ULTRASOUND-STIMULATED BEHAVIORS ON BIOMASS HYDROGEL MEDICINES FOR DRUG RELEASE APPLICATION

(バイオマスヒドロゲル薬剤での薬剤放出応用における超音波刺激挙動)

Ranpati Devage Harshani Iresha

Energy and Environment Science
Nagaoka Univeristy of Technology, Nagapka, Japan.

March 2022

Acknowledgement

This doctoral thesis is a final outcome of a loads of supports given by plentiful people. Here, I would like to offer my sincere gratitude in sentences for all of them while keeping them in heart forever.

Professor. Dr. Takaomi Kobayashi in the Department of Science of Technology Innovation, Nagaoka University of Technology (NUT), Japan, who is my academic supervisor throughout my research in Biosustainable Environmental Materials Engineering Laboratory, Nagaoka University of Technology, is truly a supervisor with a vision plus up to date knowledge and years of experiences in the fields so the researcher is eventually shaped to a professional who is versatile to relay the professional race. Professor Kobayashi's enormous guidance in knowledge and experiences, advices for research and career, support given during the stay in Japan are invaluable for me. I am always thankful for Professor Kobayashi for everything I received from him from the beginning and I am honored to have Professor Kobayashi as my academic supervisor.

Next, I would like to offer my sincere thankfulness to Associate Professor Nobu Saito, Associate Professor Motohiro Tagaya, and Associate Professor Yukiko Takahashi in the Department of Materials Science and Technology, NUT, and Professor Minoru Satoh in Ibaraki National College of Technology, for their valuable suggestions, and criticisms to streamline the research for the final outcome.

Also, I would like to express my appreciation to Assistant Professor Siriporn Taokaew, in the Department of Materials Science and Technology, NUT for the support in research and kind companionship. Another person I would like to thank here is Ms. Naomi Tominaga, in Biosustainable Environmental Materials Engineering Laboratory, NUT, for big support given during my studies in NUT and be kind to me in person. Further, all of my laboratory members including Ms. Sarara Noguchi, who was my tutor at first and friend, guide and supporter forever in Japan, Ms. Ayano Ibaraki, another kind hearted friend who is fully supportive whenever I am in need, and all the other Japanese and International laboratory friends (2016 – present), thank you very much for all the support given for the research and more importantly for your kind companionship shared with me during my stay in NUT. I am truly thankful for you all at this moment and I am lucky to have you all around.

I am extending my gratitude for the NUT administrative staff members, ‘Mutsumikai’ voluntary group members, and Sri Lankan friends in NUT and Japan for their enormous support given to smoothly flow the life in NUT. Without your kind support balancing the academic and personal life would be extremely difficult during my Doctoral study.

In the meantime, behind the screen, there are some who did invaluable sacrifices while I am focusing on my Doctoral research. My beloved late-father who was silently looking for my success, my loving mother who is the strongest person in my life and always wish for my happiness, my two beautiful sisters and little brother who are genuinely supportive every time unlimitedly, my loving husband who always looking after me, encourage me, and direct me with much love, and my two little gems, my everything, did irreplaceable sacrifices for me and I am always in debt for you all.

Also, I would like to thank all of my university teachers in NUT-Japan and University of Moratuwa-Sri Lanka and school teachers in Vijayaba National College, and Sir Jhon Kothalawala College-Sri Lanka for making me whom I am today. Further, I am expressing my thankfulness to all of my friends and relations for your kind support given so far.

Finally, I am expressing my honorable gratitude to the Japanese Government for the financial support given for my stay in Japan. That support led me to pursue research in a state-of-the-art research facility which I am forever grateful.

Ranpati Devage Harshani Iresha

March 2022

Table of Content

Chapter 1 - Introduction

1.1 Controlled drug release and drug delivery

Drug release (DR) and drug delivery (DD) are key sectors in biomedical therapies with number of evolving advanced technologies. The history evidences the progress of DR and DD from 1952 with the first invention of controlled drug release formulation of dextroamphetamine (Dexedrine) drug by Smith Klein Beecham [1]. As introduced by Kinam Park [2] the progression of the DR and DD in the first generation was oral and transdermal mechanisms with basic dissolution, diffusion, osmosis and ion-exchange methods. Then, in the second-generation delivery systems (1980 – 2010), DR and DD systems having smart functionalities were investigated by "smart" DD system (SDDS) referring to the controlled or sustained drug administration by using smart polymers [3] and hydrogels [4,5]. Such controlled and stimulated DD and DR were achieved by the surrounding factors like pH [4,6] and temperature [5]. Progress has been made of nanotechnology based research commenced in the late part of this generation opening up a wide space for more research paths in DD systems [7,8]. With the continual progression the DD systems for six decades, today, DR and DD researches are in its third generation with more unsolved problems left behind from the previous decades mainly because of difficult formulations and difficulty of predicting *in vitro-in vivo* correlation (IVIVC) of such formulations [1]. In the generation with advanced technologies in any field, addressing the

possible problems in on going or incomplete research in DD and DR would make a tangible outcomes and progression in the DR and DD. With this motivation, the current report showcases research approach for some potential SDDSs.

Briefing the history of DR and DD, the elaboration about the technologies in the SDDS is expressed hereafter. The ultimate desires of the SDDS for a specific disease or a treatment are effective and efficient in drug administration to the targeted site with less or no drug toxicity. Thus, designing of a SDDS is a mutual combination of drug or medicine, administration route, drug carrier, potential stimulant, and drug release and delivery mechanisms as shown in the Figure 1- 1 [2]. Once the drug is defined for a specific therapy, by knowing physicochemical properties of the drug, DR kinetics need to be well studied to deliver the drug efficiently. Simultaneously, DD/ DR material combining with driving mechanism using diffusion, dissolution, osmosis or ion exchange, and the release routes must be determined. To make the formulation as a successful clinical product as the ultimate target, IVIVC of the SDDS must also be verified using proper experiment series *in vitro* and *in vivo*.

In SDDS, stimulation comes related to release kinetics in combination with the release mechanisms. However, stimulation mechanism of DD and DR depends on mode of stimulation, material, delivery route etc. as described previously.

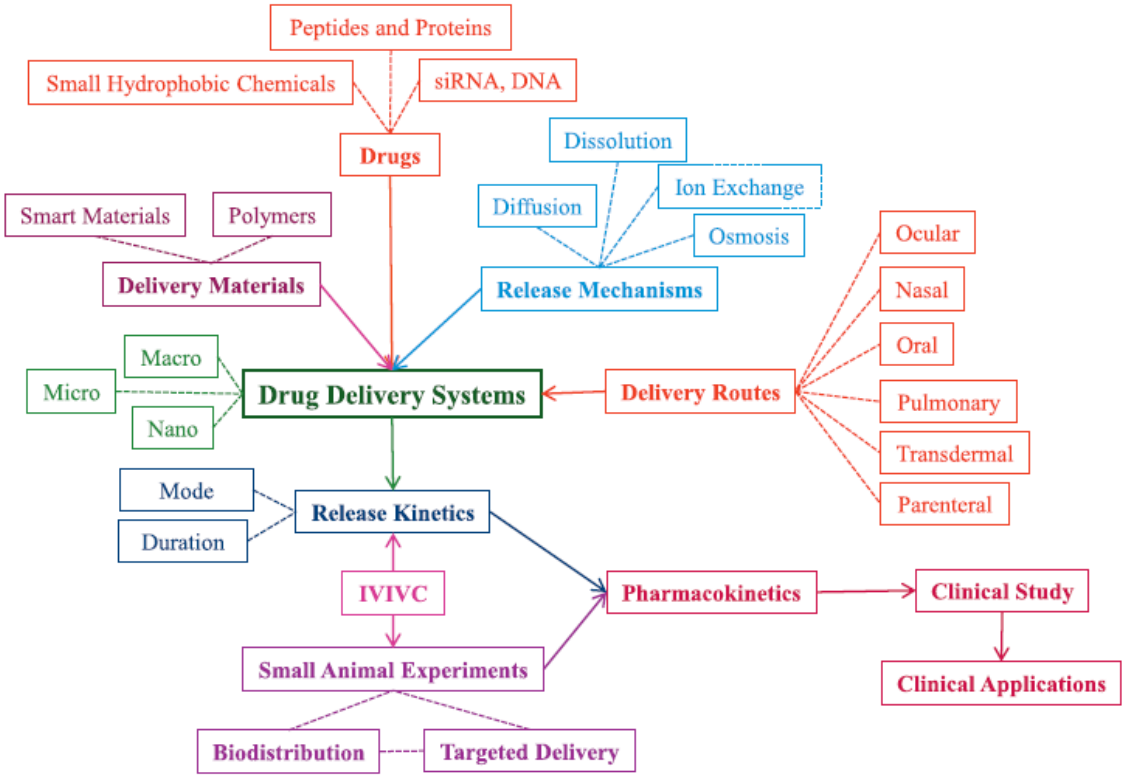

Figure 1- 1 The main components of DD systems [2]. IVIVC: *In vivo-in vitro* correlation

1.1.1 Stimulants in SDDS

Stimulant or the trigger is the most emphasizing feature when introducing a SDDS [9]. The reason could be the unique DR and DD stimulating mechanism exert by each stimulant in a specific SDDS which ultimately facilitate the drug administration. The stimulants can be categorized as exogenous and endogenous stimulants as shown in Figure 1- 2. Exogenous refers to the external stimulants such as temperature, electric fields, light, ultrasound, magnetic fields, while the endogenous stimulants are the pH, enzymes, and redox changes [10]. These stimulants have different trigger mechanism/s for DD and DR thus applicable to specific treatments depend on the drug carries and targeting site. Some common DD and DR stimulants, their research highlights including drug carrier type and material are listed in Table 1- 1. According to Table 1- 1, different SDDS with different stimulants have been investigated for years and their release mechanisms are differed from one another. Such systems are discussed in later paragraphs.

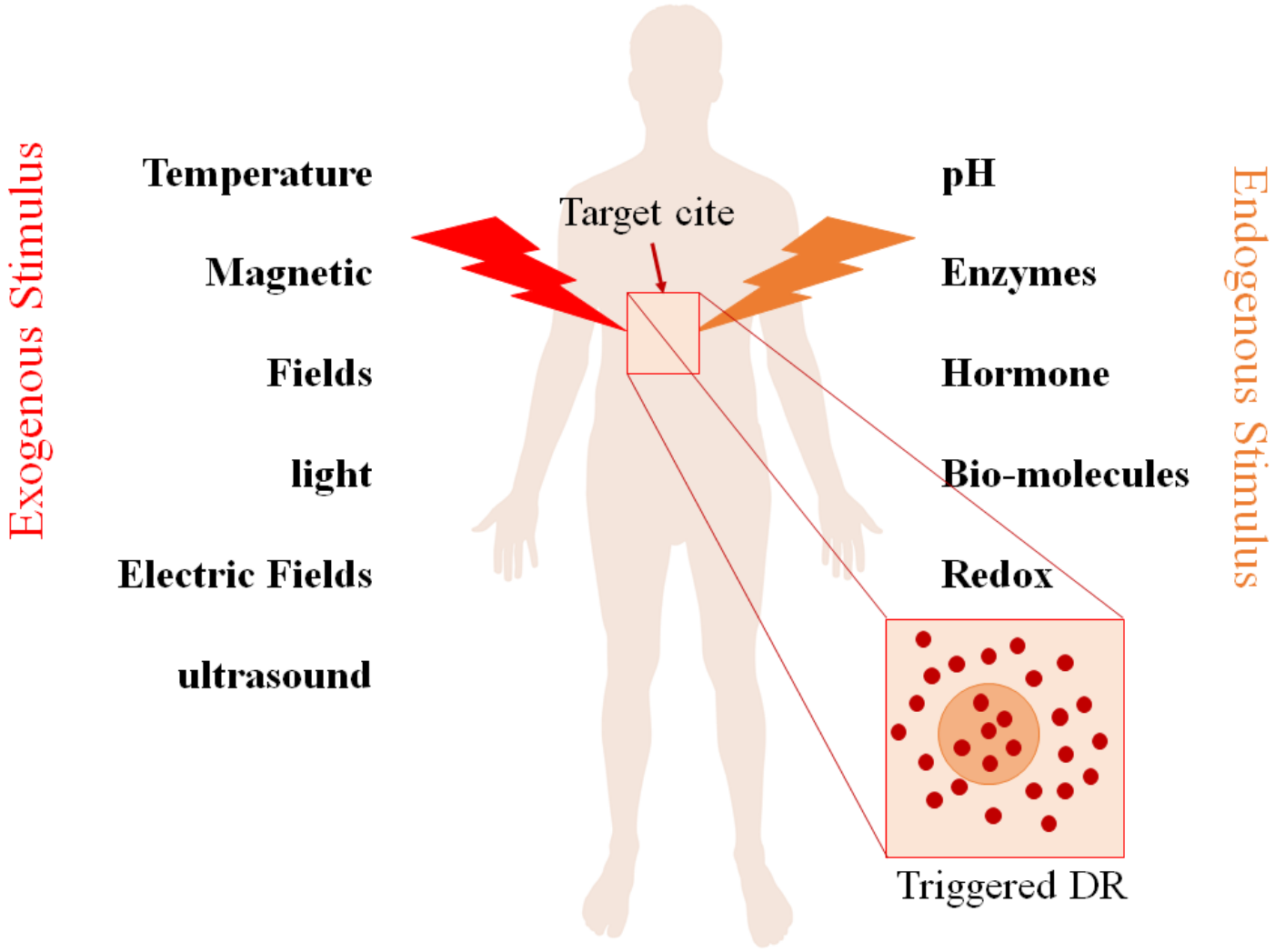

Figure 1- 2 Exogenous and endogenous stimulants in SDDSs

Among the exogenous stimulants, temperature-responsive systems are basically nanocarriers such as liposomes, micelles, or nanoparticles with lower critical solution temperature and are widely studied in oncology [10]. Triggering strategy for such thermosensitive carriers are disruption of the nanocarrier upon the elevated temperature (~ 40 – 45 ˚C) above the body temperature [11–14]. For example, a hybrid self-assembled nanocarrier composed with leucine zipper peptide – lipid bilayer was dissociated in its zipper peptide sequence above its melting point of ~ 40 ˚C and thus the enhanced DR is permitted [11]. Another system of long-circulating thermosensitive liposome was shown almost 100 % oxaliplatin release at 42 ˚C, while the release was 10 % at 37 ˚C [14]. Combined technologies were also used in creating hyperthermic effects as described in [13], where a magnetic resonance-guided high intensity focused ultrasound combined system was enhanced the doxorubicin concentration on tumor cites. Another stimulant used in SDDS was magnetic fields which provided stimulation effect to promote DR either by magnetic effect [15–17] or by temperature increment under alternative magnetic field [18–22]. A ferrogel system developed with superparamagnetic iron oxide and Pluronic F127 micelles promoted DR upon squeezing micelles by iron oxide nanoparticles by the magnetic effect [16]. Magnetic trigger in dualled on/off DR was switched as a multireservoir system with magnetic particles [17]. However, the magnetic fields which are using in oscillating or alternating form can be used to generate heat in the surrounding medium of the drug carrier thus the drug release from thermo-sensitive drug carriers [10]. One example was Fe_3O_4-

based magnetic thermal seeds coated with molecular imprinted polymer, and the loaded methotrexate drug showed 80 % release at 60 ˚C under alternate current magnetic field [18]. Another nano system containing both iron oxides and thermo-sensitive polymer promoted DR at 35 – 40 ˚C under alternating magnetic field [19].

Light-responsive DD and DR were another type of SDDS and achieved as stimuli for photochemical trigger, photoisomerization and photothermal effect [23]. Photochemical effect permitted the encapsulated drug to cleavage from the carrier composed with moieties such as ortho-nitrobenzyl, coumarin derivatives and pyrene derivatives. Those are affected to irreversibly split the covalent bonds by the lights. Then the chemical change was applicable for DD and DR systems. Gold nanoparticle system loaded with 5-fluorouracil anticancer drug by the ortho-nitrobenzyl linkage was photo cleavage the drug and thus promoted DR upon the UV light irradiation at 365 nm [24]. Photoisomerization of molecules like azobenzene, spiropyran (a class of photochromic molecule) was another stimulation in light-responsive SDDS [23]. Azobenzene-based nanoimpeller system was led to the release of camptothecin upon light excitation at 413 nm [25]. A photoswichable nanoparticle systems using spiropyran enhanced tissue penetration and DD by the reversible photoisomerization [26]. There were photothermal effects of materials with a chromophore converting light in to heat and a thermo-responsive component, and applied for light responsiveness in SDDSs [23]. For example, near-infrared light-activated microneedle

system containing photosensitive lanthanum hexaboride was developed to release of doxorubicin by the photothermal effect [27].

SDDSs have developed with electro-responsivity because of the accessibility in clinics despite the lower tissue penetrability and harmfulness to the body as caused by the presence of higher voltages and longer exposure [23]. Electro-responsive SDDSs have developed with wide range of materials like conductive polymer-contained nano-particles [28], alginate-based hydrogel [29], transdermal patch made by electrospinning [30], chitosan-based nanocomposite hydrogels [31]. Each system acted accordingly with the designed material under electric fields. As an example, a drug contain-nanoparticle system developed with a conductive polymer of polypyrrole showed triggered DR upon pulsed electric field. The release mechanism was synergistic process of the oxidation-reduction reaction and the net movement of charged molecules by the application of electric field [28]. In another SDDS, electro-sensitivity of a electrospun-transdermal patch was designed by introducing multi-walled carbon nanotubes which can dissolve the networking polymer under electric field to release the encapsulated drug [30].

It was also seen that pH variations in a specific body organ, intracellular compartments or happened due to the changes of normal body environment by diseases such as cancers or inflammation. The pH stimulated DD and DR were possible from drug carriers to be sensitive to external changes [10]. Many of such systems have designed with acidic pH responsiveness [32–36].

Discussion of the above stimulants in SDDS is summarized in Table 1- 2. Considering the feasibility of them, many of the stimulants are engaged with critically formulated materials like nanoparticles. Importantly, materials used for drug carriers in magnetic, light, electric, pH have high chances of adverse health effects. Also, conditions like hyperthermia, electric and pH are questioning the health effect of using such systems. However, consequently, yet promising stimulus are accepted for therapies using SDDSs.

Ultrasound (US) is considered clean and green technology for wide spectrum of applications including in smart DD and DR systems. US has exerted key favorable advantages for SDDSs as mentioned in Table 1- 2. From outside to inside the body manipulation ability is advantageous along with deep penetrability into the deeper tissues. This depends on the US frequency which different penetrations can be achieved for different therapies. Few mechanisms to stimulate DD or DR such as oscillatory motion, acoustic streaming, cavitation effect and hyperthermia, non-invasiveness, etc. [10,37–39] is another factor to be considered US as a SDD stimulant. Hereafter, US stimulation will be discussed elaborately as the next section.

Table 1- 1 Stimulants in DD and DR applications

Stimulant	Drug carrier		Drug	Reference
	Type of carrier	Material		
Temperature	Thermosensitive hydrogel	N-isopropyl acrylamide copolymerized with butyl methacrylate (hydrophobic) or acrylic acid (hydrophilic)	Heparin	[40]
Temperature	Liposome	Liposome co-modified with single standard DNA aptamers and thermosensitive polymers	• Calcein • Doxorubicin	[41]
Temperature	Nanoparticles	Chitosan-g-poly(*N*-isopropylacrylamide) co-polymeric nanoparticles loaded with curcumin	Curcumin	[42]
Temperature	Liposomes	Clinical-grade doxorubicin encapsulated low temperature sensitive liposomes	Doxorubicin	[13]
Temperature	Liposomes	DPPC (1 ,2-dipalmitoyl-*sn*-glycero-3-phosphocholine) and DSPC (1,2-distearoyl-*sn*-glycero-3-phosphocholine) phospholipid-based thermosensitive nanocarriers.	Idarubicin	[12]
Temperature	Liposome	Long-circulating thermosensitive liposomes using DPPC as main thermosensitive material and 1,2-distearoyl-sn-glycero-3-phosphoethanolamine-N- [maleimide (polyethylene glycol)-2000] (PEG2000-DSPE) as the long-circulating material	Oxaliplatin	[14]
Temperature	Lipid Peptide nanoscale vesicle	Leucine zipper peptide lipid hybrid nanoscale vesicles	Doxorubicin	[11]
Magnetic fields	Highly magnetic nanocarrier	Nanocarrier composed of an Fe3O4 core and poly [N-(1-one-butyric acid)] aniline (SPAnH) shell	1,3-bis (2-chloroethyl)-1-nitrosourea	[15]
Magnetic fields	Hybrid nanocarrier with magnetic and thermal sensitivity	Thermosensitive molecular imprinted polymer coated with Fe_3O_4 nanoparticles (magnetic thermal seeds)	Methotrexate	[18]
Magnetic fields	Nanoparticles	Mesoporous silica nanoparticles (MSNs) embedded with iron oxide nanocrystals and coated with a thermo-responsive	Protein	[19]

		copolymer of poly(ethyleneimine)-b-poly(N-isopropylacrylamide)		
Magnetic fields	Nanoparticle	MSNs loaded with iron oxide nanocrystals and the nanoparticle surface was immobilized with single-stranded DNA	Fluorescein	[20]
Magnetic fields	Nanoparticle	MSNs with zinc-doped iron oxide nanocrystals and the surface modified with pseudorotaxanes	Doxorubicin	[21]
Magnetic fields	Nanocomposite membrane	Ethyl cellulose membrane matrix contain superparamagnetic iron oxide and thermo-reversible poly(N-isopropylacrylamide) (PNIPAm)	Fluorescein-labeled dextran	[22]
Light	Nanoparticle	MSNs modified with nanoimpeller control function using azobenzene moieties	Camptothecin	[25]
UV light	Nanoparticle	Photoswitchable nanoparticles contained with spiropyran (a class of photochromic molecules) and lipids	Rhodamine 6B dye	[26]
UV light	Nanoparticles	Gold nanoparticles consisting with photocleavable ligands which serves to adhere the 5-fluorouracil anticancer drug and nanoparticle surface via *ortho*-nitrobenzyl linkage	5-fluorouracil	[24]
NIR light	Nanoparticles	EphB4-targeting hollow gold nanospheres	Doxorubicin	[43]
Light	Nanoparticles	Gold nanoparticle-capped MSNs	Paclitaxel	[44]
NIR light	Microneedle array system	Polycaprolactone microneedle consisting with photosensitive nanomaterial (lanthanum hexaboride) and dissolvable poly (vinyl alcohol)/polyvinylpyrrolidone supporting array patch	Doxorubicin	[27]
Electric field	Hydrogel system with dispersed nanoparticle	Dispersion of drug-loaded polypyrrole nanoparticles in PBS solution containing 25 wt% of PLGA-PEG-PLGA (PLGA-PEG-PLGA is polymer poly [(D, L-lactic acid)-co- (glycolic acid)]-b-poly (ethylene oxide)-b-poly-[(D, L-lactic acid)-co- (glycolic acid)]).	Fluorescein, Daunorubicin	[28]
Electric field	Hydrogel	Hydrogel made with mixture of poly(3,4-ethylenedioxythiophene):	Curcumin	[29]

		polystyrene sulfonate (PEDOT: PSS) and alginate (Alg)		
Electric field	Transdermal patch	Semi-interpenetrating polymer network by electrospinning using polyethylene oxide/pentaerythritol triacrylate/ Multi-walled carbon nanotubes/drug	Ketoprofen	[30]
Electric field	Nanoparticle	Orthogonal self-assembly of two end-decorated homopolymers of poly(styrene)-β-cyclodextrin and poly (ethylene oxide)-ferrocene	Rhodamine B	[45]
Electric Field	Nanocomposite hydrogel	Chitosan and montmorillonite composite hydrogel	Vitamin B_{12}	[31]
pH	Micelles	pH-responsive diblock copolymer, poly (ethylene glycol)-block-poly(2-(diisopropylamino)ethyl methacrylate) , and a vitamin E derivate (D-a-tocopheryl polyethylene glycol 1000 succinate, TPGS)	Doxorubicin	[32]
pH	Nanoparticles	MSNs combined with *β*-cyclodextrin nanovalves which are responsive for pH changes	Doxorubicin	[33]
pH	Nanoparticles	MSNs capped with gold nanoparticles by acid-labile acetal linker	[Ru(bipy)3] Cl2 (dye)	[34]
pH	Nanoparticles	Surface charge-switching poly (D, L-lactic-co-glycolic acid)-b-poly(L-histidine)-b-poly-(ethylene glycol)	Vancomycin	[35]
pH	Liposomes	PEGylated unilamellar lipid vesicles composed of tunable heterogeneous bilayers. Lipid vesicles are composed of diheneicosanoyl phosphatidylcholine (n.21), and of the titratable distearoyl phosphatidyl serine (n.18) with PEGylated lipids (distearoyl phosphatidylethanolamine PEGylated lipid, n. 18), and biotin-labeled lipids	Doxorubicin	[36]

Table 1- 2 Positive and negative points of existing stimulants in DD and DR

Stimulant	Positive	Negative
Temperature	• Cancer cells are sensitive to hyperthermic conditions thus increased control of cell growth • Several technologies such as magnetic, US, light can be used to induce heat	• Complication in technologies • Drug carrier fabrication is difficult with complex methodologies • Risk of internal tissues or organs due to applied external heat in deep penetration • Biocompatibility of drug carriers is questionable
Magnetic fields	• Stimulated DR, magnetically guided drug targeting and contrast agent for imaging is possible with magnetic fields • Reached to clinical trials for magnetically stimulated DD and DR	• Complex equipment set for focusing, intensity controlling and deep penetration • Health risk of exposing to magnetic fields are yet unsolved • Possible toxicity by iron oxide and other chemicals used in drug carriers
Light	• Non-invasive nature • High degree of spatiotemporal precision	• Low penetrating depth due to strong scattering properties of soft tissues • Complex fabrication procedures of drug carriers • Questionable biocompatibility of drug carriers
Electric fields	• Accessibility of electric fields due to the existing iontophoresis devices in clinics • Safe levels of electric fields have been studied extensively	• Risk if damage to internal tissues by the electric sources in deep penetration • Electro-responsiveness is subjected to change due to environmental factors like presence of ionizable molecules, concentration of electrolytes.
pH	• Small changes of pH make the drug carriers responsive in DR by the changes of chemical and physical functions • Abnormal cites in body such as cancers and inflation show characteristic pH changes thus	• pH changes in diseased cites could be vary depend on the patient and nature of the disease • Drug carriers may react adversely by the altered compositions of the targeted due to disease

	can be used as a stimulant without using outside stimulus.	
Ultrasound	• Non-invasive nature • Deep penetrability into tissues • Ultrasound is already a well-established technology in medicine thus capable of modifying for DD and DR • Several mechanisms to stimulate DD and DR by oscillatory motion, acoustic streaming, cavitation, thermal effect. • Easy to use • Outside to body manipulation ability	• Drug carriers need to be developed • Long exposure may affect for healthy tissues

1.1.2 US as a drug release stimulant in SDDSs

In the medical field, US is widely established as a diagnostic tool, and it is called sonography. Currently, sonography is applied for the diagnoses in vascular, abdominal, obstetrics, gynecology, neurology, cardiography, ophthalmology, etc. [46]. Thus, extending US for therapeutic applications is obvious and therefore, US is trending as a DD and DR stimulant now a days.

It is known that US is pressure wave that transmitted through a tangible medium such as water by compressing and expanding the molecules [38,47]. The range of US frequencies is above 20 kHz. Applications of US depend on the US frequency, and such frequencies have dividing at low (20 – 200 kHz), intermediate (200 – 700 kHz), medium (0.7 – 3 MHz), and high (1 – 20 MHz) ranges [48]. The low-frequency US is typical for therapeutic medical applications [48] as a promising stimulant for DR and DD systems because US power can be transmitted through the body organs with frequency-dependent penetrability, thereby can act on the focused biological systems. Also, US is a non-invasive stimulant to the human and animal, while it can be easily manipulated externally [47].

As an external trigger source, for US, there are following characteristics. Under precise monitoring and controlling, the local temperature of the body for a specific time of treatment, which is favorable for a specific therapy, can be elevated by the hyperthermic effects of US [49]. For that, high intensity focused US is developed and mainly studied for tumor therapies. For the US DR and DD applications, thermo-sensitive liposomes widely

use carriers in US-induced hyperthermic treatments, and such liposomal DD are used for cancer treatment applications. [50–53]. Another incident is collapse of cavitation bubbles, i.e., transient, or inertial cavitation, generating more microbubbles. Thus, the process continues, emitting shock waves to damage the drug carriers, enhancing drug delivery [39], and polymer decomposition, thereby enhancing drug uptake [54,55]. Furthermore, transient cavitation can induce membrane permeabilization, thus the drug transportation [56]. The US-induced drug permeation through the skin is also possible due to the cavitation effected at the low-frequency range [57–60]. In addition, acoustic streaming, which is the circulatory motion of the liquid near to the oscillating bubbles [61], is one of the characteristics of US inducing the drug release due to the motions of the surrounding liquid of vibrating micro-drug [61–63]. Such microstreaming is mechanically, high powerful phenomenon. Thus, US has exerted sufficient effect on matrix permeability and stimulation cell activities [63,64]. Also, the bulk streaming, which happens when the US propagates in the medium while the medium is also flowing unidirectional to the US wave, can cause radiation forces. Such radiation forces are capable of transporting particles near the targeted tissues [65,66]. Therefore, with the availability of several mechanisms of stimulation, US-triggered DD and DRs are promising in medical fields.

1.2 Biomass hydrogel drug carriers in SDD and DR

In addition to the importance of external triggers in SDDS, the choice of materials to serve as the drug matrix is also inevitable. For suitable drug release stimulant in SDDSs, loading the drug in a proper drug carrier or a capsule is also one of the major factors. In SDDSs, drug carrier not only provides a temporary habitat for the drug until release but also responds to the respective stimulant for the sake of controlled/ stimulated release. As shown in Table 1- 1, there are many kinds of drug carriers or matrices namely, nanoparticles, liposomes, micelles, hydrogels, transdermal patches, etc. designed for desired applications of DDSs. Out of these drug carriers, hydrogels are one of advanced material in biomedical applications due to its unique features exert by its water retaining 3D porous structure [67,68]. Especially for the release of drugs into the human body, the materials use are mostly hydrophilic materials, and hydrogel is the most commonly utilized carrier.

In hydrogels, high porosity and the functional groups presented in the networking materials allows loading drugs in the hydrogels which can account as drug carriers [69,70]. These hydrogels were made of using synthetic polymers [71,72] or natural polymer extracts [57,69,70,73]. Nevertheless, hydrogel prepared by natural materials have many advantages over synthetic hydrogels. More importantly, biocompatibility and non-toxicity are major favorability in medical applications especially for DD/ DR and tissue culture [67,68]. Table 1- 3 summarizes different biomass hydrogels used in SDD and DR applications under different stimulants. However, so called hydrogels in here refers to biomass hydrogels are

yet little as known DD and DR matrices in the applications under US stimulations. Therefore, featuring as sustainable material for US-stimulated DD and DR, biomass hydrogels would be a promising drug capsule to experiment.

Among the natural polymers, it is known that cellulose and chitin are the world's most abundant polysaccharides [74]. Other than these, there are natural polysaccharides, namely, chitosan, carrageenan, alginate, hyaluronic acid, guar gum, etc., for DD or DR matrices. However, natural polymer hydrogels are still newly emerging into the US triggered DD and DR since drug hydrogel matrices in the fabrication hinder technological progress for cellulose and chitin. Table 1- 4 lists the summary of biomass hydrogels in US-triggered DD.

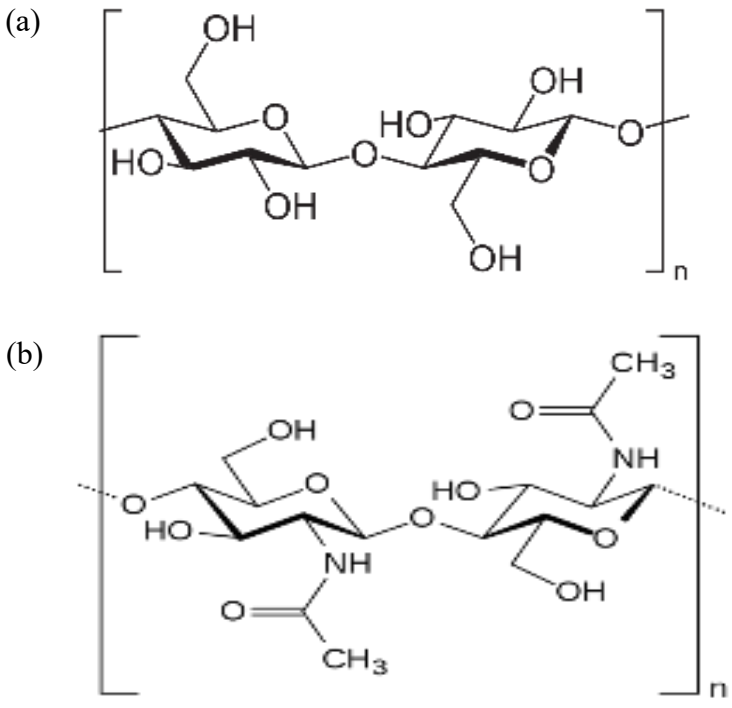

Figure 1- 3 Chemical structure of (a) cellulose and (b) chitin

Table 1- 3 Summary of biomass hydrogels in SDD and DR under different stimulants

Polysaccharide Hydrogel	Drug	Stimulant	Reference
Cellulose Hydrogel	Mimosa	US	[69]
Chitin Hydrogel	Gallic acid	US	[70]
Cationic cellulose hydrogels	Diclofenac Sodium	pH- and ion-sensitivity	[75]
Bacterial cellulose/ acrylic acid hydrogel	Bovine serum albumin	Temperature and pH	[76]
Chitin nanogels conjugated with MPA-capped-CdTe-Quantum Dots	Bovine serum albumin	pH	[77]
Hydroxypropylmethyl cellulose films	Nicotine	pH and ionic strength	[78]
Kappa-carrageenan/ polyvinyl alcohol hydrogel	β-carotene	pH	[73]
Bacterial Cellulose/ Acrylamide based hydrogel	Theophylline	Released to phosphate buffer (pH 7.4) at 37 ^{0}C	[79]
Cellulose nanocrystals-gelatin hydrogels	Theophylline	Released to simulated gastric fluid (HCl at pH 1.2) at 37 ^{0}C	[80]
Carboxymethyl cellulose/ carboxymethyl β-cyclodextrin hydrogel	Tetracycline	Released to PBS buffer (pH 7.4), at 37 ^{0}C	[81]
Carboxymethylcellulose sodium/ cellulose hydrogel	Bovine serum albumin	Released to phosphate buffer (pH 7.4) at 37 ^{0}C	[82]

Chitin/PLGA blend microspheres	Bovine serum albumin	Released to PBS buffer (pH 7.4) at 37 ^{0}C	[83]
Cellulose hydrogel and Chitin Hydrogel	Nicotine	US	[84]
Chitosan/ alginate beads	Indomethacin	pH	[85]
Poly (ethylene glycol)/ carboxymethyl chitosan hydrogel	5-fluorouracil	pH	[86]
Carboxymethyl chitosan/ poly(N-isopropylacrylamide) semi-interpenetrating polyampholyte hydrogel	Coenzyme A	Temperature and pH	[87]
Thiolated hydroxypropyl cellulose nanogels		Temperature and redox	[88]
Bacterial cellulose nanofiber/ sodium alginate hybrid hydrogel	Ibuprofen	pH and electric field	[89]

Table 1- 4 Natural polysaccharide hydrogels used for US triggered DD and DR applications

Natural polysaccharide hydrogels	Encapsulated drug	Reference
Cellulose hydrogel	Mimosa	[69]
Chitin hydrogel Cellulose hydrogel Carrageenan hydrogel Agar hydrogel	Gallic acid	[70]
Alginate Hydrogels	Bone morphogenetic protein-2 conjugated with gold nanoparticles (BMP-2 AuNPs)	[90]
chitosan/β-glycerophosphate hydrogel	Doxorubicin loaded into Lysolipid thermally sensitive liposomes	[91]
Chitosan/ perflurohexane nanodroplets	Curcumin	[92]
Ca^{2+}-crosslinked alginate hydrogels	Mitoxantrone Condensed plasmid DNA (pDNA) Stromal cell-divided factor 1α (SDF-1α)	[57]
Cellulose hydrogel	Short-chain fatty acid	[93]

Each natural polysaccharide brings unique properties depending on its nature-provided chemical structure, which is compatible with its original functions. For example, cellulose is created with β-(1→4) glycosidic bonds connecting D-glucose units (Figure 1- 3 (a)). Thus, the structure of cellulose can create rigid rod-like crystalline fibrous materials and rigid cellulose fibrils, coming with the strong inter-and intra- molecular hydrogen bonds of cellulose with -OH and -O- functional groups [94]. Therefore, especially for green plants, cellulose is a key structural element and determines the framework of cell walls [95]. In contrast, the structure of chitin is similar to that of cellulose, but the hydroxyl group on the second carbon is an acetamide group. Similarly, the chitin in its structure given in Figure 1-3 (b) brings stronger hydrogen bonds than cellulose, by the presence of many hydrogen bonding sites are available in chitin, namely, -NH, -C═O, -CH_3-OH, and -OH [96]. Thus the chitin has hard exoskeletal structures of insects, including crabs and shrimps [97]. Because of such stable characteristics, especially their insolubility in common solvents, the preparation of cellulose and chitin hydrogels was not possible until 2013 [67,98].

Some of the advanced applications of materials derived from cellulose, chitin, and their derivatives are summarized in Table 1- 5. The content of Table 1- 5 clearly shown for the competence of cellulose and chitin together with their derivatives in applications such as DD and DR, scaffold materials, wound healing materials in different forms.

Table 1- 5 Cellulose, chitin, and cellulose/ chitin-based materials in medical applications

Materials from chitin and cellulose for medical applications	Medicinal values	Reference
Chitin extracted from shrimp wastes	Chitin exhibited a bacteriostatic effect on Gram-negative bacteria, Escherichia coli ATCC 25922, Vibrio cholerae, Shigella dysenteriae, and Bacteroides fragilis	
Chitosan obtained from deacetylation of chitin	Bacteriostatic effect on Gram-positive bacteria: Staphylococcus aureus ATCC 25923, S. aureus ATCC 43300, Bacillus subtilis and Bacillus cereus, and seven Gram-negative bacteria: Escherichia coli ATCC 25922, Pseudomonas aeruginosa ATCC 27853, Vibrio cholerae, Shigella dysenteriae, Prevotella melaninogenica, and Bacteroides fragilis.	[99]
N-acetyl chito-oligosaccharides and chito-oligosaccharides derived from chemical hydrolysis of chitin	Bactericidal effect on Gram-positive bacteria: Staphylococcus aureus ATCC 25923, S. aureus ATCC 43300, Bacillus subtilis and Bacillus cereus and seven Gram-negative bacteria: Escherichia coli ATCC 25922, Pseudomonas aeruginosa ATCC 27853, Salmonella typhimurium, Vibrio cholerae, Shigella dysenteriae, Prevotella melaninogenica, and Bacteroides fragilis.	
Chitosan-ulvan hydrogel reinforced with Epidermal Growth Factor (EGF)	Non-toxic, Excellent cell proliferation, Sustained release of EGF and 100 % wound contraction within 15 days, Efficient wound healing by faster granulations tissue formation and collagen deposition	[100]
Cellulose hydrogel films from Bamboo Fibres	Fibroblast cell cultivation with higher cell density	[101]
Cellulose hydrogel from Agave fibres		[67]
Cellulose hydrogels from sugar cane bagasse	In vivo biocompatibility as a scaffold material for cell culture	[68]

Chitosan microneedle array encapsulated with vascular endothelial growth factor (VEGF)	Controlled VEGF release promotes inflammatory inhibition, collagen deposition, angiogenesis, and tissue regeneration during the wound closure.	[102]
Cellulose/ carboxymethylcellulose sodium (CMC) hydrogel	Controlled release of bovine serum albumin (BSA) based on the different compositions of the hydrogel	[103]
Cellulose-lignin hydrogel	Controlled release of polyphenols based on the different compositions of the hydrogel	[104]
Cellulose/poly(N-isopropylacrylamide) hydrogels	Controlled release of dimethyl methylene blue as a model drug based on the different compositions of the hydrogel	[105]
methylcellulose, hydroxyethylcellulose, and hydroxypropylcellulose hydrogels	Alaptide release capability	[106]
carboxymethylcellulose (CMC)/ poly(N-isopropylacrylamide) hydrogel	Temperature, pH and redox responsive lysozyme release behaviour	[107]
Chitin-carbon nanotube composite hydrogel	Biocompatible scaffold for neuron repair/ regeneration with excellent neuron adhesion and support of synaptic function of neurons	[108]
Chitin-glucan and polyphenols extracted from pomegranate as a supplement	Recovery of endothelial dysfunction by reducing the inflammatory disorder in a mouse model	[109]
Chitin nanofibrils	Suppression of skin inflammation in atopic dermatitis	[110]
Chitin nanoparticles	Efficient release of ellagic acid from chitin nanoparticles thus inhibition of breast cancer cell growth	[111]

1.2.1 Biomass hydrogels in US-triggered DR applications

On the other hand, polysaccharide hydrogels composed of fundamental polymeric linkages like glucose segments are possible to produce film-like matrices. For biomass hydrogels, as summarized in Table 1- 4, there are several matrices made from different natural polymers for different drug systems. Those hydrogel matrices exhibited enhanced release of drugs under US-triggering. Extensive studies on the US parameters-based DR from biomass hydrogels were clearly discussed in gallic acid-chitin hydrogel system [70] and mimosa-cellulose hydrogel [69]. Chitin hydrogel system with gallic acid expressed enhanced DR under the triggering of US at different output powers at 43 kHz US. Here, gallic acid is natural polyphenolic compound with excellent pharmacological and biological benefits [112]. The different US power irradiated to the chitin-gallic acid hydrogel enhanced the release of gallic acid as compared with that of non-US case, which has about 3 μg/(min・min) in the releasing rate. Especially, the 30W US clearly enhanced the release with 10 times efficiency about 30 μg/(min・min) rate. Similar behavior was exhibited for the mimosa-loaded cellulose hydrogels [69] and cellulose-chitin composite hydrogel loaded with nicotine. In other words, US power controlled the release of such drugs from cellulose or chitin matrix, which those gel drugs retained excellent biocompatibility and cell culture properties [67,68,113].

1.2.2 Specialty and properties of biomass hydrogels for US DR applications

It is general that hydrogel structure is a major factor to be considered in DDS because of affecting the drug loading capacity, responsiveness to a stimulant, applicability in a decided root, etc. Hydrogels, in their born nature, consist of a 3-dimensional (3D) porous network. Thus, for drug encapsulation the structure should have high porosity inside the hydrogel, high surface area due to the high porosity and leading to higher surface affinity with the drug. Increased drug loading at lower cellulose loading was possible due to the high porosity and high swelling properties [93]. Other than this, due to hydrophilic nature in hydrogels hydrophobic drugs is significantly difficult to load in the matrix, this is disadvantage to use such drugs developed effectively for therapies [114]. Thus, hydrogel systems are primarily favorable for biological agents because of their hydrophilicity [115] as summarized in Figure 1- 4.

Considering the US-stimulated DD applications, hydrogel must be well-tailored in order to achieve the US stimulation effect on DD and DR. Currently, the most used drug carriers for US-responsive DD and DR systems are polymeric micelles [116–118], liposomes [41,51,119], microbubbles with gas-filled core with lipid, polymer/ protein shell [120,121]. Even though the biomass hydrogel systems for US DD are limited yet, the acquired progress of hydrogel development is worth considering.

During US exposure, the stability of the hydrogels is an intrinsic need for a DR system. Comparison was made for carrageenan hydrogel and agar hydrogel loaded with gallic acid

cellulose and chitin for US-DR [70]. The US forces was serious to the carrageenan hydrogel, leading to the matrix broken and while made the matrix weaken for agar gel. Only the gallic acid-loaded chitin and cellulose hydrogels kept the hydrogel state untouched under the US exposure, while maintaining controlled and enhanced gallic acid release over the period of 60 min exposure. In the case of alginate, this natural anionic polymer making into a gel form by adding divalent cation crosslinker Ca^{2+} [122]. The gel form of alginate was successfully used for US-stimulated digital release of drugs [57]. The ionic crosslink bonds were disrupted by the US irradiation, but reforming of hydrogel was occurred without US in the same as cellulose and chitin hydrogels. When the alginate hydrogels were irradiated with US, the hydrogel was incubated in Ca^{2+} medium with 2.6 mM, 13.3 mM, and without the salt. Over the 8 cycles of US exposure, the normalized dry mass and the normalized elastic modulus of the alginate hydrogels in the medium without Ca^{2+} were reduced [57]. Furthermore, Recent studies presented that the accelerated drug release by US was attributed to the softening of the cellulose hydrogel carrier under the exposure [123] by using sono-deviced rheometer. Here, the cyclic US irradiation cause the cyclic change of viscoelastic properties of the cellulose hydrogel. If explains extensively, when US was irradiated into the cellulose hydrogel, the viscoelastic properties were dropped suddenly and once the US was switched off, the properties returned to the original values. This behaviour is an interesting finding in the field of biomass hydrogel because this cyclic property change ensures repeatability against US irradiation for many applications.

Thus, in conclusion, biomass hydrogel material development for the US-stimulated DR applications and study the hydrogel behaviours against US may concrete their applicability in clinical applications in future.

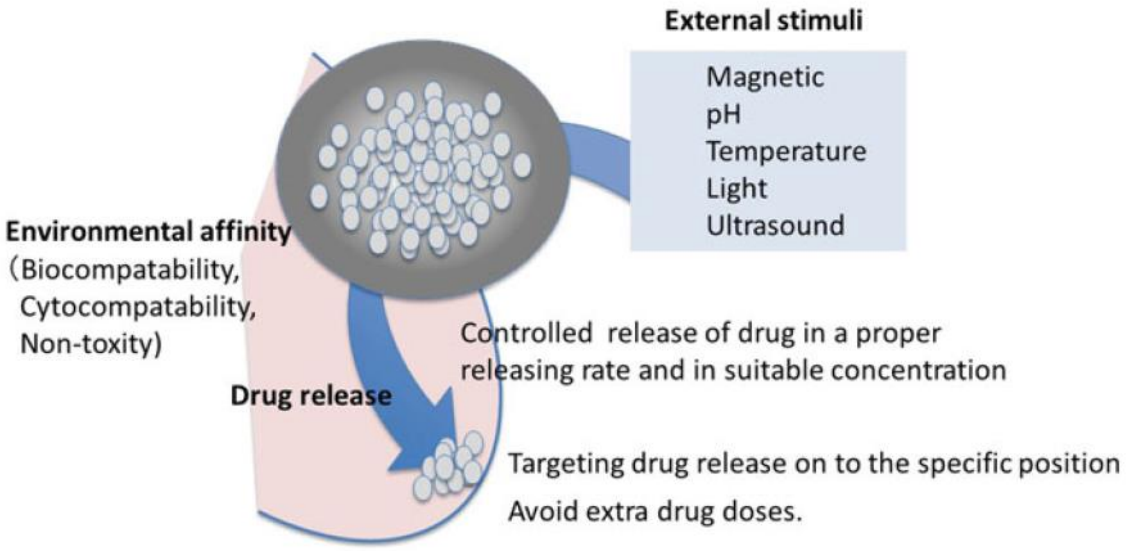

Figure 1- 4 Schematic representation of smart DR using biomass hydrogels [9]

1.3 Scope of the current study

In this thesis study, biomass polymers of cellulose and chitin and in composites were moulded to biomass hydrogels and focused for drug release under US stimulation for sustainable way of medical applications. Nicotine was used as the drug considering as candidate for popping-up medicinal values for neuro-regenerative therapies. Nicotine release behaviours from hydrogels were tested under US irradiation. Further, viscoelastic properties and FTIR were analysed to identify the effects of US on the hydrogel matrix.

Chapter 2 discussed about the nicotine-loaded cellulose hydrogels prepared in three cellulose loadings. Nicotine release was enhanced by the US exposure and the release was

increased with the US power in the hydrogel made with 0.9 wt% cellulose. Cellulose hydrogel system was compatible with the release in PBS medium also which analogues to the physiological environment. Hydrogels were softened upon US irradiation and FTIR analysis together with deconvolution analysis ensured the nicotine release due to the breakage of nicotine-cellulose hydrogen bonds in the matrix upon US stimulation.

In Chapter 3, composite hydrogel of cellulose-chitin was newly introduced, and its behavioural changes of *in-situ* viscoelastic properties were studied under cyclic US irradiation using sono-deviced rheometer. US-triggered viscoelastic property drops upon US irradiation and returning the values to the initials when US was stopped was noted in cyclic US exposure. Different compositions of cellulose and chitin in the hydrogel matrix showed different behaviours in viscoelasticity. Especially, the chitin containing hydrogels show gradual decline of properties up to second cycle and then in the third cycle, sudden drop was noted. FTIR analysis concluded the strong hydrogen bonding network in the cellulose-chitin composite hydrogel while changes of the initial hydrogen bonding network was happened after the cyclic US irradiation making the matrix more uniform than the initial. Ultimately, the composite hydrogels loaded with nicotine were tested for nicotine release under cyclic US trigger to consider the feasibility of the composite hydrogel for cyclic DD and DR applications.

Finally, the study summary was presented in Chapter 4.

References

[1] Y.H. Yun, B.K. Lee, K. Park, Controlled Drug Delivery: Historical perspective for the next generation., J. Control. Release. 219 (2015) 2–7. https://doi.org/10.1016/j.jconrel.2015.10.005.

[2] K. Park, Controlled drug delivery systems: Past forward and future back, J. Control. Release. 190 (2014) 3–8. https://doi.org/10.1016/j.jconrel.2014.03.054.

[3] A. V. Kabanov, E. V. Batrakova, N.S. Melik-Nubarov, N.A. Fedoseev, T.Y. Dorodnich, V.Y. Alakhov, V.P. Chekhonin, I.R. Nazarova, V.A. Kabanov, A new class of drug carriers: micelles of poly(oxyethylene)-poly(oxypropylene) block copolymers as microcontainers for drug targeting from blood in brain, J. Control. Release. 22 (1992) 141–157. https://doi.org/10.1016/0168-3659(92)90199-2.

[4] R.A. Siegel, M. Falamarzian, B.A. Firestone, B.C. Moxley, pH-Controlled release from hydrophobic/polyelectrolyte copolymer hydrogels, J. Control. Release. 8 (1988) 179–182. https://doi.org/10.1016/0168-3659(88)90044-2.

[5] A.S. Huffman, A. Afrassiabi, L.C. Dong, Thermally reversible hydrogels: II. Delivery and selective removal of substances from aqueous solutions, J. Control. Release. 4 (1986) 213–222. https://doi.org/10.1016/0168-3659(86)90005-2.

[6] L. chang Dong, A.S. Hoffman, A novel approach for preparation of pH-sensitive hydrogels for enteric drug delivery, J. Control. Release. 15 (1991) 141–152. https://doi.org/10.1016/0168-3659(91)90072-L.

[7] T. Kawano, M. Yamagata, H. Takahashi, Y. Niidome, S. Yamada, Y. Katayama, T. Niidome, Stabilizing of plasmid DNA in vivo by PEG-modified cationic gold nanoparticles and the gene expression assisted with electrical pulses, J. Control. Release. 111 (2006) 382–389. https://doi.org/10.1016/J.JCONREL.2005.12.022.

[8] M.M. Ow Sullivan, J.J. Green, T.M. Przybycien, Development of a novel gene

delivery scaffold utilizing colloidal gold–polyethylenimine conjugates for DNA condensation, Gene Ther. 2003 1022. 10 (2003) 1882–1890. https://doi.org/10.1038/sj.gt.3302083.

[9] H. Iresha, T. Kobayashi, Smart Polysaccharide Hydrogels in Drug Delivery and Release, in: A.K. Nayak, M.S. Hasnain (Eds.), Adv. Biopolym. Syst. Drug Deliv., Springer Nature, 6330 Cham, Swisterlan, 2020: pp. 135–149. https://doi.org/https://doi.org/10.1007/978-3-030-46923-8.

[10] S. Mura, J. Nicolas, P. Couvreur, Stimuli-responsive nanocarriers for drug delivery, Nat. Mater. 12 (2013) 991–1003. https://doi.org/10.1038/nmat3776.

[11] Z.S. Al-Ahmady, W.T. Al-Jamal, J. V. Bossche, T.T. Bui, A.F. Drake, A.J. Mason, K. Kostarelos, Lipid–Peptide Vesicle Nanoscale Hybrids for Triggered Drug Release by Mild Hyperthermia in Vitro and in Vivo, ACS Nano. 6 (2012) 9335–9346. https://doi.org/10.1021/NN302148P.

[12] T. Lu, D. Haemmerich, H. Liu, A.L.B. Seynhaeve, G.C. van Rhoon, A.B. Houtsmuller, T.L.M. ten Hagen, Externally triggered smart drug delivery system encapsulating idarubicin shows superior kinetics and enhances tumoral drug uptake and response, Theranostics. 11 (2021) 5700–5712. https://doi.org/10.7150/THNO.55163.

[13] A. Ranjan, G.C. Jacobs, D.L. Woods, A.H. Negussie, A. Partanen, P.S. Yarmolenko, C.E. Gacchina, K. V. Sharma, V. Frenkel, B.J. Wood, M.R. Dreher, Image-guided drug delivery with magnetic resonance guided high intensity focused ultrasound and temperature sensitive liposomes in a rabbit Vx2 tumor model, J. Control. Release. 158 (2012) 487–494. https://doi.org/10.1016/J.JCONREL.2011.12.011.

[14] Y. Li, P. Xu, D. He, B. Xu, J. Tu, Y. Shen, Long-Circulating Thermosensitive Liposomes for the Targeted Drug Delivery of Oxaliplatin</p>, Int. J. Nanomedicine.

15 (2020) 6721–6734. https://doi.org/10.2147/IJN.S250773.

[15] H.W. Yang, M.Y. Hua, H.L. Liu, C.Y. Huang, R.Y. Tsai, Y.J. Lu, J.Y. Chen, H.J. Tang, H.Y. Hsien, Y.S. Chang, T.C. Yen, P.Y. Chen, K.C. Wei, Self-protecting core-shell magnetic nanoparticles for targeted, traceable, long half-life delivery of BCNU to gliomas, Biomaterials. 32 (2011) 6523–6532. https://doi.org/10.1016/j.biomaterials.2011.05.047.

[16] J. Qin, I. Asempah, S. Laurent, A. Fornara, R.N. Muller, M. Muhammed, Injectable Superparamagnetic Ferrogels for Controlled Release of Hydrophobic Drugs, Adv. Mater. 21 (2009) 1354–1357. https://doi.org/10.1002/ADMA.200800764.

[17] K. Cai, Z. Luo, Y. Hu, X. Chen, Y. Liao, L. Yang, L. Deng, Magnetically Triggered Reversible Controlled Drug Delivery from Microfabricated Polymeric Multireservoir Devices, Adv. Mater. 21 (2009) 4045–4049. https://doi.org/10.1002/ADMA.200900593.

[18] T. Kubo, K. Tachibana, T. Naito, S. Mukai, K. Akiyoshi, J. Balachandran, K. Otsuka, Magnetic Field Stimuli-Sensitive Drug Release Using a Magnetic Thermal Seed Coated with Thermal-Responsive Molecularly Imprinted Polymer, ACS Biomater. Sci. Eng. 5 (2018) 759–767. https://doi.org/10.1021/ACSBIOMATERIALS.8B01401.

[19] A. Baeza, E. Guisasola, E. Ruiz-Hernández, M. Vallet-Regí, Magnetically Triggered Multidrug Release by Hybrid Mesoporous Silica Nanoparticles, Chem. Mater. 24 (2012) 517–524. https://doi.org/10.1021/cm203000u.

[20] E. Ruiz-Hernández, A. Baeza, M. Vallet-Regí, Smart Drug Delivery through DNA/Magnetic Nanoparticle Gates, ACS Nano. 5 (2011) 1259–1266. https://doi.org/10.1021/nn1029229.

[21] C.R. Thomas, D.P. Ferris, J.-H. Lee, E. Choi, M.H. Cho, E.S. Kim, J.F. Stoddart, J.-

S. Shin, J. Cheon, J.I. Zink, Noninvasive Remote-Controlled Release of Drug Molecules in Vitro Using Magnetic Actuation of Mechanized Nanoparticles, J. Am. Chem. Soc. 132 (2010) 10623–10625. https://doi.org/10.1021/JA1022267.

[22] T. Hoare, B.P. Timko, J. Santamaria, G.F. Goya, S. Irusta, S. Lau, C.F. Stefanescu, D. Lin, R. Langer, D.S. Kohane, Magnetically Triggered Nanocomposite Membranes: A Versatile Platform for Triggered Drug Release, Nano Lett. 11 (2011) 1395–1400. https://doi.org/10.1021/NL200494T.

[23] C.S. Linsley, B.M. Wu, Recent advances in light-responsive on-demand drug-delivery systems, Ther. Deliv. 8 (2017) 89. https://doi.org/10.4155/TDE-2016-0060.

[24] S.S. Agasti, A. Chompoosor, C.-C. You, P. Ghosh, C.K. Kim, V.M. Rotello, Photoregulated Release of Caged Anticancer Drugs from Gold Nanoparticles, J. Am. Chem. Soc. 131 (2009) 5728–5729. https://doi.org/10.1021/JA900591T.

[25] J. Lu, E. Choi, F. Tamanoi, J.I. Zink, Light-Activated Nanoimpeller-Controlled Drug Release in Cancer Cells, Small. 4 (2008) 421–426. https://doi.org/10.1002/SMLL.200700903.

[26] R. Tong, H.D. Hemmati, R. Langer, D.S. Kohane, Photoswitchable Nanoparticles for Triggered Tissue Penetration and Drug Delivery, J. Am. Chem. Soc. 134 (2012) 8848–8855. https://doi.org/10.1021/JA211888A.

[27] M.-C. Chen, Z.-W. Lin, M.-H. Ling, Near-Infrared Light-Activatable Microneedle System for Treating Superficial Tumors by Combination of Chemotherapy and Photothermal Therapy, ACS Nano. 10 (2015) 93–101. https://doi.org/10.1021/ACSNANO.5B05043.

[28] J. Ge, E. Neofytou, T.J. Cahill, R.E. Beygui, R.N. Zare, Drug Release from Electric-Field-Responsive Nanoparticles, ACS Nano. 6 (2011) 227–233. https://doi.org/10.1021/NN203430M.

[29] A. Puiggalí-Jou, E. Cazorla, G. Ruano, I. Babeli, M.P. Ginebra, J. Garciá-Torres, C. Alemán, Electroresponsive Alginate-Based Hydrogels for Controlled Release of Hydrophobic Drugs, ACS Biomater. Sci. Eng. 6 (2020) 6228–6240. https://doi.org/10.1021/ACSBIOMATERIALS.0C01400/SUPPL_FILE/AB0C01400_SI_001.PDF.

[30] J.S. Im, B.C. Bai, Y.S. Lee, The effect of carbon nanotubes on drug delivery in an electro-sensitive transdermal drug delivery system, Biomaterials. 31 (2010) 1414–1419. https://doi.org/10.1016/J.BIOMATERIALS.2009.11.004.

[31] K.H. Liu, T.Y. Liu, S.Y. Chen, D.M. Liu, Drug release behavior of chitosan–montmorillonite nanocomposite hydrogels following electrostimulation, Acta Biomater. 4 (2008) 1038–1045. https://doi.org/10.1016/J.ACTBIO.2008.01.012.

[32] P. Yu, H. Yu, C. Guo, Z. Cui, X. Chen, Q. Yin, P. Zhang, X. Yang, H. Cui, Y. Li, Reversal of doxorubicin resistance in breast cancer by mitochondria-targeted pH-responsive micelles, Acta Biomater. 14 (2015) 115–124. https://doi.org/10.1016/j.actbio.2014.12.001.

[33] H. Meng, M. Xue, T. Xia, Y.-L. Zhao, F. Tamanoi, J.F. Stoddart, J.I. Zink, A.E. Nel, Autonomous in Vitro Anticancer Drug Release from Mesoporous Silica Nanoparticles by pH-Sensitive Nanovalves, J. Am. Chem. Soc. 132 (2010) 12690–12697. https://doi.org/10.1021/ja104501a.

[34] R. Liu, Y. Zhang, X. Zhao, A. Agarwal, L.J. Mueller, P. Feng, pH-Responsive Nanogated Ensemble Based on Gold-Capped Mesoporous Silica through an Acid-Labile Acetal Linker, J. Am. Chem. Soc. 132 (2010) 1500–1501. https://doi.org/10.1021/ja907838s.

[35] A.F. Radovic-Moreno, T.K. Lu, V.A. Puscasu, C.J. Yoon, R. Langer, O.C. Farokhzad, Surface charge-switching polymeric nanoparticles for bacterial cell wall-targeted

delivery of antibiotics, ACS Nano. 6 (2012) 4279–4287. https://doi.org/10.1021/NN3008383/SUPPL_FILE/NN3008383_SI_001.PDF.

[36] S. Karve, A. Bandekar, M.R. Ali, S. Sofou, The pH-dependent association with cancer cells of tunable functionalized lipid vesicles with encapsulated doxorubicin for high cell-kill selectivity, Biomaterials. 31 (2010) 4409–4416. https://doi.org/10.1016/J.BIOMATERIALS.2010.01.064.

[37] A. Carovac, F. Smajlovic, D. Junuzovic, Application of Ultrasound in Medicine, Acta Inform. Medica. 19 (2011) 168. https://doi.org/10.5455/aim.2011.19.168-171.

[38] W.G. Pitt, G.A. Husseini, B.J. Staples, Ultrasonic drug delivery--a general review., Expert Opin. Drug Deliv. 1 (2004) 37–56. https://doi.org/10.1517/17425247.1.1.37.

[39] S.R. Sirsi, M.A. Borden, State-of-the-art materials for ultrasound-triggered drug delivery, Adv. Drug Deliv. Rev. 72 (2014) 3–14. https://doi.org/10.1016/J.ADDR.2013.12.010.

[40] A. Gutowska, Y.H. Bae, J. Feijen, S.W. Kim, Heparin release from thermosensitive hydrogels, J. Control. Release. 22 (1992) 95–104. https://doi.org/10.1016/0168-3659(92)90194-V.

[41] K. Ninomiya, T. Yamashita, S. Kawabata, N. Shimizu, Targeted and ultrasound-triggered drug delivery using liposomes co-modified with cancer cell-targeting aptamers and a thermosensitive polymer, Ultrason. Sonochem. 21 (2014) 1482–1488. https://doi.org/10.1016/j.ultsonch.2013.12.023.

[42] N. Sanoj Rejinold, P.R. Sreerekha, K.P. Chennazhi, S. V. Nair, R. Jayakumar, Biocompatible, biodegradable and thermo-sensitive chitosan-g-poly (N-isopropylacrylamide) nanocarrier for curcumin drug delivery, Int. J. Biol. Macromol. 49 (2011) 161–172. https://doi.org/10.1016/J.IJBIOMAC.2011.04.008.

[43] J. You, R. Zhang, C. Xiong, M. Zhong, M. Melancon, S. Gupta, A.M. Nick, A.K.

Sood, C. Li, Effective Photothermal Chemotherapy Using Doxorubicin-Loaded Gold Nanospheres That Target EphB4 Receptors in Tumors, Cancer Res. 72 (2012) 4777–4786. https://doi.org/10.1158/0008-5472.CAN-12-1003.

[44] J.L. Vivero-Escoto, I.I. Slowing, C.-W. Wu, V.S.-Y. Lin, Photoinduced Intracellular Controlled Release Drug Delivery in Human Cells by Gold-Capped Mesoporous Silica Nanosphere, J. Am. Chem. Soc. 131 (2009) 3462–3463. https://doi.org/10.1021/JA900025F.

[45] Q. Yan, J. Yuan, Z. Cai, Y. Xin, Y. Kang, Y. Yin, Voltage-responsive vesicles based on orthogonal assembly of two homopolymers, J. Am. Chem. Soc. 132 (2010) 9268–9270. https://doi.org/10.1021/JA1027502/SUPPL_FILE/JA1027502_SI_001.PDF.

[46] S.V. Ranganayakulu, Ultrasound applications in Medical Sciences, Int. J. Mod. Trends Eng. Res. 3 (2016) 287–293.

[47] T. Boissenot, A. Bordat, E. Fattal, N. Tsapis, Ultrasound-triggered drug delivery for cancer treatment using drug delivery systems: From theoretical considerations to practical applications, J. Control. Release. 241 (2016) 144–163. https://doi.org/10.1016/J.JCONREL.2016.09.026.

[48] F. Ahmadi, I. V. McLoughlin, S. Chauhan, G. Ter-Haar, Bio-effects and safety of low-intensity, low-frequency ultrasonic exposure, Prog. Biophys. Mol. Biol. 108 (2012) 119–138. https://doi.org/10.1016/j.pbiomolbio.2012.01.004.

[49] J.E. Kennedy, G.R. Ter Haar, D. Cranston, High intensity focused ultrasound: surgery of the future?, Br. J. Radiol. 76 (2003) 590–599. https://doi.org/10.1259/bjr/17150274.

[50] E. Mylonopoulou, M. Bazán-Peregrino, C.D. Arvanitis, C.C. Coussios, A non-exothermic cell-embedding tissue-mimicking material for studies of ultrasound-induced hyperthermia and drug release, Int. J. Hyperth. 29 (2013) 133–144.

https://doi.org/10.3109/02656736.2012.762553.

[51] M.A. Santos, D.E. Goertz, K. Hynynen, Focused ultrasound hyperthermia mediated drug delivery using thermosensitive liposomes and visualized with in vivo two-photon microscopy, Theranostics. 7 (2017) 2718–2731. https://doi.org/10.7150/thno.19662.

[52] P.C. Lyon, C. Mannaris, M. Gray, R. Carlisle, F. V. Gleeson, D. Cranston, F. Wu, C.C. Coussios, Large-Volume Hyperthermia for Safe and Cost-Effective Targeted Drug Delivery Using a Clinical Ultrasound-Guided Focused Ultrasound Device, Ultrasound Med. Biol. 47 (2021) 982–997. https://doi.org/10.1016/j.ultrasmedbio.2020.12.008.

[53] J.R. Tacker, R.U. Anderson, Delivery of antitumor drug to bladder cancer by use of phase transition liposomes and hyperthermia, J. Urol. 127 (1982) 1211–1214. https://doi.org/10.1016/S0022-5347(17)54299-8.

[54] J. Kost, K. Leong, R. Langer, Ultrasound-enhanced polymer degradation and release of incorporated substances., Proc. Natl. Acad. Sci. U. S. A. 86 (1989) 7663–7666. https://doi.org/10.1073/pnas.86.20.7663.

[55] H. Jiang, T. Kobayashi, Ultrasound Effect on Cellulose Decomposition in Solution and Hydrogels, 0869 (2017) 45–52.

[56] J. Sundaram, B.R. Mellein, S. Mitragotri, An experimental and theoretical analysis of ultrasound-induced permeabilization of cell membranes, Biophys. J. 84 (2003) 3087–3101. https://doi.org/10.1016/S0006-3495(03)70034-4.

[57] N. Huebsch, C.J. Kearney, X. Zhao, J. Kim, C.A. Cezar, Z. Suo, D.J. Mooney, Ultrasound-triggered disruption and self-healing of reversibly cross-linked hydrogels for drug delivery and enhanced chemotherapy, Proc. Natl. Acad. Sci. 111 (2014) 9762–9767. https://doi.org/10.1073/pnas.1405469111.

[58] S. Mitragotri, D. Blankschtein, R. Langer, Ultrasound-mediated transdermal protein delivery, Science (80-.). 269 (1995) 850–853. https://doi.org/10.1126/science.7638603.

[59] S. Mitragotri, Healing sound: The use of ultrasound in drug delivery and other therapeutic applications, Nat. Rev. Drug Discov. 4 (2005) 255–260. https://doi.org/10.1038/nrd1662.

[60] B.E. Polat, D. Blankschtein, R. Langer, Low-frequency sonophoresis: Application to the transdermal delivery of macromolecules and hydrophilic drugs, Expert Opin. Drug Deliv. 7 (2010) 1415–1432. https://doi.org/10.1517/17425247.2010.538679.

[61] W.L. Nyborg, Ultrasonic microstreaming and related phenomena, Br. J. Cancer. 45 (1982) 156–160. /pmc/articles/PMC2149335/?report=abstract (accessed June 15, 2021).

[62] P. Marmottant, S. Hilgenfeldt, Controlled vesicle deformation and lysis by single oscillating bubbles, Nature. 423 (2003) 153–156. https://doi.org/10.1038/nature01613.

[63] K.G. Baker, V.J. Robertson, F.A. Duck, A review of therapeutic ultrasound: Biophysical effects, Phys. Ther. 81 (2001) 1351–1358. https://doi.org/10.1093/ptj/81.7.1351.

[64] J.A. Rooney, Hemolysis near an ultrasonically pulsating gas bubble, Science (80-.). 169 (1970) 869–871. https://doi.org/10.1126/science.169.3948.869.

[65] M.J. Shortencarier, P.A. Dayton, S.H. Bloch, P.A. Schumann, T.O. Matsunaga, K.W. Ferrara, A method for radiation-force localized drug delivery using gas-filled lipospheres, IEEE Trans. Ultrason. Ferroelectr. Freq. Control. 51 (2004) 822–831. https://doi.org/10.1109/TUFFC.2004.1320741.

[66] P.A. Dayton, J.S. Allen, K.W. Ferrara, The magnitude of radiation force on

ultrasound contrast agents, J. Acoust. Soc. Am. 112 (2002) 2183–2192. https://doi.org/10.1121/1.1509428.

[67] K.L. Tovar-carrillo, S.S. Sueyoshi, M. Tagaya, T. Kobayashi, Fibroblast Compatibility on Scaffold Hydrogels Prepared from Agave Tequilana Weber Bagasse for Tissue Regeneration, 52 (2013) 11607–11613. https://doi.org/doi.org/10.1021/ie401793w.

[68] K. Nakasone, S. Ikematsu, T. Kobayashi, Biocompatibility Evaluation of Cellulose Hydrogel Film Regenerated from Sugar Cane Bagasse Waste and Its in Vivo Behavior in Mice, Ind. Eng. Chem. Res. 55 (2016) 30–37. https://doi.org/10.1021/acs.iecr.5b03926.

[69] H. Jiang, K. Tovar-Carrillo, T. Kobayashi, Ultrasound stimulated release of mimosa medicine from cellulose hydrogel matrix, Ultrason. Sonochem. 32 (2016) 398–406. https://doi.org/10.1016/j.ultsonch.2016.04.008.

[70] H. Jiang, T. Kobayashi, Ultrasound stimulated release of gallic acid from chitin hydrogel matrix, Mater. Sci. Eng. C. 75 (2017) 478–486. https://doi.org/10.1016/j.msec.2017.02.082.

[71] X.Z. Zhang, D.Q. Wu, C.C. Chu, Synthesis, characterization and controlled drug release of thermosensitive IPN-PNIPAAm hydrogels, Biomaterials. 25 (2004) 3793–3805. https://doi.org/10.1016/j.biomaterials.2003.10.065.

[72] L.R. Brown, E.R. Edelman, F. Fischel-Ghodsian, R. Langer, Characterization of Glucose-Mediated Insulin Release from Implantable Polymers, J. Pharm. Sci. 85 (1996) 1341–1345. https://doi.org/10.1021/js9600686.

[73] H. Hezaveh, I.I. Muhamad, Controlled drug release via minimization of burst release in pH-response kappa-carrageenan/polyvinyl alcohol hydrogels, Chem. Eng. Res. Des. 91 (2013) 508–519. https://doi.org/10.1016/j.cherd.2012.08.014.

[74] D. Verma, E. Fortunati, Biopolymer processing and its composites: An introduction, in: D. Verma, E. Fortunati, J. Siddharth, X. Zhang (Eds.), Biomass, Biopolym. Mater. Bioenergy Constr. Biomed. Other Ind. Appl., 1st ed., Elsevier, 2019: pp. 3–23. https://doi.org/10.1016/B978-0-08-102426-3.00001-1.

[75] R. Rodríguez, C. Alvarez-Lorenzo, A. Concheiro, Cationic cellulose hydrogels: Kinetics of the cross-linking process and characterization as pH-/ion-sensitive drug delivery systems, J. Control. Release. 86 (2003) 253–265. https://doi.org/10.1016/S0168-3659(02)00410-8.

[76] M.C.I. Mohd Amin, N. Ahmad, N. Halib, I. Ahmad, Synthesis and characterization of thermo- and pH-responsive bacterial cellulose/acrylic acid hydrogels for drug delivery, Carbohydr. Polym. 88 (2012) 465–473. https://doi.org/10.1016/j.carbpol.2011.12.022.

[77] S. Rejinold N, K.P. Chennazhi, H. Tamura, S. V. Nair, J. Rangasamy, Multifunctional chitin nanogels for simultaneous drug delivery, bioimaging, and biosensing, ACS Appl. Mater. Interfaces. 3 (2011) 3654–3665. https://doi.org/10.1021/am200844m.

[78] P.L. Marani, G.D. Bloisi, D.F.S. Petri, Hydroxypropylmethyl cellulose films crosslinked with citric acid for control release of nicotine, Cellulose. 22 (2015) 3907–3918. https://doi.org/10.1007/s10570-015-0757-1.

[79] M. Pandey, M.C.I. Mohd Amin, N. Ahmad, M.M. Abeer, Rapid synthesis of superabsorbent smart-swelling bacterial cellulose/acrylamide-based hydrogels for drug delivery, Int. J. Polym. Sci. 2013 (2013) 10 pages. https://doi.org/10.1155/2013/905471.

[80] S.Y. Ooi, I. Ahmad, M.C.I.M. Amin, Cellulose nanocrystals extracted from rice husks as a reinforcing material in gelatin hydrogels for use in controlled drug delivery

systems, Ind. Crops Prod. 93 (2016) 227–234. https://doi.org/10.1016/j.indcrop.2015.11.082.

[81] D. Jeong, S.W. Joo, Y. Hu, V.V. Shinde, E. Cho, S. Jung, Carboxymethyl cellulose-based superabsorbent hydrogels containing carboxymehtyl β-cyclodextrin for enhanced mechanical strength and effective drug delivery, Eur. Polym. J. 105 (2018) 17–25. https://doi.org/10.1016/j.eurpolymj.2018.05.023.

[82] C. Chang, B. Duan, J. Cai, L. Zhang, Superabsorbent hydrogels based on cellulose for smart swelling and controllable delivery, Eur. Polym. J. 46 (2010) 92–100. https://doi.org/10.1016/j.eurpolymj.2009.04.033.

[83] F.L. Mi, S.S. Shyu, Y.M. Lin, Y.B. Wu, C.K. Peng, Y.H. Tsai, Chitin/PLGA blend microspheres as a biodegradable drug delivery system: A new delivery system for protein, Biomaterials. 24 (2003) 5023–5036. https://doi.org/10.1016/S0142-9612(03)00413-7.

[84] H. Iresha, T. Kobayashi, Cellulose and Chitin Hydrogels as Drug Carriers in Ultrasound-stimulated Nicotine Release System, in: Proceeding 27th Annu. Meet. Japan Soc. Sonochemistry, The Japan Society of Sonochemistry, Tokyo, 2018: pp. 76–77.

[85] F.L. Mi, H.W. Sung, S.S. Shyu, Drug release from chitosan-alginate complex beads reinforced by a naturally occurring cross-linking agent, Carbohydr. Polym. 48 (2002) 61–72. https://doi.org/10.1016/S0144-8617(01)00212-0.

[86] I.M. El-Sherbiny, H.D.C. Smyth, Poly(ethylene glycol)-carboxymethyl chitosan-based pH-responsive hydrogels: Photo-induced synthesis, characterization, swelling, and in vitro evaluation as potential drug carriers, Carbohydr. Res. 345 (2010) 2004–2012. https://doi.org/10.1016/j.carres.2010.07.026.

[87] B.L. Guo, Q.Y. Gao, Preparation and properties of a pH/temperature-responsive

carboxymethyl chitosan/poly(N-isopropylacrylamide)semi-IPN hydrogel for oral delivery of drugs, Carbohydr. Res. 342 (2007) 2416–2422. https://doi.org/10.1016/j.carres.2007.07.007.

[88] J. Tan, H. Kang, R. Liu, D. Wang, X. Jin, Q. Li, Y. Huang, Dual-stimuli sensitive nanogels fabricated by self-association of thiolated hydroxypropyl cellulose, Polym. Chem. 2 (2011) 672–678. https://doi.org/10.1039/c0py00348d.

[89] X. Shi, Y. Zheng, G. Wang, Q. Lin, J. Fan, PH- and electro-response characteristics of bacterial cellulose nanofiber/sodium alginate hybrid hydrogels for dual controlled drug delivery, RSC Adv. 4 (2014) 47056–47065. https://doi.org/10.1039/c4ra09640a.

[90] C.J. Kearney, H. Skaat, S.M. Kennedy, J. Hu, M. Darnell, T.M. Raimondo, D.J. Mooney, Switchable Release of Entrapped Nanoparticles from Alginate Hydrogels, Adv. Healthc. Mater. 4 (2015) 1634–1639. https://doi.org/10.1002/adhm.201500254.

[91] A. López-Noriega, C.L. Hastings, B. Ozbakir, K.E. O'Donnell, F.J. O'Brien, G. Storm, W.E. Hennink, G.P. Duffy, E. Ruiz-Hernández, Hyperthermia-Induced Drug Delivery from Thermosensitive Liposomes Encapsulated in an Injectable Hydrogel for Local Chemotherapy, Adv. Healthc. Mater. 3 (2014) 854–859. https://doi.org/10.1002/adhm.201300649.

[92] F. Baghbani, M. Chegeni, F. Moztarzadeh, S. Hadian-Ghazvini, M. Raz, Novel ultrasound-responsive chitosan/perfluorohexane nanodroplets for image-guided smart delivery of an anticancer agent: Curcumin, Mater. Sci. Eng. C. 74 (2017) 186–193. https://doi.org/10.1016/j.msec.2016.11.107.

[93] L. Yan, L. Wang, S. Gao, C. Liu, Z. Zhang, A. Ma, L. Zheng, Celery cellulose hydrogel as carriers for controlled release of short-chain fatty acid by ultrasound, Food Chem. 309 (2019) 125717. https://doi.org/10.1016/j.foodchem.2019.125717.

[94] L.J. del Valle, A. Díaz, J. Puiggal, Hydrogels for Biomedical Applications: Cellulose,

Chitosan, and Protein/Peptide Derivatives, Gels. 3 (2017) 27. https://doi.org/10.3390/gels3030027.

[95] H. Chen, Biotechnology of lignocellulose: Theory and practice, in: Biotechnol. Lignocellul. Theory Pract., Chemical Industry Press, Beijing and Springer ScienceCBusiness Media Dordrecht, Beijing, 2014: pp. 1–511. https://doi.org/10.1007/978-94-007-6898-7.

[96] T. Kameda, M. Miyazawa, H. Ono, M. Yoshida, Hydrogen Bonding Structure and Stability of α-Chitin Studied by13C Solid-State NMR, Macromol. Biosci. 5 (2005) 103–106. https://doi.org/10.1002/mabi.200400142.

[97] Y. Duan, A. Freyburger, W. Kunz, C. Zollfrank, Cellulose and chitin composite materials from an ionic liquid and a green co-solvent, Carbohydr. Polym. 192 (2018) 159–165. https://doi.org/10.1016/j.carbpol.2018.03.045.

[98] T. Kobayashi, Fabrication of cellulose hydrogels and characterization of their biocompatible films, in: F. Atta-ur-Rahman (Ed.), Stud. Nat. Prod. Chem., Elsevier B.V., 2015: pp. 1–15. https://doi.org/10.1016/B978-0-444-63473-3.00001-0.

[99] M.S. Benhabiles, R. Salah, H. Lounici, N. Drouiche, M.F.A. Goosen, N. Mameri, Antibacterial activity of chitin, chitosan and its oligomers prepared from shrimp shell waste, Food Hydrocoll. 29 (2012) 48–56. https://doi.org/10.1016/J.FOODHYD.2012.02.013.

[100] K. Mariia, M. Arif, J. Shi, F. Song, Z. Chi, C. Liu, Novel chitosan-ulvan hydrogel reinforcement by cellulose nanocrystals with epidermal growth factor for enhanced wound healing: In vitro and in vivo analysis, Int. J. Biol. Macromol. 183 (2021) 435–446. https://doi.org/10.1016/j.ijbiomac.2021.04.156.

[101] K.L. Tovar-Carrillo, M. Tagaya, T. Kobayashi, Bamboo Fibers Elaborating Cellulose Hydrogel Films for Medical Applications, J. Mater. Sci. Chem. Eng. 01 (2013) 7–12.

https://doi.org/10.4236/msce.2013.17002.

[102] J. Chi, X. Zhang, C. Chen, C. Shao, Y. Zhao, Y. Wang, Antibacterial and angiogenic chitosan microneedle array patch for promoting wound healing, Bioact. Mater. 5 (2020) 253–259. https://doi.org/10.1016/j.bioactmat.2020.02.004.

[103] C. Chang, B. Duan, J. Cai, L. Zhang, Superabsorbent hydrogels based on cellulose for smart swelling and controllable delivery, Eur. Polym. J. 46 (2010) 92–100. https://doi.org/10.1016/J.EURPOLYMJ.2009.04.033.

[104] D. Ciolacu, A.M. Oprea, N. Anghel, G. Cazacu, M. Cazacu, New cellulose–lignin hydrogels and their application in controlled release of polyphenols, Mater. Sci. Eng. C. 32 (2012) 452–463. https://doi.org/10.1016/J.MSEC.2011.11.018.

[105] J. Wang, X. Zhou, H. Xiao, Structure and properties of cellulose/poly(N-isopropylacrylamide) hydrogels prepared by SIPN strategy, Carbohydr. Polym. 94 (2013) 749–754. https://doi.org/10.1016/J.CARBPOL.2013.01.036.

[106] Z. Sklenář, Z. Vitková, P. Herdová, K. Horáčková, V. Šimunková, Formulation and release of alaptide from cellulose-based hydrogels, Acta Vet. Brno. 81 (2013) 301–306. https://doi.org/10.2754/AVB201281030301.

[107] S. Dutta, P. Samanta, D. Dhara, Temperature, pH and redox responsive cellulose based hydrogels for protein delivery, Int. J. Biol. Macromol. 87 (2016) 92–100. https://doi.org/10.1016/J.IJBIOMAC.2016.02.042.

[108] N. Singh, J. Chen, K.K. Koziol, K.R. Hallam, D. Janas, A.J. Patil, A. Strachan, J.G. Hanley, S.S. Rahatekar, Chitin and carbon nanotube composites as biocompatible scaffolds for neuron growth, Nanoscale. 8 (2016) 8288–8299. https://doi.org/10.1039/C5NR06595J.

[109] A.M. Neyrinck, E. Catry, B. Taminiau, P.D. Cani, L.B. Bindels, G. Daube, C. Dessy, N.M. Delzenne, Chitin–glucan and pomegranate polyphenols improve endothelial

dysfunction, Sci. Reports 2019 91. 9 (2019) 1–12. https://doi.org/10.1038/s41598-019-50700-4.

[110] R. Izumi, K. Azuma, H. Izawa, M. Morimoto, M. Nagashima, T. Osaki, T. Tsuka, T. Imagawa, N. Ito, Y. Okamoto, H. Saimoto, S. Ifuku, Chitin nanofibrils suppress skin inflammation in atopic dermatitis-like skin lesions in NC/Nga mice, Carbohydr. Polym. 146 (2016) 320–327. https://doi.org/10.1016/J.CARBPOL.2016.03.068.

[111] S. Pirzadeh-Naeeni, M.R. Mozdianfard, S.A. Shojaosadati, A.C. Khorasani, T. Saleh, A comparative study on schizophyllan and chitin nanoparticles for ellagic acid delivery in treating breast cancer, Int. J. Biol. Macromol. 144 (2020) 380–388. https://doi.org/10.1016/J.IJBIOMAC.2019.12.079.

[112] C.-R. Jo, I.-Y. Jeong, N.-Y. Lee, K.-S. Kim, M.-W. Byun, Synthesis of a Novel Compound from Gallic Acid and Linoleic Acid and its Biological Functions -Food Science and Biotechnology | Korea Science, Food Sci. Biotechnol. 15 (2006) 317–320. https://www.koreascience.or.kr/article/JAKO200609905840956.page (accessed June 17, 2021).

[113] H. Tamura, T. Furuike, S. V. Nair, R. Jayakumar, Biomedical applications of chitin hydrogel membranes and scaffolds, Carbohydr. Polym. 84 (2011) 820–824. https://doi.org/10.1016/j.carbpol.2010.06.001.

[114] R. Narayanaswamy, V.P. Torchilin, Hydrogels and their applications in targeted drug delivery, Molecules. 24 (2019) 603. https://doi.org/10.3390/molecules24030603.

[115] V. Pérez-Luna, O. González-Reynoso, Encapsulation of Biological Agents in Hydrogels for Therapeutic Applications, Gels. 4 (2018) 61. https://doi.org/10.3390/gels4030061.

[116] P. Mohan, N. Rapoport, Doxorubicin as a molecular nanotheranostic agent: Effect of doxorubicin encapsulation in micelles or nanoemulsions on the ultrasound-mediated

intracellular delivery and nuclear trafficking, Mol. Pharm. 7 (2010) 1959–1973. https://doi.org/10.1021/mp100269f.

[117] G.A. Husseini, D.A. Christensen, N.Y. Rapoport, W.G. Pitt, Ultrasonic release of doxorubicin from Pluronic P105 micelles stabilized with an interpenetrating network of N,N-diethylacrylamide, J. Control. Release. 83 (2002) 303–305. https://doi.org/10.1016/S0168-3659(02)00203-1.

[118] G.A. Husseini, G.D. Myrup, W.G. Pitt, D.A. Christensen, N.Y. Rapoport, Factors affecting acoustically triggered release of drugs from polymeric micelles, J. Control. Release. 69 (2000) 43–52. https://doi.org/10.1016/S0168-3659(00)00278-9.

[119] A. Schroeder, R. Honen, K. Turjeman, A. Gabizon, J. Kost, Y. Barenholz, Ultrasound triggered release of cisplatin from liposomes in murine tumors, J. Control. Release. 137 (2009) 63–68. https://doi.org/10.1016/j.jconrel.2009.03.007.

[120] R.E. Vandenbroucke, I. Lentacker, J. Demeester, S.C. De Smedt, N.N. Sanders, Ultrasound assisted siRNA delivery using PEG-siPlex loaded microbubbles, J. Control. Release. 126 (2008) 265–273. https://doi.org/10.1016/j.jconrel.2007.12.001.

[121] S. Chen, J.H. Ding, R. Bekeredjian, B.Z. Yang, R. V. Shohet, S.A. Johnston, H.E. Hohmeier, C.B. Newgard, P.A. Grayburn, Efficient gene delivery to pancreatic islets with ultrasonic microbubble destruction technology, Proc. Natl. Acad. Sci. U. S. A. 103 (2006) 8469–8474. https://doi.org/10.1073/pnas.0602921103.

[122] K.Y. Lee, D.J. Mooney, Alginate: Properties and biomedical applications, Prog. Polym. Sci. 37 (2012) 106–126. https://doi.org/10.1016/j.progpolymsci.2011.06.003.

[123] S. Noguchi, K. Takaomi, Ultrasound response of viscoelastic changes of cellulose hydrogels triggered with Sono-deviced rheometer, Ultrason. Sonochem. 67 (2020) 105143. https://doi.org/10.1016/j.ultsonch.2020.105143.

Chapter 2. Ultrasound-triggered nicotine release from nicotine-loaded cellulose hydrogel

Abstract

Ultrasound (US)-triggered nicotine release system in a cellulose hydrogel drug carrier was developed with three different cellulose concentrations of 0.45 wt%, 0.9 wt%, and 1.8 wt%. The nicotine-loaded cellulose hydrogels were fabricated by the phase inversion method when the nicotine and cellulose mixture in the 6 wt% LiCl/ *N*, *N*-dimethylacetamide solvent was exposed to water vapor at room temperature. Nicotine was used as the medicine due to its revealed therapeutic potential for neurodegenerative diseases like Alzheimer's and Parkinson's diseases. The behavior of US-triggered nicotine release from nicotine-cellulose hydrogel was studied at 43 kHz US frequency at the changing US output powers of 0 W, 5 W, 10 W, 20 W, 30 W, and 40 W. The significant US-triggered nicotine release enhancement was noted for the hydrogels made with 0.9 wt% and 1.8 wt% cellulose loading. The matrix made with 0.9 wt% cellulose was exhibited the highest nicotine release at the 40 W US power, and differences in nicotine release at different US powers were noticeable than at 0.45 wt% and 1.8 wt% cellulose loadings. For the three cellulose hydrogel systems, the storage modulus (G') values at the 0.01 wt% strain rate were dropped from their initial values due to the US irradiation. This reduction was proportionately decreased when the US power was increased. The deconvolution of FTIR spectra of nicotine-loaded cellulose films before and after US exposure was suggested breakage

of cellulose-nicotine and cellulose-water in the matrix; thus, the stimulated nicotine release from the cellulose matrix was promoted by the US irradiation.

2.1 Introduction

US becomes an advanced stimulant as used in smart drug delivery systems (SDDSs) consisting of a number of state-of-the-art drug carriers [1]. The development has upgraded SDDSs as modern drug delivery systems (DDSs) due to the requirement of enhancing therapeutic efficiency by limiting drug toxicity caused by over-exposure to drugs [2,3]. Thus, the stimulation action of SDDSs is a crucial factor for designing advanced SDDSs. Therefore, researches have been expanding to identify prospective drug delivery and drug-release with some stimulants like temperature [4], light [5], magnetic field [6], pH [7], and US [8–11]. Among these stimulants, US brings advantages over the behavioral features of other SDDS, since US behaves deep penetrability, inside the body manipulation ability from outside the body, non-invasiveness, and harmlessness in addition to easy and convenient use with low cost [1,10,11]. US nebulization and imaging are some key diagnostic processes due to deep penetrability to the human body [12,13]. More interestingly, US-triggered drug release and drug transportation were induced by several physical factors like oscillatory motion of surrounded fluid, acoustic streaming, cavitation, and thermal effect [1,14]. Recent researches revealed the enhancement of drug release under US irradiation as compared to conventional diffusion release and other stimulants [8–10,15,16]. On the other hand, the combination of US and biomass hydrogel matrix containing medicine behaved interestingly as an advanced DDS.

For example, in the mimosa-cellulose hydrogel, the enhanced drug release was performed by US trigger due to the US promoted hydrogen bonding breakage between the medicine and the hydrogel matrix [8]. Similar US triggered behavior was observed for chitin-gallic acid medicine [9]. Also, the controlled dual drug release from the electrospun composite matrix was achieved due to both thermal and non-thermal effects of US [15]. Therefore, US is interested in the possibility of gene delivery to cardiac, vascular, tumor, and bone tissues, transdermal release of proteins, hormones, and medical techniques like therapeutic drug systems. For particular applications, designing a suitable drug carrier becomes another key step to develop a SDDS [17]. Currently, comprehensive attention is drawn to a wide range of drug carriers in the uses of transdermal patches [18], hydrogels [16,19,20], polymer-nanoparticle composite fibers [15], multilayered capsules [21], core-shell capsules [22], and other nanocarriers [10,11,23]. In these functional materials, some of the drug carriers were used for US drug release and DDSs. Among them, hydrogel DDSs were becoming more popular as drug carriers in drug delivery and release [8,9,16,19,24]. This was due to their less toxicity by the high-water retention in the polymer networking, high drug loading in the volumetric space, and the better affinity with the human body by water promoted soften role. Also, such a matrix had extreme biocompatibility and cytocompatibility with nontoxicity in the hydrogel [20,25]. Especially, natural polysaccharide-based hydrogels were emerging into biomedical applications. For example, agave cellulose hydrogel was reported as an excellent material for regenerative applications with fibroblast compatibility [25]. Also, cellulose hydrogels from purified

sugarcane bagasse waste were successfully tested for *in vivo* biocompatibility using mice [26]. Nevertheless, the research numbers of such biomass hydrogels as drug carriers in US-triggered DDSs are still limited. In the present study, nicotine-loaded cellulose hydrogels are highlighted for US triggering DR system. It is known that nicotine is considered as a potential therapeutic drug for Alzheimer's disease (AD) and Parkinson's disease (PD) [27,28], which are known as neurodegenerative diseases. Nicotine is a natural alkaloid and is well known as an addictive drug due to smoking. Despite such a famous application, nicotine exhibits values as a medicine. Quik et al. reviewed the protective actions of nicotine against nigrostriatal degeneration for PD [29]. The improved perception and sustained visual attention were seen for AD patients treated with nicotine [30]. Also, manganese and iron toxicities led to neurodegenerative disorders like PD, but this was completely blocked by the nicotine pretreatments [31]. However, a controlled nicotine treatment is necessary for AD and PD patients due to their extreme sensitivity to drug overdoses. Therefore, as a novel drug release system, the US-stimulated nicotine release was studied by using nicotine-entrapped hydrogel prepared with cellulose matrix. The US trigger for nicotine release is described as a prospective therapeutic application especially in neurodegenerative diseases like AD and PD. The present article includes the preparation of nicotine-loaded cellulose hydrogels and US-triggered nicotine release behavior.

2.2 Materials and Methods

2.2.1 Materials

Cotton was purchased from Kawamoto Sangyo Co., Ltd, Osaka, Japan. Lithium Chloride (LiCl), *N, N*-Dimethylacetamide (DMAc), Ethanol (EtOH), and Potassium Hydroxide (KOH) were purchased from Nacali Tesque, Inc. (Kyoto, Japan). Nicotine was a product of Tokyo Kasei Kogyo Co., Ltd. (Tokyo, Japan). Phosphate buffered Saline was purchased from Thermo Fisher Scientific Co., Ltd. (Tokyo, Japan). Cotton was dissolved in DMAc/ 6 wt% LiCl solvent to obtain the required percentages of cellulose solutions. DMAc was dried in KOH for 3 – 7 days at room temperature, and LiCl was vacuum dried for 24 h at 80 $^{\circ}$C prior to making cellulose solutions.

2.2.2 Fabrication of nicotine-loaded cellulose hydrogels

According to our previous reports, the solvent DMAc/ 6 wt% LiCl was used to dissolve cotton cellulose [8,25]. By using the cellulose solution, nicotine-cellulose hydrogels were prepared according to the procedure shown in the figure (Figure 2- 1). First, cotton was soaked in an abundant amount of distilled water for 24 h while stirring. For 1 g of cotton, 150 ml of distilled water was used. This step promotes swelling of cellulose fibers. After 24 h, swollen fibers were separated using vacuum-induced adapter glass filtration. Then, the cotton was stirred in 150 ml ethanol for 24 h and continued the same with 150 ml DMAc. After stirring with DMAc, filtered cotton was dried in a vacuum drier for 24 h to evaporate excess DMAc in cotton. Then, DMAc/ 6 wt% LiCl solvent was prepared by dissolving 6 g of dried LiCl in 93

ml of dried DMAc. The DMAc/ 6 wt% LiCl solvent and the cotton were stirred until the cotton dissolved for 1 wt% cellulose solution, at room temperature. After dissolution, the clear cellulose solution was centrifuged at 10000 rpm for 99 min to remove impurities to maintain the purity of the cellulose solution. The same procedure was applied to obtain initial cellulose solutions with 0.5 wt% and 2 wt% cellulose concentrations. Parallelly, nicotine solution with 1 wt% nicotine concentration was prepared by dissolving 95 % nicotine in DMAc/ 6 wt% LiCl solvent. After 48 h mixing of cellulose solutions with the nicotine solution in 9:1 ratio by weight, nicotine-cellulose solutions were obtained. Table 1 shows the concentration details for three samples in different cellulose concentrations of 0.45 wt%, 0.9 wt%, and 1.8 wt% in nicotine-cellulose solutions. Then, the nicotine -cellulose solutions (10 g) was poured into a glass petri dish (50 mm diameter). For the gelation of the nicotine-cellulose solutions, the dish with nicotine-cellulose solution was kept in a closed container with 20 ml of distilled water. After 24 h of phase inversion under the water vapor atmosphere at room temperature, the formed cellulose hydrogel entrapped with nicotine was seen in the dish. The hydrogels having 3.4 ± 0.3 mm thickness and 29 ± 1.5 mm diameter nicotine-cellulose hydrogels were obtained for the 0.45 wt%, 0.9 wt%, and 1.8 wt% cellulose solutions with nicotine. To remove DMAc, LiCl, and unbound nicotine, the hydrogels were washed abundantly by 20 ml × 30 times of distilled water. Table 1 lists the nicotine-cellulose hydrogels samples. There were six samples in the presence and absence of nicotine having the sample name of NC0.45, NC0.9, and NC1.8 for nicotine-loaded cellulose hydrogels and C0.45, C0.9, and C1.8 in the absence of nicotine,

with different cellulose concentration where 0.45 wt%, 0.9 wt%, and 1.8 wt% cellulose, respectively. Here, the nicotine concentration was fixed at 0.1 wt% in the former sample groups. Figure 2- 2 contains the pictures of the NC0.9 in comparison with only cellulose hydrogel of C0.9. It was appeared that the nicotine-cellulose hydrogel showed yellowish color compared to cellulose hydrogel (C0.9).

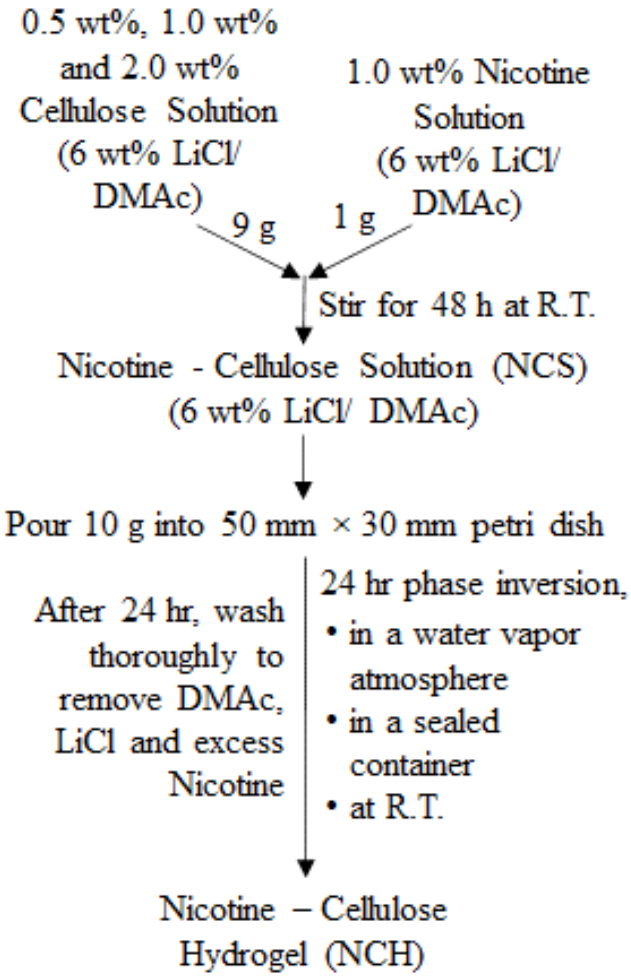

Figure 2- 1 Procedure of preparing nicotine-cellulose hydrogels

(a). (b).

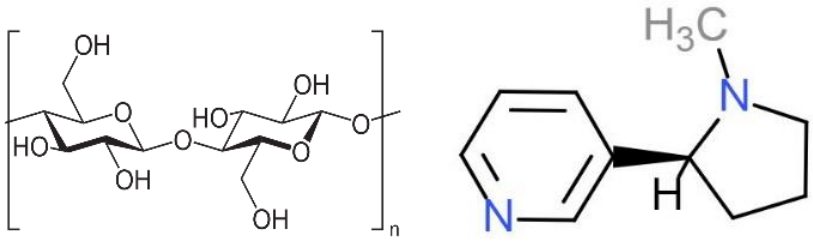

(c). (d).

Figure 2- 2 Chemical structure of **(a)** cellulose and **(b)** nicotine. Cellulose hydrogels **(c)** without and **(d)** with nicotine

2.2.3 Characterization of nicotine-cellulose hydrogels

Water contents of the prepared hydrogels were calculated using the equation $\frac{W_w - W_d}{W_d} \times 100\%$ where the W_w and W_d are the weight of the hydrogel in the wet and dry state, respectively. Before the value of W_w was measured, hydrogel surface was wiped softly. Hydrogels were dried in a vacuum drier at 80 °C for 24 h to obtain the dry weight of hydrogels. Three samples from each sample category were used to ensure its repeatability [8]. Density of the nicotine-cellulose hydrogels and cellulose hydrogels were measured using the multifunction balance (GX-200, A&D Company Limited, Japan). The densities of hydrogels were measured at 25 °C. This measurement was independently triplicated per each sample to ensure the consistency of results. To observe the cross-sections of the nicotine-cellulose hydrogels, SEM images were measured using TM3030Plus tabletop microscope (HITACHI Hight-Tech, Japan) for the freeze-dried hydrogels with gold sputtering on the cross-sections. Nicotine amounts entrapped in NC0.45, NC0.9, and NC1.8 hydrogels were measured according to a reported method with few modifications [4]. Nicotine-cellulose hydrogel was cut into small pieces and stirred with 20 ml × 3 times of distilled water for 1 h, 1 h, and 24 h consecutive stirring steps allowing trapped nicotine to release to the water medium, at 40 °C. At each stirring, water was filtered and collected together. Here the amount of trapped nicotine in the hydrogel is the nicotine amount diffused into the total 60 ml of water. The experiment was continued independently for three samples to confirm the reproducibility.

2.2.4 Experimental setup for US-triggered nicotine release from nicotine-cellulose hydrogels and the analysis of the hydrogel matrix after US exposure

The prepared hydrogels were exposed to US using the schematic experimental setup shown in Figure 2- 3. The nicotine-cellulose hydrogel was inserted into a bottle filled with 60 ml of distilled water, and then the bottle was immersed in the water-fed sonoreactor (HSR-305R, Honda Electronics Co., Ltd, Japan), 13 cm × 12.5 cm × 8 cm in size. The distance from the surface of the US transducer to the middle of the bottle was fixed at 6.5 cm, and the bottom of the bottle was adjusted in 2.5 cm from the bottom of the sonoreactor throughout the experiments. In the bottle, the nicotine-cellulose hydrogel was placed horizontally, as illustrated. The bath temperature was controlled at 25 °C using heating circular device (Lauda E100, Hansen & Co., Ltd., Japan) during the sonoreactor was running. The required US frequency and output powers were controlled with a Wave factory (15 MHz WF1943B multifunction synthesizer, NF, Japan). The generated signal amplified using high-speed bipolar amplifier (DC-1MHz/10GVA HAS 4032, NF, Japan) was finally sent via a wave homogenizer (Honda Electronics, Japan) before transducing. In the US-triggered experiments, repeatability was confirmed by triplicating the experiment in each US condition for the respective nicotine-cellulose hydrogel.

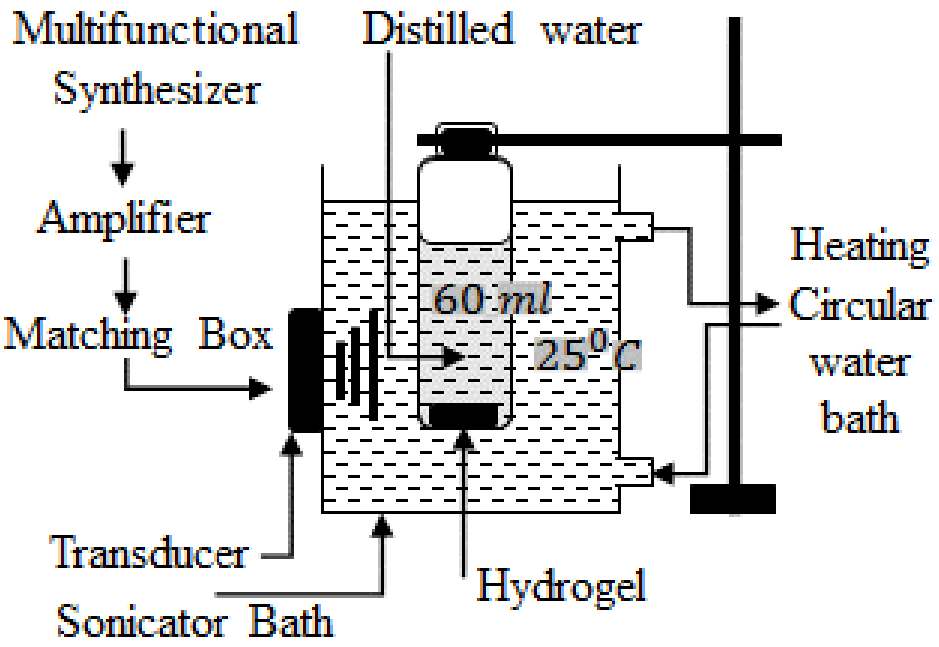

Figure 2- 3 US experimental setup

To measure the nicotine concentration in the water filled bottle in the sonoreactor, the absorption peak of the nicotine in the 60 ml of water containing the nicotine-cellulose hydrogel was determined at 260 nm wavelength by using UV/VIS/NIR spectrophotometer (Jasco V-570, UV/VIS/NIR spectrophotometer, Jasco Corporation, Japan). This absorption peak having the characteristic band for nicotine was due to the $\pi \rightarrow \pi^*$ electron transition in pyridine ring present in nicotine [32].

Nicotine release behavior from NC0.9 hydrogel was further studied under physiological environment with phosphate buffered saline (PBS) solution at 37 ˚C. The same experimental system explain above was used with 60 ml PBS solution at 37 ˚C. Here, the absorption peak of nicotine UV-Vis spectra obtained in PBS was shifted to 258 nm wavelength.

The US effect on viscoelastic behavior on the nicotine-cellulose hydrogels was analyzed using rheometer (Physica MCR 301, Anton Paar, Austria). The measurements were taken from 0.01 % - 10 % strain range at 1 Hz frequency at 25 ℃ for the storage modulus (G') and the loss modulus (G"). Further, the values of tan δ = G"/G' were recorded at each strain rate.

FT-IR analysis was carried out using the JASCO FT/IR-4100 instrument (JASCO Corporation, Japan) for the nicotine-cellulose hydrogel films before and after the US exposure. The sample films of the NC0.9 nicotine-cellulose hydrogel was used in the measurement after vacuum dried for 24 h at room temperature. The entrapment of nicotine inside the dried nicotine-cellulose hydrogel film was confirmed with the absorption peak that appeared at 260

nm in the UV-Vis spectra for the dried nicotine-cellulose hydrogel film. Then, the dried film was introduced with 2 µl distilled water drop to swell the film. The swollen film was sandwiched in between two CaF_2 plates (30 mm Ø × 2 mm) and sealed the opening at the circumference with a sealing tape (0.1 mm × 13 mm, SAN-EI, Japan). FT-IR spectra were obtained for the wavelength range of 4000 cm^{-1} – 1000 cm^{-1} and were smoothed using the Savitzky-Golay filter in the Spectra Manager 2.0 software of the FT-IR machine and baseline corrected using Origin 2018. A set of FT-IR spectra for the NC0.9 nicotine-cellulose hydrogel films with five different thicknesses were recorded without exposing to US. These spectra were used to obtain generalized two-dimensional correlation spectra (2D-CoS) of the OH-stretching region at 3000 cm^{-1} – 3700 cm^{-1}, using 2Dshige version 1.3 software (2Dshige (c) Shigeaki Morita, Kwansei-Gakuin University, Japan, 2004 – 2005). Those synchronous and asynchronous 2D maps were drawn using Origin 2018, and negative correlation intensities were shaded, while positive correlation intensities were remained unshaded. In order to identify the effect of US on the FT-IR spectra of the hydrogel film, those analyses were compared before and after the US exposure at 43 kHz/ 40 W for 60 min. FT-IR measurements were taken at the same point of the sample. With the correlation peaks identified from the 2D maps, the OH-stretching region was deconvoluted into Gaussian peaks using Fit peaks (Pro) in the Origin 2018 software. The correctness of fitted curves were ensured with the $R^2 > 0.9$.

2.3 Results and discussion

2.3.1 US-triggered nicotine release from nicotine-cellulose hydrogels

In order to investigate the US-triggered nicotine release behavior of the nicotine-cellulose hydrogels, the fabricated hydrogel was exposed to US using the experimental setup, as shown in Figure 2- 3. This disk-shaped nicotine-cellulose hydrogel can be suggested to use external to body to administrate drug via the skin. However, further development and studies are required until the final application. In the current work, possibility to use nicotine-loaded cellulose hydrogel under US-triggered drug release and the preliminary analysis is discussed extensively. The nicotine concentration in the distilled water was measured at each US exposure time by UV-Vis absorption. The figures, Figure 2- 4 (a), (b), and (c) are described for the time change in nicotine release behavior of NC0.45, NC0.9, and NC1.8, respectively. Here, at different US output powers of 5W, 10 W, 20 W, 30 W, and 40 W, the comparison was made with the nicotine release in each releasing system without US. The open symbols in their plots were relevant to the release without US. For the NC0.45 Figure 2- 4 (a), it was seen that the nicotine release behavior was almost the same at each US power and, poor release enhancement was seen when compared in the absence of US. Here, the release amount of nicotine became about 2 µg/ml at 60 min exposure in each of the cases for NC0.45. In contrast, the NC0.9 and NC1.8 were significant in the enhancement of US-triggered nicotine release, as given in Figure 2- 4 (b) and (c). Here, it is important to note that the initial nicotine contents inside the respective nicotine-cellulose hydrogels were affected for the released nicotine amount during

US exposure. As seen in Table 2- 1, the amounts of nicotine entrapped in the nicotine-cellulose hydrogels were 179 µg, 602 µg, and 537 µg for NC0.45, NC0.9, and NC1.8, respectively. These differences in the entrapped nicotine amounts in the formed hydrogels with different cellulose concentrations were due to the cellulose density and matrix structure. Here, the cellulose amounts in the hydrogel films were changed when the hydrogels were formed from 0.45 wt%, 0.9 wt%, and 1.8 wt% of cellulose in the solution. As a result, the formed hydrogel films possessed different water contents, as given in Table 2- 1. In the lower cellulose-loaded hydrogel of NC0.45, higher water was contained, while higher cellulose-loaded hydrogel (NC1.8) showed lower water content. This meant that the hydrogel film formed from lower cellulosic solutions contained loose hydrogel structure having lower cellulose density. However, higher cellulosic concentrations led to tight cellulose hydrogels in the structure, showing the degree of the entanglements of the cellulose chains formed the tight hydrogel matrix. In the SEM, the cross-section images of NC0.45, NC0.9, and NC1.8 in Figure 2- 6 had evidence of the different cellulose matrix density and structure in each hydrogel. Here, the loose hydrogel matrix was seen for NC0.45 (Figure 2- 6 (a)), while the matrix density was increased for NC1.8 as (Figure 2- 6 (g)). For the NC0.9 hydrogel in Figure 2- 6 (d), the structure showed high porosity with intermediate matrix density. Therefore, the NC0.9 and NC1.8 hydrogels were capable of more space for nicotine loading in the cellulose network in the hydrogel due to the higher cellulose density and the porosity.

Moreover, the NC0.9 showed distinguishable deviations in the amounts of nicotine released over the range of US powers used from 5 W to 40 W, compared to the NC0.45 and NC1.8 under the same conditions. More interestingly, among the three nicotine-cellulose hydrogels, the highest nicotine release of 5 µg/ml at 60 min exposure was observed for NC0.9, at 40 W. Even though the NC1.8 contained considerably high amount of nicotine inside, the responses to different US powers were not noticeable in nicotine release as shown in Figure 2- 4 (c). This might be because of the tightest hydrogel matrix of NC1.8, as shown in Figure 2- 4 (g). Out of the total nicotine content, the percentage amounts of the released nicotine at 60 min were measured for NC0.45 as 60 %, 70 %, 74 % and 80 % at 0 W, 5 W, 20 W and 40 W. Similar measurement was done for NC0.9 as 19 %, 32 %, 34 % and 50 % and for NC1.8 as 17 %, 35 %, 36 % and 41 %. When the US power was changed from 5 W to 40 W, the releasing percentage was increased. But this was comparatively narrow for the NC0.45 in 70 % - 80 % and NC1.8 in 35 % - 41 %. In fact, the US triggering effect on the nicotine releasing depended upon the hydrogel matrix. In figures, Figure 2- 6 (b), (e), and (h), the SEM images were obtained after US irradiation, showing that the shrunk structure of the matrix was caused by the US irradiation. According to figures, Figure 2- 6 (b) and (d), the NC0.45 was easily shrunk by the US irradiation because, in the SEM view, the loose matrix could be easily affected under the external US powers. Thus, the entrapped nicotine was easily released out even under small US powers like 5 W and 10 W. However, in the case of NC1.8, the hydrogel matrix was hardened more after US exposure, as given in Figure 2- 6 (h), and a tight and hard wall of the

cellulose matrix was observed at X2500 magnification. It was seen that the NC1.8 had the densest matrix in the samples, and thus the stimulation effects of US on the NC1.8 matrix limited the change in the cellulose wall in the matrix even at higher US powers like 40 W. Nevertheless, for the NC0.9, the triggering effect of US on the nicotine release was well-noticeable as seen in Figure 2- 4 (c). This was because the matrix was responded in order with the changing US powers from 5 W to 40 W. Here, after the US irradiation, the porous structure of the NC0.9 was disappeared and became laminar-structured walls as observed at higher magnification of X2500 in Figure 2- 6 (f). This was signs for the loaded nicotine in the matrix could be released in a controlled manner accordingly at different US powers due to this laminar structure. This is because such a layered structure of the matrix could easily respond to the US than the one relative to the hard thick wall like the NC1.8.

Table 2- 1 Nicotine and cellulose wt% of solutions which were used to fabricate respective hydrogels, nicotine content trapped inside the washed nicotine-cellulose hydrogels, density, and water content before and after exposure to US (40 W/ 43 kHz, 25 ^{0}C, 60 min), of prepared nicotine-cellulose hydrogels and its respective cellulose hydrogels

Sample	Cellulose and Nicotine wt% in solutions used to fabricate hydrogels		Nicotine content trapped inside the washed nicotine-cellulose hydrogels(µg)	Density of Hydrogels (g/cm^3)	Water content (%) Dry basis	
	Cellulose wt%	Nicotine wt%			Before US exposure	After US exposure
NC0.45	0.45	0.1	179±15	1.010±0.000	3075±52	2924±41
NC0.9	0.9	0.1	602±68	1.016±0.000	1971±25	1915±23
NC1.8	1.8	0.1	537±68	1.021±0.000	1329±11	1290±13
C0.45	0.45	-	-	1.006±0.001	3231±70	3093±66
C0.9	0.9	-	-	1.013±0.001	2005±65	1863±66
C1.8	1.8	-	-	1.019±0.001	1448±69	1340±79

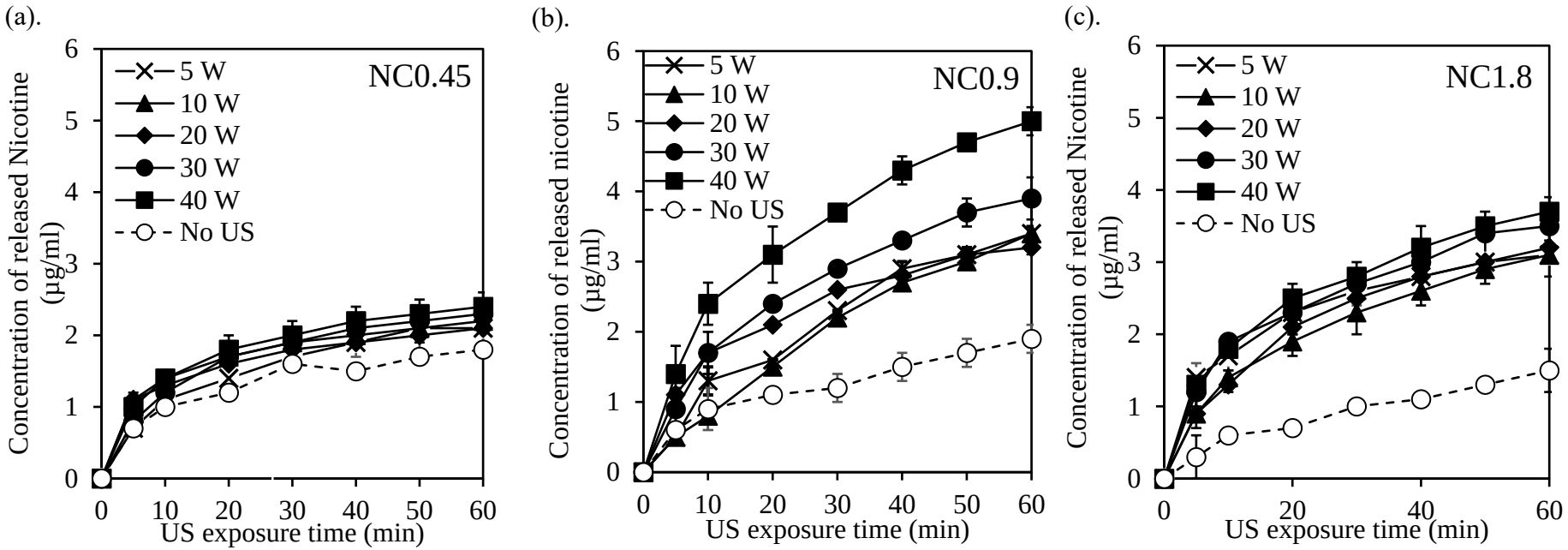

Figure 2- 4 Nicotine release behavior from nicotine-cellulose hydrogels prepared with different cellulose concentrations (a) 0.45 wt% (b) 0.9 wt% and (c) 1.8 wt%. US output powers ranged as 5 W, 10 W, 20 W, 30 W and 40 W at 43 kHz US frequency, at 25 ^{0}C, for 60 min. The US-triggered behavior was compared with the release at no US conditions in distilled water environment.

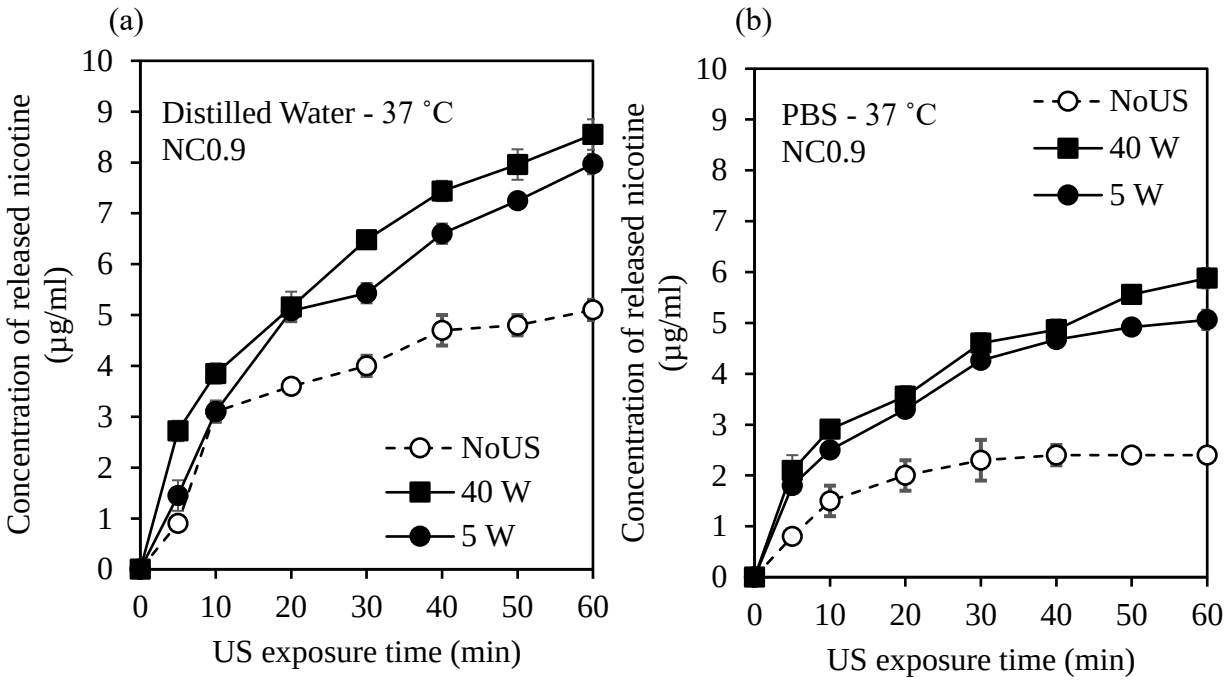

Figure 2- 5 Nicotine release behavior from NC0.9 hydrogel in (a) distilled water and (b) PBS environment at 37 ˚C. US at 43 kHz frequency and 5 W and 40 W output power for 60 min irradiation

In Figure 2- 5, results of nicotine release from NC0.9 hydrogel in physiological environment of PBS was compared with the release in distilled water at 37 ˚C. According to the results, the release of nicotine in PBS Figure 2- 5 (b) is lower compared in distilled water Figure 2- 5 (a). The reason could be the lower diffusion of nicotine in salt medium [33]. However, US was triggered the nicotine release both in distilled water and PBS while lower basal release of nicotine was shown in PBS at 37 ˚C than in distilled water. This meant that the US-triggered nicotine release is possible in the physiological environment as well. However, in both mediums, at 5 W and 40 W differences in nicotine release was not noticeable. Here, the reason could be the loosen cellulose hydrogel matrix at 37 ˚C. Due to the high temperature, the hydrogen bonds have broken thus the matrix was loosened. Further, the nicotine-cellulose interactions were also broken and thus nicotine was release easily despite the US power.

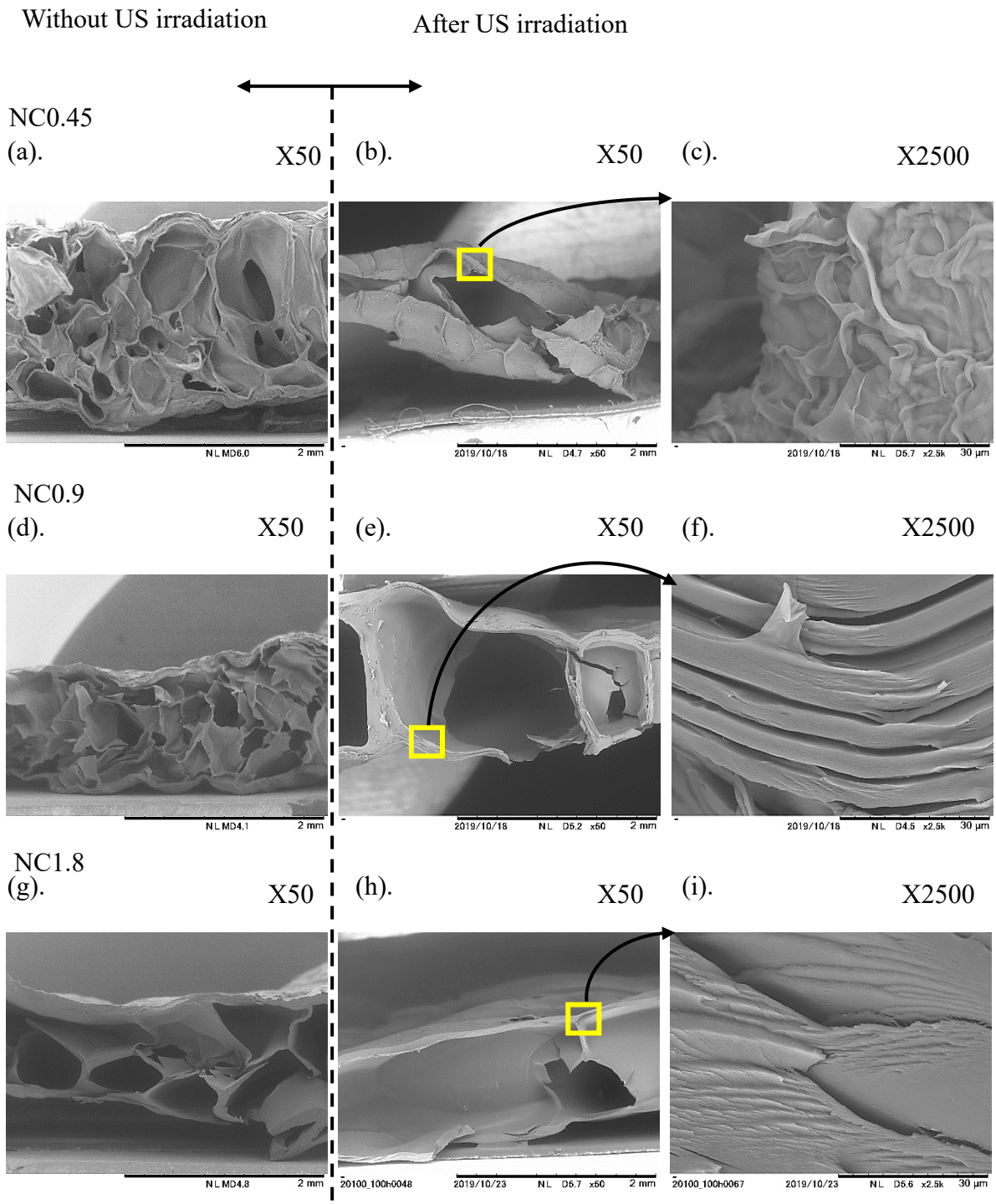

Figure 2- 6 Cross section Scanning Electron Microscopic (SEM) images of **(a), (b), (c)** NC0.45, **(d), (e), (f)** NC0.9, and **(g), (h), (i)** NC1.8 hydrogels. **(a), (d), (g)** show hydrogels before expose to US, in X50 magnification. **(b), (e), (h)** show hydrogels after exposing to US, in X50 magnification while **(c), (f), (i)** show the same hydrogels in X2500 magnifications. Hydrogels were exposed to US at 40 W/ 43 kHz, for 60 min, at 25 ^{0}C

2.3.2 Effect of US on the nicotine-cellulose matrix

The properties of the nicotine-cellulose hydrogel matrix are crucial to consider the differences in US-triggered nicotine release for each nicotine-cellulose hydrogel. The figures, Figure 2- 7 (a), (c), and (e) exhibit storage modulus (G') and loss modulus (G") of NC0.45, NC0.9, and NC1.8, respectively, before and after the US irradiation. According to the results, it was clearly visible that the G' value at 0.01 % strain rate was increased when the cellulose loading was increased from 0.45 wt% to 1.8 wt%. The reason was the loose cellulose network at lower cellulose loading, like 0.45 wt%, forming a soft hydrogel. The tight hydrogel network of the hydrogels in the 1.8 wt% cellulose makes the hydrogel stiffer (Figure 2- 6 (g)). However, the US exposure at 40 W output power for 60 min was caused to reduce the G' of the nicotine-cellulose hydrogels at 0.01 % strain. The G' values were decreased for NC0.45 from 5.9×10^4 Pa to 4.3×10^4 pa, while for the NC0.9 from 1.8×10^5 Pa to 1.3×10^5 Pa, and for NC1.8 from 3.2×10^5 Pa to 2.4×10^5 pa. This reduction of the G' values in their hydrogels meant that the US was transmitted through the nicotine-cellulose hydrogel matrix, and thus some internal hydrogen bonds between cellulose segments were broken upon the difference in the cellulose matrix. Considering the stimulated-nicotine release behavior and the reduction of water contents during the US triggering (Table 2- 1), the breakage of cellulose-nicotine and cellulose-water hydrogen bonds in the matrix might be possible by the US exposure. Furthermore, the % strain rate at $\tan\delta = G''/G' = 1$, was changed to increase from 2.5 % to 5.8 % in the NC0.45 and in NC0.9 from 1.9 % to 2.4 %, which meaning that the matrix elasticity was increased in

the US exposure. Therefore, this suggested the formation of inter and intramolecular hydrogen bonds in the cellulose network. However, the formation of cellulose hydrogen bonds reduced the elasticity for NC1.8 due to the dense structure. Thus, significant US effects on the viscoelastic properties were seen in the hydrogels. Elaborately, the effect of different US powers on the G' and G" values of NC0.9 hydrogel were plotted in Figure 2- 8 (a). For the NC0.9 hydrogel, the G' values at the 0.01 % strain rate at 0 W, 5 W, 20 W, and 40 W were 1.8 × 10^5 Pa, 1.5 × 10^5 Pa, 1.4 × 10^5 Pa, and 1.3 × 10^5 Pa, respectively. As per the results, the G' values were trending downward when the US output power was increasing. A similar tendency was observed for NC0.45 as 5.9 × 10^4 Pa, 5.3 × 10^4 Pa, 5.2 × 10^4 Pa, and 4.3 × 10^4 Pa, and for NC1.8 as 3.2 × 10^4 Pa, 3.1 × 10^4 Pa, 2.7 × 10^4 Pa, and 2.4 × 10^4 Pa, as summarized in Figure 2- 8 (b). This meant that when the US power was increasing, the release of nicotine and water from the cellulose matrix was augmented proportionately by the increased energy transfer to the hydrogel during the transmittance of US through it. Also, this stimulation function of US to the cellulose matrix was occurred irrespective of the differences in the cellulose concentrations in the three hydrogel systems.

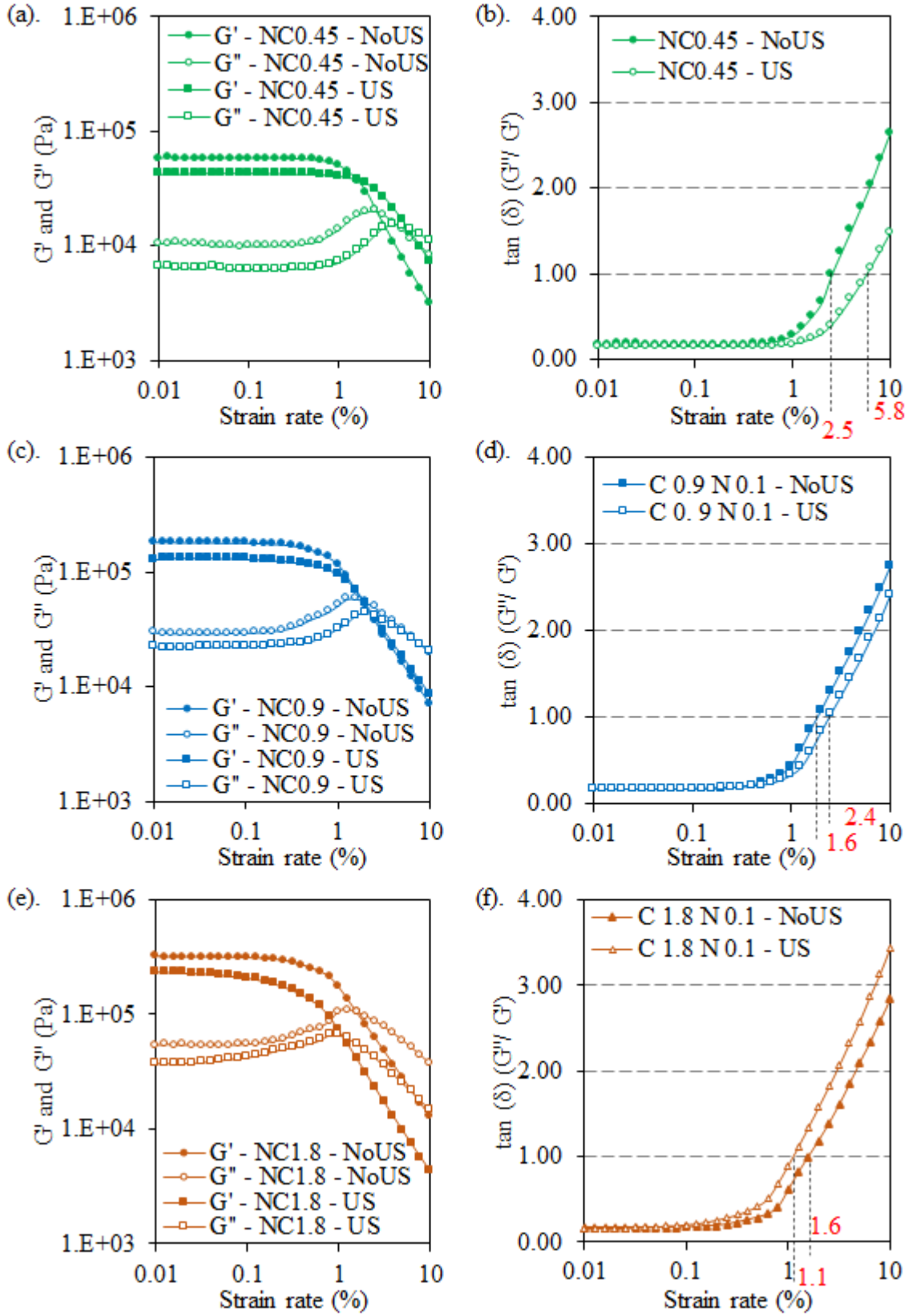

Figure 2- 7(a), (c), (e) amplitude sweep measurement of nicotine-cellulose hydrogels and (b), (d), (f) tan δ, with and without US irradiation. (a), (b) NC0.45, (c), (d) NC0.9 and (e), (f) NC1.8. US conditions were 40 W/ 43 kHz and irradiation time was 60 min, at 25 0C. The measurements were taken within 0.01 % - 10 % strain rate, at 1 Hz, at 25 0C. tan δ = G''/ G'

(a).

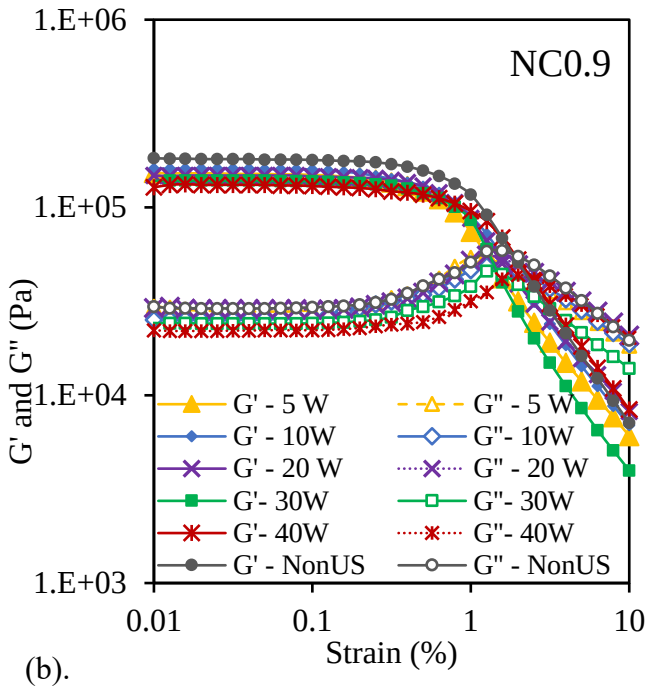

(b).

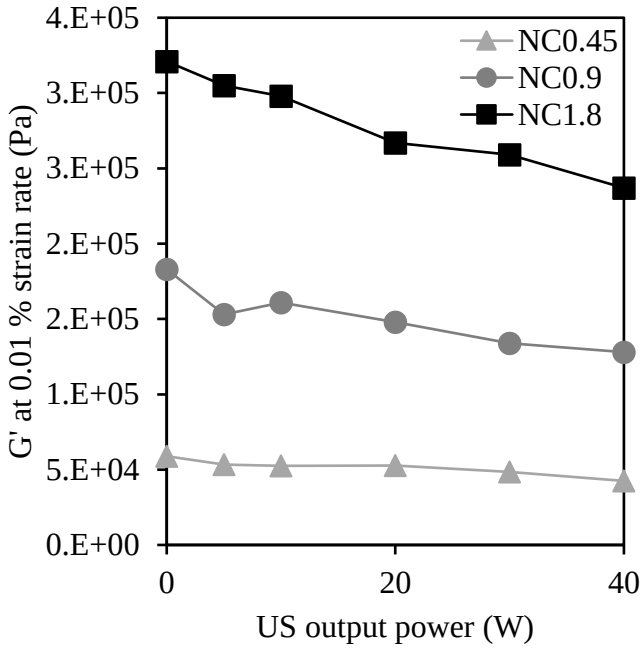

Figure 2- 8 (a) Amplitude sweep measurement of NC0.9 nicotine-cellulose hydrogels exposed to different US output powers (5 W, 10 W, 20 W, 30 W and 40 W) at 43 kHz US frequency **(b)** G' at 0.01 % strain rate for NC0.45, NC0.9 and NC1.8 nicotine-cellulose hydrogels exposed to different US output powers. US exposure time was 60 min, at 25 ^{0}C. The measurements were taken within 0.01 % - 10 % strain rate, at 1 Hz, at 25 ^{0}C

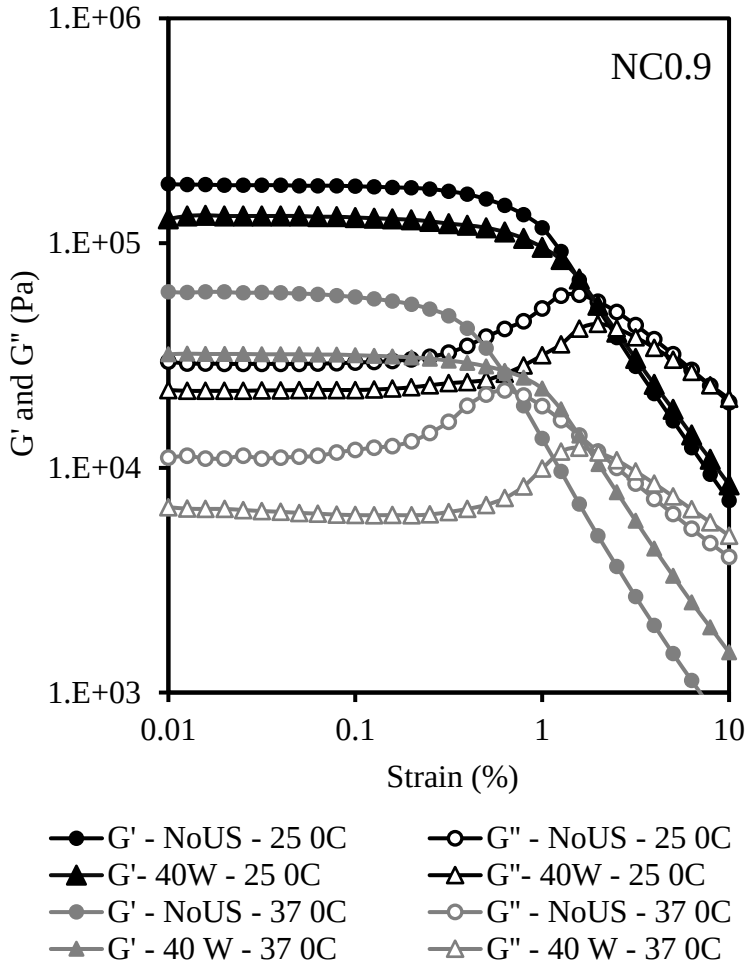

Figure 2- 9 Amplitude sweep measurement of NC0.9 hydrogels exposed to US at 05 W and 40 W at 43 kHz frequency, at 25 ˚C and 37 ˚C in distilled water. US exposure time was 60 min. The measurements were taken within 0.01 % - 10 % strain rate, at 1 Hz

However, comparing the viscoelastic properties of NC0.9 hydrogels at 25 ˚C and 37 ˚C, the G' at 0.01 % stain was 1.8×10^5 Pa and 6.1×10^4 Pa, respectively, without exposing to US (Figure 2- 9). Which means, at 37 ˚C the NC0.9 matrix has softened due to the high temperature. At 37 ˚C, the matrix strength was further decreased by the US exposure at 37 ˚C. The results suggest the matrix softening at high temperature and this behavior further confirms the enhanced drug release behavior at 37 ˚C as discussed in Figure 2- 5.

In order to investigate the hydrogen bonds in the nicotine-cellulose hydrogel films, FTIR spectra for the NC0.9 were measured in the presence and the absence of US (Figure 2- 10 (a)). Their deconvolution analysis is shown in Figure 2- 11. The baseline correction for the two spectra in Figure 2- 10 (a) was performed using base points at the same (x, y) coordinates. In the comparison, it was clearly shown an intensity reduction in the OH stretching region at 3000 cm^{-1} – 3700 cm^{-1} and in the bound water region at 1500 cm^{-1} – 1750 cm^{-1} in Figure 2- 10 (a) in the absence and presence of US. Considering the OH stretching region, the intensity reduction is possible due to both water and nicotine release out from the cellulose matrix. Prior to deconvolute the OH stretching region, the possible correlations hidden in the OH stretching region were identified using 2D-CoS obtained from 2DShige software as described[34,35]. Synchronous and asynchronous 2D-CoS are shown in Figure 2- 10 (b) and (c), respectively. In the Synchronous map, one strong auto-peak at (3407, 3407) and two cross-peaks at (3610, 3407) and (3610, 3407) have appeared. These three peaks were positive. Further, from the asynchronous map, three positive cross-peaks at (3582, 3433), (3248, 3433), and (3100, 3433),

and three negative peaks at (3433, 3582), (3433, 3248) and (3433, 3100) were recorded. Therefore, the OH stretching region of nicotine-cellulose hydrogel within 3000 cm^{-1} – 3700 cm^{-1} was identified as a combination of six peaks appeared at 3610, 3585, 3433, 3407, 3248, and 3100 cm^{-1} for the positions of hydrogen bonds.

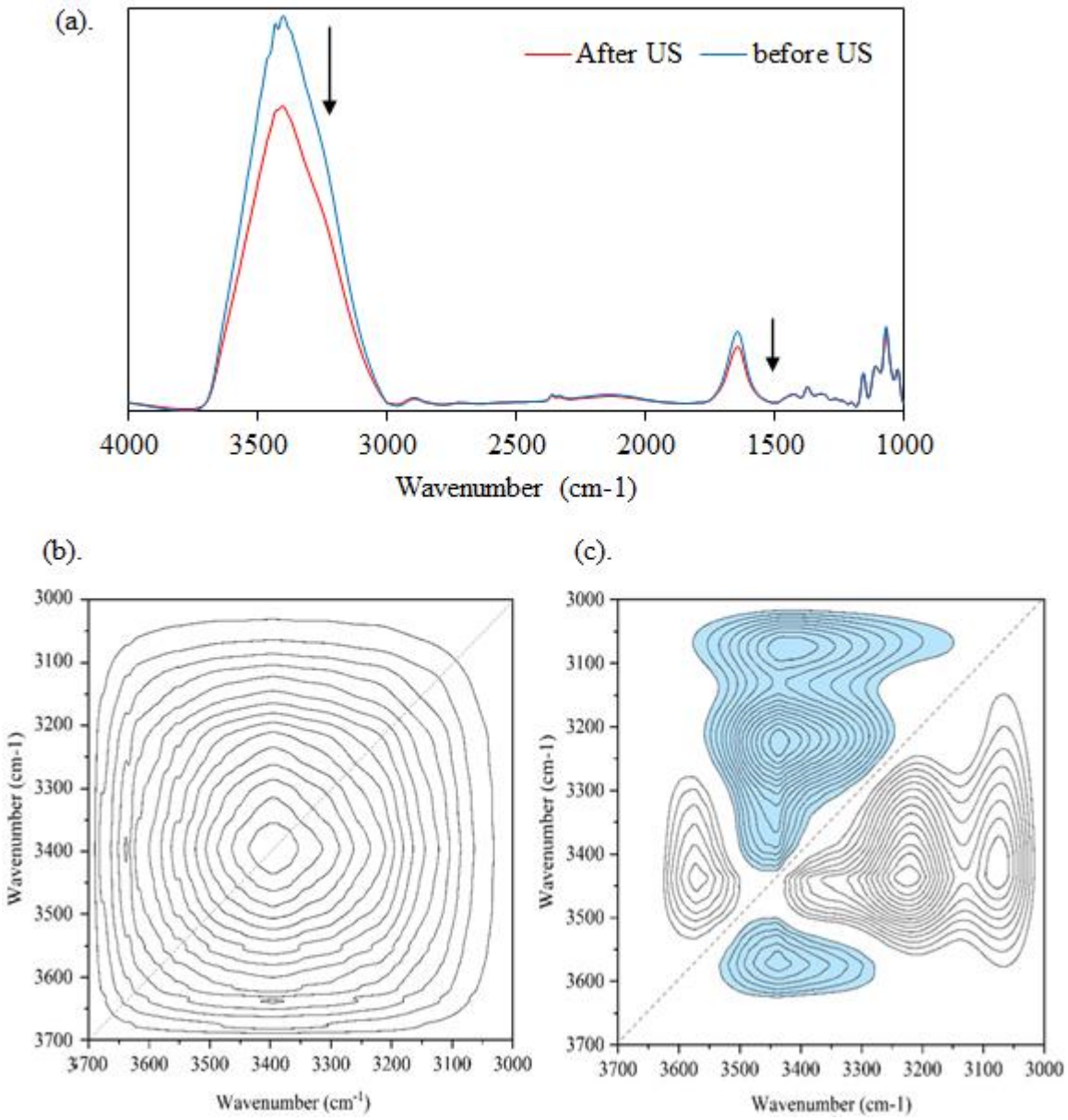

Figure 2- 10(a) FTIR spectra of NC0.9 nicotine-cellulose hydrogel film before (blue line) and after (red line) exposed to US at 40W/ 43 kHz, for 60 min at 25 ^{0}C. **(b)** Synchronous and **(c)** asynchronous two-dimensional correlation spectra obtained for the OH stretching regions at 3000 cm^{-1} - 3700 cm^{-1} of FTIR spectra of NC0.9 films

Deconvolution of the OH region of FT-IR spectra of nicotine-cellulose hydrogels was performed using Origin 2018 software according to the recent works [8,9,36]. Depending on the peaks obtained from the 2D-CoS, the OH stretching band was deconvoluted into six Gaussian peaks, and comparison was made before and after US irradiation, as shown in Figure 2- 11 (a) and (b), respectively. Here, the peak 1, 2, and 4 at 3610 cm^{-1}, 3585 $cm^{-1,}$ and 3407 cm^{-1} are assigned to free water in the matrix [37], free OH in the cellulose molecules [38,39], and OH stretching of the intermolecular hydrogen bonding of hydroxyl groups of cellulose [37,39,40], respectively. Peak 5 at 3248 cm^{-1} was assigned to cellulose-water as the cellulose -OH strongly bonded to water appears around 3200 cm^{-1} [40]. The peak 3 at 3433 cm^{-1} was assigned to cellulose-nicotine as this bond is less strong compared to cellulose-water because the –HO---H_2O is stronger than –HO---N– in nicotine. Thus, the cellulose-nicotine peak should be at a higher wavenumber than the cellulose-water peak. According to Bailey et al., at lower water concentrations, the interaction of hydrogen bond between nitrogen atom in pyridine moieties and water is higher [41]. Therefore, the nicotine-water peak was assigned as peak 6 at 3100 cm^{-1} in the shorter wavenumber end. Furthermore, the deconvolution of the FT-IR band at 1500 cm^{-1} – 1750 cm^{-1} was performed, and two hidden peaks at 1680 cm^{-1} (peak a) and 1645 cm^{-1} (peak b) were identified (Figure 2- 11 (c) and (d)). Here, peak **a** was assigned to C=N stretching of the pyridine ring [42] while peak **b** was assigned to –OH bending of bound water [43].

In the US effect on the OH stretching region, the FTIR intensities of the peaks 3 and 5 of OH region were greatly reduced after exposure to US for 60 min at 40W/ 43kHz US conditions. This meant that the US promoted breaking hydrogen bonds between cellulose-nicotine and cellulose-water, resulting in releasing nicotine and water. Water removal from the matrix was further proved by the intensity reduction of the peak **b** (Figure 2- 11 (c) and (d)). Further, the intensity of peak 4 in Figure 2- 11 (a) and (b) was increased after US irradiation, meaning the formation of intermolecular hydrogen bonds in the cellulose matrix. Collectively, the results concluded that the nicotine release behavior was stimulated by breaking hydrogen bonds of nicotine – cellulose under US irradiation.

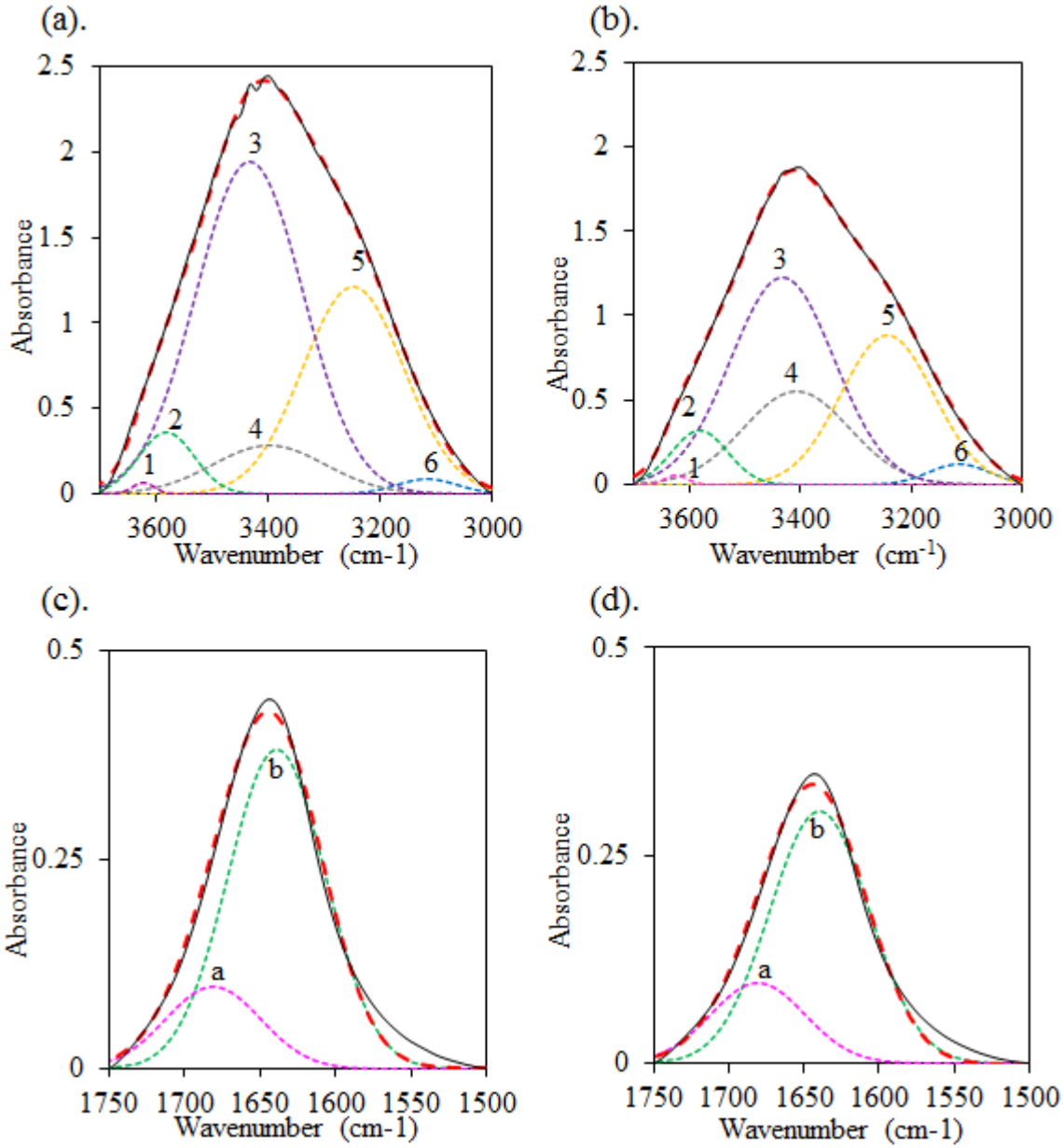

Figure 2- 11 Deconvolution of **(a), (b)** 3000 cm^{-1} – 3700 cm^{-1} and **(c), (d)** 1500 cm^{-1} – 1750 cm^{-1} regions of FTIR spectra obtained for NC0.9 films **(a), (c)** before and **(b), (d)** after expose to US at 40W/ 43 kHz at 25 ^{0}C for 60 min. The solid lines represent the original peak while dotted lines represent the fitted curves

2.4 Conclusion

In the present study, US-stimulated nicotine release behavior from nicotine-loaded cellulose hydrogel was studied. In NC0.9, the entrapment of the highest amounts of nicotine in the cellulose hydrogel due to the high porous structure and the laminar-structured wall reformation acted on the efficient nicotine releasing under US triggering. Also, the NC0.9 matrix was stimulated accordingly against US powers observed from 0 W to 40 W while the highest stimulated nicotine release efficiency was observed for NC0.9 at 40 W US power. The viscoelastic properties of the cellulose matrix were lowered by the US irradiation. The combined results of 2D-CoS and deconvolution of the FT-IR OH stretching region suggest hydrogen bond breaking of nicotine-cellulose, which leads to the stimulated nicotine release under US.

References

[1] S.R. Sirsi, M.A. Borden, State-of-the-art materials for ultrasound-triggered drug delivery, Adv. Drug Deliv. Rev. 72 (2014) 3–14. https://doi.org/10.1016/J.ADDR.2013.12.010.

[2] D. Liu, F. Yang, F. Xiong, N. Gu, The smart drug delivery system and its clinical potential, Theranostics. 6 (2016) 1306–1323. https://doi.org/10.7150/thno.14858.

[3] S. Hossen, M.K. Hossain, M.K. Basher, M.N.H. Mia, M.T. Rahman, M.J. Uddin, Smart nanocarrier-based drug delivery systems for cancer therapy and toxicity studies: A review, J. Adv. Res. 15 (2019) 1–18. https://doi.org/10.1016/J.JARE.2018.06.005.

[4] K.L. Deng, H.B. Zhong, T. Tian, Y.B. Gou, Q. Li, L.R. Dong, Drug release behavior of a pH/temperature sensitive calcium alginate/poly(N-acryloylglycine) bead with core-shelled structure, Express Polym. Lett. 4 (2010) 773–780. https://doi.org/10.3144/expresspolymlett.2010.93.

[5] Q. Feng, Y. Zhang, W. Zhang, Y. Hao, Y. Wang, H. Zhang, L. Hou, Z. Zhang, Programmed near-infrared light-responsive drug delivery system for combined magnetic tumor-targeting magnetic resonance imaging and chemo-phototherapy, Acta Biomater. 49 (2017) 402–413. https://doi.org/10.1016/j.actbio.2016.11.035.

[6] A. Baeza, E. Guisasola, E. Ruiz-Hernández, M. Vallet-Regí, Magnetically Triggered Multidrug Release by Hybrid Mesoporous Silica Nanoparticles, Chem. Mater. 24 (2012) 517–524. https://doi.org/10.1021/cm203000u.

[7] H. Hezaveh, I.I. Muhamad, Controlled drug release via minimization of burst release in pH-response kappa-carrageenan/polyvinyl alcohol hydrogels, Chem. Eng. Res. Des. 91 (2013) 508–519. https://doi.org/10.1016/j.cherd.2012.08.014.

[8] H. Jiang, K. Tovar-Carrillo, T. Kobayashi, Ultrasound stimulated release of mimosa medicine from cellulose hydrogel matrix, Ultrason. Sonochem. 32 (2016) 398–406.

https://doi.org/10.1016/j.ultsonch.2016.04.008.

[9] H. Jiang, T. Kobayashi, Ultrasound stimulated release of gallic acid from chitin hydrogel matrix, Mater. Sci. Eng. C. 75 (2017) 478–486. https://doi.org/10.1016/j.msec.2017.02.082.

[10] W. Chen, J. Du, Ultrasound and pH dually responsive polymer vesicles for anticancer drug delivery, Sci. Rep. 3 (2013) 1–9. https://doi.org/10.1038/srep02162.

[11] J.L. Paris, M.V. Cabañas, M. Manzano, M. Vallet-Regí, Polymer-Grafted Mesoporous Silica Nanoparticles as Ultrasound-Responsive Drug Carriers, ACS Nano. 9 (2015) 11023–11033. https://doi.org/10.1021/acsnano.5b04378.

[12] Z. Zhou, W. Fan, M. Lang, Y. Wang, Transdermal bFGF delivery using low-frequency sonophoresis: An innovative potential therapy for osteoradionecrosis of jaws, J. Med. Hypotheses Ideas. 9 (2015) 9–12. https://doi.org/10.1016/j.jmhi.2014.07.001.

[13] C.M. Panje, D.S. Wang, M.A. Pysz, R. Paulmurugan, Y. Ren, F. Tranquart, L. Tian, J.K. Willmann, Ultrasound-mediated gene delivery with cationic versus neutral microbubbles: Effect of DNA and microbubble dose on In Vivo transfection efficiency, Theranostics. 2 (2012) 1078–1091. https://doi.org/10.7150/thno.4240.

[14] W.G. Pitt, G.A. Husseini, B.J. Staples, Ultrasonic drug delivery--a general review., Expert Opin. Drug Deliv. 1 (2004) 37–56. https://doi.org/10.1517/17425247.1.1.37.

[15] B. Song, C. Wu, J. Chang, Ultrasound-triggered dual-drug release from poly(lactic-co-glycolic acid)/mesoporous silica nanoparticles electrospun composite fibers, Regen. Biomater. 2 (2015) 229–237. https://doi.org/10.1093/rb/rbv019.

[16] N. Huebsch, C.J. Kearney, X. Zhao, J. Kim, C.A. Cezar, Z. Suo, D.J. Mooney, Ultrasound-triggered disruption and self-healing of reversibly cross-linked hydrogels for drug delivery and enhanced chemotherapy, Proc. Natl. Acad. Sci. 111 (2014) 9762–9767. https://doi.org/10.1073/pnas.1405469111.

[17] K. Park, Controlled drug delivery systems: Past forward and future back, J. Control. Release. 190 (2014) 3–8. https://doi.org/10.1016/j.jconrel.2014.03.054.

[18] B.E. Polat, D. Hart, R. Langer, D. Blankschtein, Ultrasound-Mediated Transdermal Drug Delivery: Mechanisms, Scope, and Emerging Trends, J. Control. Release. 152 (2011) 330–348. https://doi.org/10.1016/j.jconrel.2011.01.006.

[19] F. Camponeschi, A. Atrei, G. Rocchigiani, L. Mencuccini, M. Uva, R. Barbucci, New Formulations of Polysaccharide-Based Hydrogels for Drug Release and Tissue Engineering, Gels. 1 (2015) 3–23. https://doi.org/10.3390/gels1010003.

[20] T.R. Hoare, D.S. Kohane, Hydrogels in drug delivery: Progress and challenges, Polymer (Guildf). 49 (2008) 1993–2007. https://doi.org/10.1016/j.polymer.2008.01.027.

[21] B.G. De Geest, A.G. Skirtach, A.A. Mamedov, A.A. Antipov, N.A. Kotov, S.C. De Smedt, G.B. Sukhorukov, Ultrasound-triggered release from multilayered capsules, Small. 3 (2007) 804–808. https://doi.org/10.1002/smll.200600441.

[22] Y. Jing, Y. Zhu, X. Yang, J. Shen, C. Li, Ultrasound-triggered smart drug release from multifunctional core-shell capsules one-step fabricated by coaxial electrospray method, Langmuir. 27 (2011) 1175–1180. https://doi.org/10.1021/la1042734.

[23] I. Lentacker, B. Geers, J. Demeester, S.C. De Smedt, N.N. Sanders, Design and Evaluation of Doxorubicin-containing Microbubbles for Ultrasound-triggered Doxorubicin Delivery: Cytotoxicity and Mechanisms Involved, Mol. Ther. 18 (2010) 101–108. https://doi.org/10.1038/MT.2009.160.

[24] H. Epstein-Barash, G. Orbey, B.E. Polat, R.H. Ewoldt, J. Feshitan, R. Langer, M.A. Borden, D.S. Kohane, A microcomposite hydrogel for repeated on-demand ultrasound-triggered drug delivery, Biomaterials. 31 (2010) 5208–5217. https://doi.org/10.1016/j.biomaterials.2010.03.008.

[25] K.L. Tovar-carrillo, S.S. Sueyoshi, M. Tagaya, T. Kobayashi, Fibroblast Compatibility

on Scaffold Hydrogels Prepared from Agave Tequilana Weber Bagasse for Tissue Regeneration, 52 (2013) 11607–11613. https://doi.org/doi.org/10.1021/ie401793w.

[26] K. Nakasone, S. Ikematsu, T. Kobayashi, Biocompatibility Evaluation of Cellulose Hydrogel Film Regenerated from Sugar Cane Bagasse Waste and Its in Vivo Behavior in Mice, Ind. Eng. Chem. Res. 55 (2016) 30–37. https://doi.org/10.1021/acs.iecr.5b03926.

[27] M. Quik, X.A. Perez, T. Bordia, Nicotine as a potential neuroprotective agent for Parkinson's disease, Mov. Disord. 27 (2012) 947–957. https://doi.org/10.1002/mds.25028.

[28] L.I. Golbe, M.H. Mark, J.I. Sage, Parkinson ' s Disease Handbook, 2010.

[29] M. Quik, M. O'Neill, X.A. Perez, Nicotine neuroprotection against nigrostriatal damage: importance of the animal model, Trends Pharmacol. Sci. 28 (2007) 229–235. https://doi.org/10.1016/j.tips.2007.03.001.

[30] G.M.M. Jones, B.J. Sahakian, R. Levy, D.M. Warburton, J.A. Gray, Effects of acute subcutaneous nicotine on attention, information processing and short-term memory in alzheimer's disease, Psychopharmacology (Berl). 108 (1992) 485–494. https://doi.org/10.1007/BF02247426.

[31] B. Getachew, A.B. Csoka, M. Aschner, Y. Tizabi, Nicotine protects against manganese and iron-induced toxicity in SH-SY5Y cells: Implication for Parkinson's disease, Neurochem. Int. 124 (2019) 19–24. https://doi.org/10.1016/j.neuint.2018.12.003.

[32] P.M. Clayton, C.A. Vas, T.T.T. Bui, A.F. Drake, K. McAdam, Spectroscopic studies on nicotine and nornicotine in the UV region, Chirality. 25 (2013) 288–293. https://doi.org/10.1002/chir.22141.

[33] C.-Y. Chen, K.D. Papadopoulos, Temperature and Salting out Effects on Nicotine Dissolution Kinetics in Saline Solutions, ACS Omega. 5 (2020) 7738–7744.

https://doi.org/10.1021/ACSOMEGA.9B02836.

[34] I. Noda, Generalized two-dimensional correlation method applicable to infrared, Raman, and other types of spectroscopy, Appl. Spectrosc. 47 (1993) 1329–1336. https://doi.org/10.1366/0003702934067694.

[35] I. Noda, A.E. Dowrey, C. Marcott, G.M. Story, Y. Ozaki, focal point, Appl. Spectrosc. 54 (2000) 236A-248A.

[36] V.J. Addiel, T. Motohiro, K. Takaomi, Ultrasonics Sonochemistry Ultrasound stimulus inducing change in hydrogen bonded crosslinking of aqueous polyvinyl alcohols, Ultrason. Sonochem. 21 (2014) 295–309. https://doi.org/10.1016/j.ultsonch.2013.06.011.

[37] Y. Guo, P. Wu, Investigation of the hydrogen-bond structure of cellulose diacetate by two-dimensional infrared correlation spectroscopy, Carbohydr. Polym. 74 (2008) 509–513. https://doi.org/10.1016/J.CARBPOL.2008.04.005.

[38] B. Hinterstoisser, L. Salmén, Application of dynamic 2D FTIR to cellulose, Vib. Spectrosc. 22 (2000) 111–118. https://doi.org/10.1016/S0924-2031(99)00063-6.

[39] T. Kondo, The assignment of IR absorption bands due to free hydroxyl groups in cellulose, Cellulose. 4 (1997) 281–292. https://doi.org/10.1023/A:1018448109214.

[40] J.J. Shephard, P.J. Bremer, A. James McQuillan, Structure and conformation in mixtures of methyl-terminated poly(ethylene oxide) and water. principal component analysis and band fitting of infrared absorptions, J. Phys. Chem. B. 113 (2009) 14229–14238. https://doi.org/10.1021/jp905149z.

[41] H.E. Bailey, Y.-L. Wang, S.R. Lynch, M.D. Fayer, Dynamics and Microstructures of Nicotine/Water Binary Mixtures near the Lower Critical Solution Temperature, J. Phys. Chem. B. 122 (2018) 9538–9548. https://doi.org/10.1021/acs.jpcb.8b06205.

[42] S.M. Melikova, K.S. Rutkowski, A.A. Gurinov, G.S. Denisov, M. Rospenk, I.G.

Shenderovich, FTIR study of the hydrogen bond symmetry in protonated homodimers of pyridine and collidine in solution, J. Mol. Struct. 1018 (2012) 39–44. https://doi.org/10.1016/j.molstruc.2011.12.027.

[43] S.Y. Oh, D. Il Yoo, Y. Shin, G. Seo, FTIR analysis of cellulose treated with sodium hydroxide and carbon dioxide, Carbohydr. Res. 340 (2005) 417–428. https://doi.org/10.1016/j.carres.2004.11.027.

Chapter 3. *In-situ* Viscoelasticity Behavior of Cellulose-Chitin Composite Hydrogels During Ultrasound Irradiation

Part 1

Abstract

Composite hydrogels with different cellulose and chitin loading were prepared, and *in-situ* viscoelastic properties of the composite hydrogels were estimated under cyclic exposure of 43 kHz and 30 W ultrasound (US) using the sono-deviced rheometer. US transmitted into the hydrogel caused it softening within about 10 sec, thus declining G' and G'' of the hydrogels. However, when the US was stopped, the G' and G'' returned to the initial value. Here, G' behaved at the US irradiation gradually against time, especially in the first cycle. After the second and third US cycles, the G' declining was occurred much quickly within few seconds. When the chitin component increased in the hydrogel, the G' dropping was significant during the US cycles. FTIR analysis of the hydrogels suggested that the peaks of -OH stretching and the amide I vibration near 1655 cm^{-1} were shifted towards lower wavenumbers after the third US cycle, meaning that the US influenced the hydrogen bonding interaction of the amide group of chitin. This repetitive US effect contributed to the breakage of hydrogen bonds and increased interactions of the acetylamine group in chitin and in -OH groups. Thus, eventually, the matrix was turned into a more stabilized hydrogel.

3.1 Introduction

Cellulose and chitin are gaining attention as biocompatible polymer materials in medicine. They show superior properties which are favorable for such applications, especially in the form of hydrogels. By their nature, cellulose and chitin hydrogels have higher water retention [1,2] in a three-dimensional porous structure [3,4], formed by the cellulose or chitin network [5,6]. Moreover, biocompatibility [7] and cytocompatibility [8] of such polysaccharide hydrogels are advantageous for tissue engineering scaffolds [8] and drug carriers [9,10]. More recently, cellulose [11] and chitin [12] hydrogel drug carriers were used as regenerative medicine hydrogels, which exhibited the controllable drug release under US stimulation. Here, mimosa release from cellulose hydrogel and gallic acid release from chitin hydrogel was triggered due to the US promoted breakage of hydrogen bonds between the drug and the polysaccharide matrix. This meant that the US well stimulated the hydrogen-bonding networks of both hydrogels.

Recently, the cellulose hydrogels were tested for the US-triggered viscoelastic behavior by using *in-situ* sono-deviced rheometer [13]. During the analysis for evaluating viscoelastic properties, it was noted that US irradiation caused the cellulose hydrogel matrix to soften. After stopping the US, the hydrogels returned to their original viscoelastic conditions. This softening of hydrogels during US exposure will be helpful in applications like US drug delivery [14]. In addition, similar effects on the viscosity properties of US-combined aqueous polymeric systems were reported based on ex situ measurements[15–17]. However, an *in-situ* analysis of

the viscoelastic behavior of the cellulose hydrogels revealed direct US-based effects on hydrogen-bonding networks in the polymeric matrix [13]. Compared to cellulose hydrogels alone, these two polysaccharides have the possibility of forming extended, strong inter- intra-molecular hydrogen bonds in a composite cellulose–chitin polymer framework [18–21]. Even though materials developed from cellulose and chitin are composed on many inorganic and natural materials [22–25], materials from cellulose and chitin composite have a limited research history. Thus, in the present work, cellulose chitin-composite hydrogels (CCCHs) were fabricated and the US effect on their viscoelastic properties was described, based on an in-situ analysis using a sono-deviced rheometer.

3.2 Materials and Methods

3.2.1 Materials

Defatted cotton was a product of Kawamoto Sangyo Co., Ltd, Osaka, Japan, and was used as the cellulose source without further chemical treatment. According to our previous study, chitin was extracted from the crab shells obtained from the Teradomari fish market, Nagaoka, Niigata, and purified according to our previous study [12]. For the demineralization of crab shells, hydrochloric acid (HCl) was used. Then, the deproteinization of chitin was performed from sodium hydroxide (NaOH), and the decolorization of the extracted chitin was done using ethanol (EtOH). HCl, NaOH, EtOH, Lithium Chloride (LiCl), *N*, *N*-Dimethylacetamide (DMAc), and Potassium Hydroxide (KOH) were purchased from Nacali Tesque, Inc. (Kyoto, Japan). Cotton was dissolved in DMAc/ 6 wt% LiCl solvent to obtain 1 wt% of cellulose solutions. DMAc was dried in KOH for 3 days at room temperature, and LiCl was vacuum dried for 24 h at 80 °C before the preparation of cellulose or chitin solutions.

3.2.2 Extraction of chitin from crab shells

Chitin was extracted according to the former reports available [12]. The dried and crushed crab shells were stored in the freezer to maintain their original status. First, 30 g of raw crab shells were stirred with 900 ml of 1 N HCl for 24 h as the demineralization step. Then, the treated crab shells were filtered using a metal mesh and washed using distilled water till the pH become 7. Next, demineralized crab shells were treated with 900 ml of 1 N NaOH for 5 h at 90 °C for deproteinization. Again, the treated crab shells were washed until neutral pH. Next,

the sample was undergone the decolorization step by stirring with an excess of EtOH at 60 °C for 5 h. Finally, the obtained chitin was vacuum dried at room temperature (R.T). for 24 h before making chitin solutions.

3.2.3 Fabrication of cellulose-chitin composite hydrogels

According to the fabrication procedure of composite hydrogels, cotton and chitin were first dissolved individually in the 6 wt% LiCl/ DMAc solvents of each cellulose or chitin solution with 1 wt% concentration, according to our previous works [6,8]. First, 1 g of cellulose/ chitin was undergone three solvent exchange steps stirring in 150 ml of distilled water, EtOH, and DMAc, for 24 h in each solvent. After the solvent exchange steps, the cellulose or chitin was vacuum dried for 24 h at 25 ˚C. Meanwhile, the 6 wt% LiCl/ DMAc solvent was prepared by dissolving 6 g of dried LiCl in 93 ml of dried DMAc. Then, the vacuum-dried cellulose or chitin was fed into the prepared 6 wt% LiCl in DMAc solvent. This was stirred until completely dissolved to obtain a clear solution. Once the dissolution was completed for the cellulose or chitin solution, the solutions were centrifuged at 10000 rpm to remove undissolved cellulose or chitin and other impurities.

For the composite hydrogels, the cellulose and chitin solutions were mixed by stirring for 48 h at R.T. As listed in Table 1, the weight ratios of cellulose (C) and chitin (Ch) were changed as 0.7/ 0.2, 0.45/0.45, and 0.2/ 0.7 in 0.1 parts of LiCl/ DMAc solutions for C0.7Ch0.2, C0.45Ch0.45 and C0.2Ch0.7 samples, respectively. Using those mixed solutions, three kinds of composite hydrogels of C and Ch were prepared as follows. First, 10 g from the cellulose-

chitin mixture was poured into a petri dish with 50 mm diameter and kept in a sealed container carrying a water vapor atmosphere at 25 ˚C for 24 h. During the 24 h period, the gelation process was occurred, and thus the cellulose-chitin composite hydrogel was formed due to the phase inversion [1,21]. Then the formed hydrogels were washed well using 20 ml × 30 times of distilled water to remove LiCl and DMAc.

The water contents of the prepared hydrogels were evaluated by the equation $((W_w - W_d)/W_d) \times 100$ %, where the W_w and W_d are the wet and the dry weight of the hydrogel, respectively. Here, the W_w was measured for the hydrogels immediately after the washing process was completed. Before the W_w measurements, the hydrogels were carefully patted by a Kim wiper to wipe the surrounded water on the hydrogel surfaces. The W_d was measured after vacuum drying the hydrogels at 80 °C for 24 h. The experiments were triplicated for each sample to assure the consistency of the results. Further, the densities of the hydrogels were also measured using the multifunctional balance (GX-200, A&D Company Limited, Japan) at 25 ˚C and measured three times for each sample. The viscosity of the solutions was measured using the rheometer Physica MCR 301 (Anton Paar Japan, Tokyo) at 25 ˚C.

Table 3- 1 Composition of the cellulose-chitin solution (CCS) mixture used to prepare respective cellulose-chitin composite hydrogels (CCCHs)

Sample Name	Composition of CCSs used to fabricate CCCHs		
	1 wt% Cellulose (wt%)	1 wt% Chitin (wt%)	6 wt% LiCl/ DMAc (wt%)
C0.9	0.9	0	0.1
C0.7Ch0.2	0.7	0.2	0.1
C0.45Ch0.45	0.45	0.45	0.1
C0.2Ch0.7	0.2	0.7	0.1
Ch0.9	0	0.9	0.1

FTIR analysis was performed for the vacuum dried composite hydrogel thin films using the JASCO FTIR-4100 instrument (JASCO Corporation, Japan). The hydrogel film was swollen with a 2 µl of distilled water drop and then sandwiched between two clean CaF_2 plates (30 mm Ø × 2 mm). The opening was well sealed using a sealing tape (0.1 mm × 13 mm, SAN-EI, Japan). The FTIR spectra were recorded for the hydrogel films before starting the US irradiation, and after three 5 min, US cycles with 5 min NoUS intervals.

3.2.4 In-situ viscoelastic measurements using the sono-devised rheometer

Schematic diagram of the sono-devised rheometer used is shown in Figure 3- 1. The rheometer Physica MCR 301 (Anton Paar Japan, Tokyo) was used to modify the sample platform on the bottom with Langevin-type HEC-45242 M transducer (Honda electronics Co. Ltd., Japan), where the transducer was located vertically upwards. The signal generated via the wave factory (15 MHz WF1943B multifunction synthesizer, NF, Japan) was amplified by the high-speed bipolar amplifier (DC-1MHz/10GVA HAS 4032, NF, Japan). Then, the signal was sent through the wave homogenizer (Honda Electronics, Japan) and finally transduced to the

transducer equipped with a circulating water bath (86 mm diameter × 65 mm height). Here, the bottom of the water bath was covered by the SUS 316 plate (0.2 mm thickness) and hinged well onto the top surface of the transducer. The hydrogel sample was put on the US 316 plate during the *in-situ* viscoelasticity measurement. To ensure the wetting of the hydrogel and to ease the US transmission to the sample, 5 ml of distilled water was poured onto the sample plate. Water circulation caused entirely fill the water bath without any voids, and thus the US transmission was not interrupted. Water flow in the water bath was maintained to flow due to keeping the bath temperature controlled at 25 °C. The transduced US wave was passed through the water medium and transmitted via the SUS plate and then through the sample. Deformations were not noticed on the SUS plate due to the US transmittance. US was operated at a constant US frequency of 43 kHz and constant 30 W output power. The viscoelasticity measurement for the cellulose-chitin composite hydrogels was carried out using the parallel plate 25 (PP25) measuring system, at the constant 1 % strain rate and 1 Hz oscillatory frequency during the US operation. The US irradiation was cycled with 5 min intervals without and with the exposure to US written for NoUS and US, respectively. The *in-situ* measurements of the storage modulus (G') and the loss modulus (G'') were recorded with time during the cycling US operation per each hydrogel with an average diameter of 25 mm and 2.5 mm average thickness.

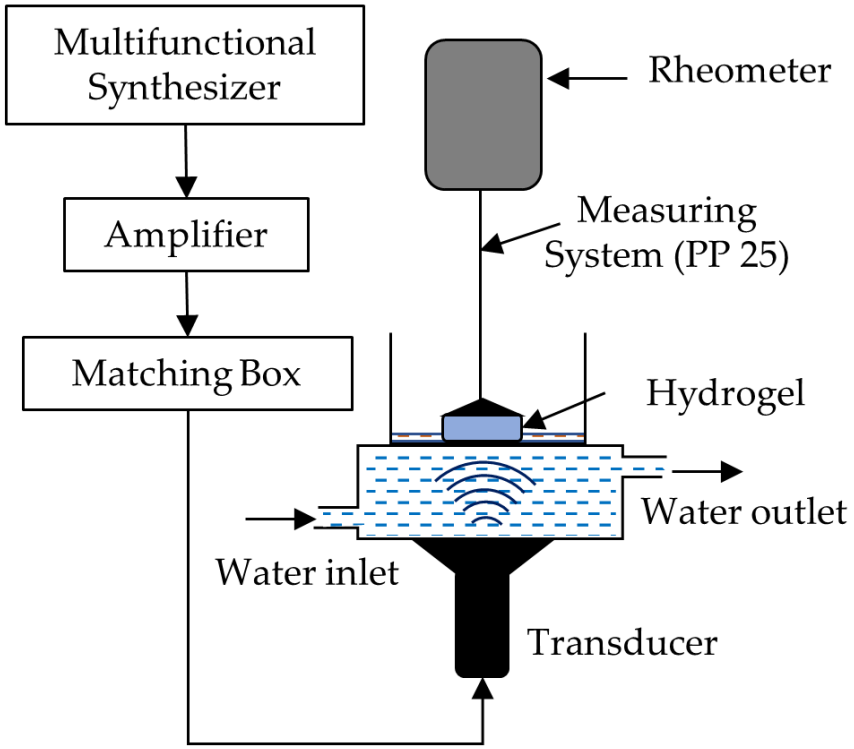

Figure 3- 1 The experimental setup equipped with US transducer for *in-situ* viscoelastic measurements

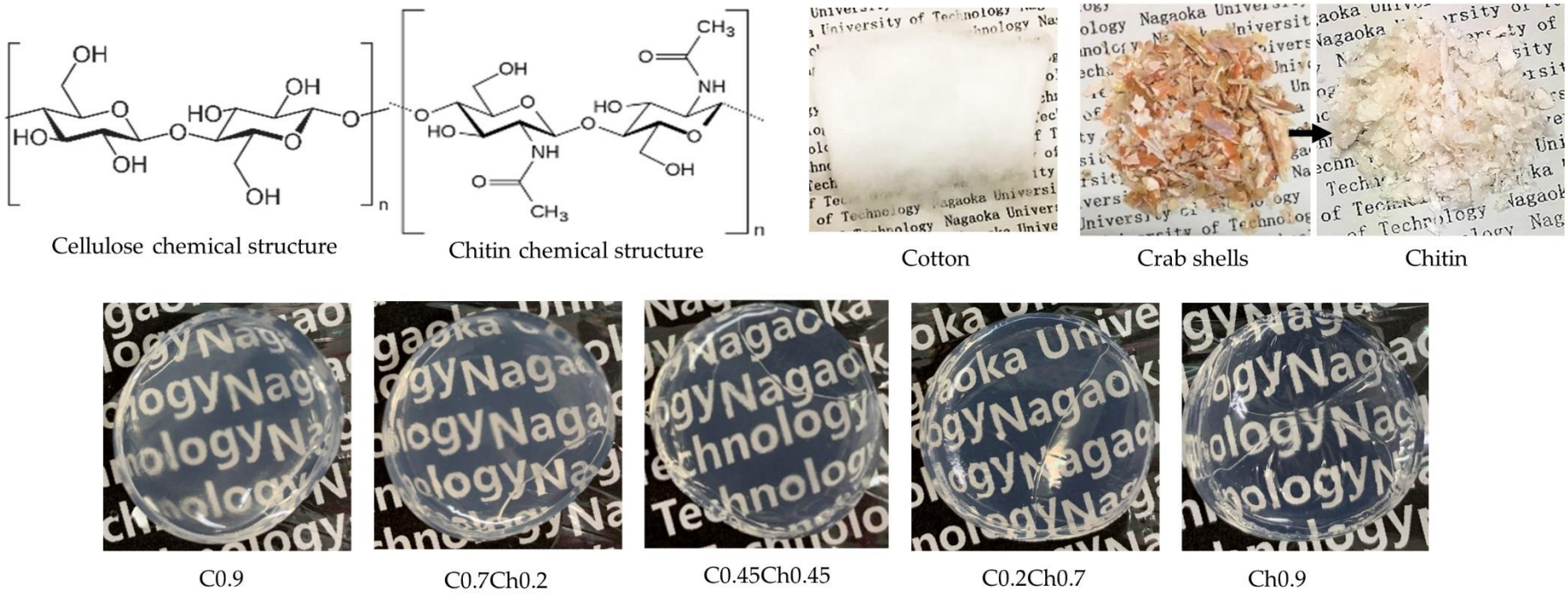

Figure 3- 2 Pictures of chemical structures of cellulose and chitin, cotton, crab shells, extracted chitin, cellulose hydrogel (C0.9), chitin hydrogel (Ch0.9), and cellulose-chitin hydrogel (C0.7Ch0.2, C0.45Ch0.45, and C0.2Ch0.7)

3.3 Results and discussion

3.3.1 Viscoelastic behavior of cellulose-chitin composite hydrogel

The CCCHs were successfully fabricated by the phase inversion of the cellulose-chitin solutions (CCSs), as seen in Figure 3- 2. Here, each hydrogel was prepared from LiCl/ DMAc solution with the composition shown in Table 3- 1. Based on the different ratios of cellulose and chitin, differences in some physical properties were noted, as given in Table 3- 2. The viscosity of the CCSs in LiCl/ DMAc was increased as the chitin component was increased. creased. Because of the presence of many hydrogen bonding sites, namely, methyl hydroxyl, and the acetyl amide, carbonyl and hydroxyl groups, chitin is more able than cellulose of forming strong hydro[20,26]. Therefore, when the chitin content was increasing in the CCSs, it tended to create more hydrogen bonds with cellulose as well. Thus, the solution behaves more and more viscous even though the total polysaccharide concentration was maintained constant at 0.9 wt%.

In the cases of CCCHs, their appearances were transparent, as seen in the pictures, and further, the transparency was increased when the chitin concentration was increased. The densities of the hydrogels were decreased slightly by the addition of chitin. The cellulose hydrogel showed the lowest water content of 1971%, while the chitin-containing hydrogels had higher water content: 2236, 2459, 2452, and 2378% for C0.7Ch0.2, C0.45Ch0.45, C0. 2Ch0.7, and Ch0.9, respectively. These suggested that the polymeric matrix for the cellulose hydrogel was formed as a denser matrix than the chitin-contained hydrogels.

The in-situ viscoelastic properties of the hydrogels were measured during the US exposure by using the experimental setup equipped with 43 kHz US device, as shown in Figure 3- 1 [13]. The same setup was used to perform the amplitude sweep test for the hydrogels before and after exposing them to continuous US at 30 W/ 43 kHz for 1 h. Figure 3- 3 shows those viscoelastic properties at different strain % values with and without continuous US irradiation. The values of the storage modulus (G') at the 0.01 % strain were 1. 83 × 10^5, 1.13 × 10^5, 8.61 × 10^4, 1.0 × 10^5, and 9.4 × 10^4 Pa, for C0.9, C0.7Ch0.2, C0.45Ch0.45, C0.2Ch0.7 and Ch0.9, respectively, without US. In the hydrogels, the highest G' value was obtained at the lower strains %, and those values were constant up to 0.13 % - 1.0 % strain. In the case of the composite hydrogels of cellulose and chitin, G' at 0.01 % strain values were decreased relative to that of C0.9. At higher strains (%) than 1 % - 2 %, the G' values were tended to decrease because of the deformation of the hydrogel structure. The G" at lower strains were retained constant similar with the range of G'. And G" were started to increase after 1 % - 2 % strains up to the gel points of each hydrogel and then changed to decline with the increased strains. Here, the gel point is the cross point of G' and G", i.e., G'=G''[1], and the strain % at the gel point was considered for the evaluations. With the increment of chitin component in hydrogels, the strain % at the gel point was shifted towards the higher strain end as 1.05, 1.1, 7.0, 4.0 %, and 5.0 % for C0.9, C0.7Ch0.2, C0.45Ch0.45, C0.2Ch0.7, and Ch0.9, respectively. Briefly, the chitin component in the hydrogels caused an increase in the elastic properties of the CCCHs. It was noted that C0.45Ch0.45 hydrogel showed the highest strain of 7.0 % at the gel point,

which suggested that high elasticity was kept at higher deformation conditions. Considering the water contents given in Table 3- 2, as explained earlier, the cellulose hydrogel had the lowest water content than the composite hydrogels and the chitin hydrogel. Also, the highest water content was seen for the C0.45Ch0.45 as 2459 %. However, the composite hydrogels contained higher water retention, meaning a loose network than cellulose hydrogel comparatively. Among them, the C0.45Ch0.45 system seemed to have the loosest network. Thus, it could retain the highest amount of water inside, while it could maintain high elastic behavior than other hydrogel systems.

Table 3- 2 Viscosity of CCSs mixtures, water contents (wet basis) of CCCHs before and after the US irradiation (30 W/ 43 kHz, 1 h), and density of CCCHs

Sample Name	Viscosity (25 ^{0}C, at 1 % strain) (Pa.s)	Water Content (%) (dry basis)		Density (g/cm^3)
		Before US	After US	
C0.9	0.209	1971	1915	1.016
C0.7Ch0.2	0.218	2236	2171	1.014
C0.45Ch0.45	0.512	2459	2380	1.014
C0.2Ch0.7	1.14	2452	2443	1.013
Ch0.9	1.82	2378	2316	1.011

According to Figure 3- 3, after 1 h continuous US irradiation at 43 kHz frequency and 30 W output power, the value of the G’ at 0.01 % strain were 1.34×10^5, 9.07×10^4, 7.74×10^4, 8.64×10^4, and 9.12×10^4 Pa for C0.9, C0.7Ch0.2, C0.45Ch0.45, C0.2Ch0.7, and Ch0.9 hydrogels, respectively. As compared with before US irradiation, these values were dropped after US exposure for each hydrogel. For 1 h exposure, US irradiation caused to decline the G"

values also. Therefore, the initial gel elasticity was somewhat dropped during the long US exposure time. As seen in Table 3- 2, after 1 h exposure to US, the water contents of the hydrogels were also decreased. Those results suggested that the US behaved to release the water trapped inside the hydrogels [11].

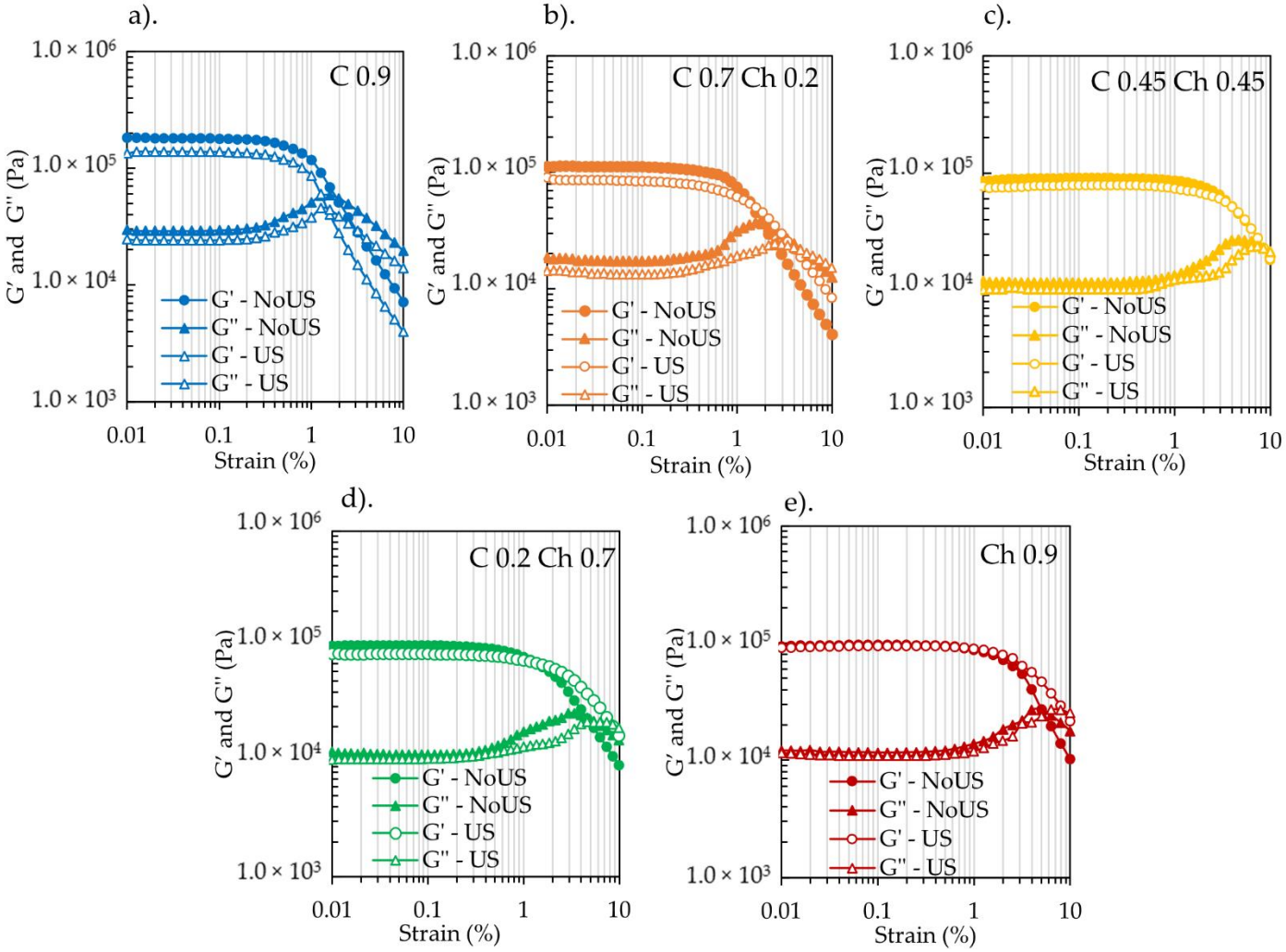

Figure 3- 3 Storage modulus (G') and loss modulus (G'') of a) C0.9, b) C0.7Ch0.2, c) C0.45Ch0.45 d) C0.2Ch0.7 and e) Ch0.9 before and after expose to continuous US irradiation for 1 h The measurements were taken within 0.01 % - 10 % strain, at 1 Hz, at 25 ^{0}C. US exposure was at 43 kHz/ 30 W for 1 h at 25 ˚C

3.3.2 Cycled US exposure in the viscoelasticity change

Figure 3- 4 shows G’ and G’’ behaviors of the hydrogels under cyclic *in-situ* US irradiation at 30 W/ 43 kHz. Here, the US irradiation was cycled with and without US in 5 min intervals, and G’ and G’’ values were monitored against the time. The G’ and G’’ variations were illustrated in closed and opened symbols, respectively. For all the samples, it was clearly visible that G’ and G’’ values were started to drop once the US irradiation was started. Interestingly, the values were fully returned to the initial value within few seconds when the US stopped. This behavior repeatedly happened at three cycles of the US – NoUS steps. Here, cyclic softening and gelation behavior of hydrogels were noted in the presence and absence of US.

The C0.9 hydrogel, the pure cellulose hydrogel, showed that the G’ and G’’ were hugely dropped compared with the initial values at the NoUS steps. Here, for C0.9, the cyclic behavior of G’ decline was looked similar in first, second, and third US processes. For the Ch0.9 of chitin hydrogel, G’ and G’’ values were dropped slower against US exposure time, especially at the first and second US cycles. It has appeared that the softening effect was cycled by US exposure, meaning that US influenced on temporary breakage of existing networking bonds of C0.9 and Ch0.9. The composite hydrogels of cellulose and chitin showed intermediate behaviors of G’ and G’’ compared to pure cellulose and chitin hydrogels. As given in Figure 3- 4 b), c) and d) for C0.7Ch0.2, C0.45Ch0.45, and C0.2Ch0.7, their G’ and G’’ were dropped during the US irradiation with a similar pattern as Ch0.9. However, the dropped percentage

was not as high as C0.9 and Ch0.9. Also, it was noted that the G' and G'' values were returned as the US exposure was stopped. Throughout the US – NoUS cycles, all the values were returned to their initial value, and since the values were the same, there was no breakage of the cellulose and chitin polymer chains in the hydrogels by the US. Therefore, the softening effect of US might be due to changes or probably the breakage of hydrogen bonds or some physical tangles.

Interestingly, the softening behavior of the hydrogels was behaved differently in the first US cycle and next to the second US cycle. The G' dropping was gradually occurred during the first US cycle in C0.9 and Ch0.9, but the Ch0.9 was slower in the G' dropping than that of C0.9. In the second and third US cycles, the G' values were dropped quicker than the first cycle, especially in Ch0.9. Considering the composite hydrogels, in the first US cycle and the second US cycle, the gradient of the G' dropping was decreased when the chitin component increased in the hydrogel. However, in the third US cycle, the G' drop was almost abrupt and stayed constant over the irradiation period for the composite hydrogels. The chitin hydrogel had the same behavior. This G' and G'' behavior in first and second cycles for the hydrogels containing chitin might be due to acetyl amine groups in the chitin. Cellulose does not have acetylamine groups or only -OH groups. Therefore, chitin-containing hydrogels may form their network with more hydrogen bonds or physical tangles, thus show slower softening behavior during US irradiation, as explained above. However, eventually, the US made the gel matrix re-arranged

into a much stable condition under the US irradiation, especially for the chitin having HN-COCH3 groups.

Figure 3- 5 shows the values of tan δ (G''/G') variation in the cyclic US processes. As exceeded over tan δ = 1, the gel state of hydrogel became the liquid state because the gel network was destroyed under the US forces. In the case of C0.9 as cellulose hydrogel, the tan δ values were reached to tan δ ≈ 5 – 6, meaning that significant softening effect as the hydrogel turned to the liquid state by US exposure. In the comparison of composite hydrogels, the values of the tan δ were ≈ 1 under the US irradiation for C0.7C0.2 than C0.45Ch0.45 and C0.2Ch0.7. Nevertheless, there was a tendency of increasing the tan δ value with the US cycles. This tendency was higher in the ascending order of C0.7Ch0.2, C0.45Ch0.45 and C0.2Ch0.7. This meant that the C0.7Ch0.2 matrix could keep the gel state even though the US forced the matrix bonds. In contrast, for the C0.45Ch0.45 and C0.2Ch0.7 composite hydrogels, at the first and second US cycles, the tan δ values were stayed below tan δ = 1, but the values exceeded tan δ = 1 at the third US cycle. For Ch 0.9, it showed much significant behavior on the same tendency. Here, the values of tan δ at the first US cycle were less than those at the second and third US cycles for Ch0.9. And at the third US cycle, the values of tan δ were reached to tan δ ≈ 5 – 6. Here, Ch0.9 matrix was more sensitive to US than the composite hydrogels. However, when the US was stopped, tan δ became tan δ < 1 for all the five hydrogel systems meaning that the matrix was returned to the gel state without permanently breaking the hydrogel networking.

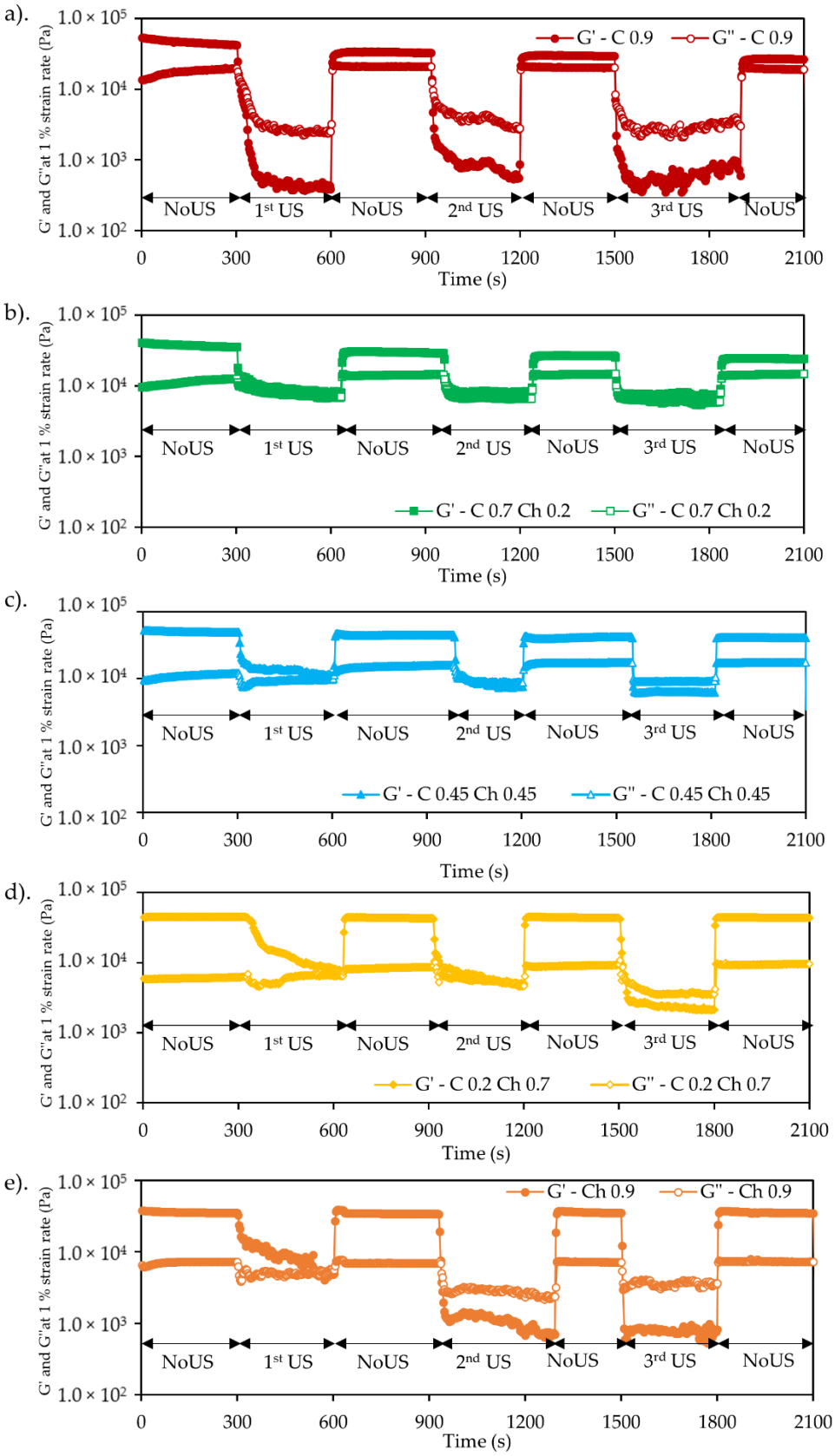

Figure 3- 4 G' and G'' vs time plots of a) C0.9, b) C0.7Ch0.2, c) C0.45Ch0.45 d) C0.2Ch0.7 and e) Ch0.9 during the cyclic US operation, i.e., in situ. G' and G' were measured at constant 1% strain and 1 Hz frequency. US exposure was at 30 W/ 43 kHz. Cyclic US and NoUS process was done in 5 min intervals

The C0.9 hydrogel, the pure cellulose hydrogel, showed that the G' and G'' were hugely dropped compared with the initial values at the NoUS steps. Here, for C0.9, the cyclic behavior of G' decline was looked similar in first, second, and third US processes. For the Ch0.9 of chitin hydrogel, G' and G'' values were dropped slower against US exposure time, especially at the first and second US cycles. It has appeared that the softening effect was cycled by US exposure, meaning that US influenced on temporary breakage of existing networking bonds of C0.9 and Ch0.9. The composite hydrogels of cellulose and chitin showed intermediate behaviors of G' and G'' compared to pure cellulose and chitin hydrogels. As given in Figure 3- 4 b), c) and d) for C0.7Ch0.2, C0.45Ch0.45, and C0.2Ch0.7, their G' and G'' were dropped during the US irradiation with a similar pattern as Ch0.9. However, the dropped percentage was not as high as C0.9 and Ch0.9. Also, it was noted that the G' and G'' values were returned as the US exposure was stopped. Throughout the US – NoUS cycles, all the values were returned to their initial value, and since the values were the same, there was no breakage of the cellulose and chitin polymer chains in the hydrogels by the US. Therefore, the softening effect of US might be due to changes or probably the breakage of hydrogen bonds or some physical tangles.

Interestingly, the softening behavior of the hydrogels was behaved differently in the first US cycle and next to the second US cycle. The G' dropping was gradually occurred during the first US cycle in C0.9 and Ch0.9, but the Ch0.9 was slower in the G' dropping than that of C0.9. In the second and third US cycles, the G' values were dropped quicker than the first cycle,

especially in Ch0.9. Considering the composite hydrogels, in the first US cycle and the second US cycle, the gradient of the G' dropping was decreased when the chitin component increased in the hydrogel. However, in the third US cycle, the G' drop was almost abrupt and stayed constant over the irradiation period for the composite hydrogels. The chitin hydrogel had the same behavior. This G' and G'' behavior in first and second cycles for the hydrogels containing chitin might be due to acetyl amine groups in the chitin. Cellulose does not have acetylamine groups or only -OH groups. Therefore, chitin-containing hydrogels may form their network with more hydrogen bonds or physical tangles, thus show slower softening behavior during US irradiation, as explained above. However, eventually, the US made the gel matrix re-arranged into a much stable condition under the US irradiation, especially for the chitin having HN-COCH3 groups.

Figure 3- 5 shows the values of tan δ (G''/G') variation in the cyclic US processes. As exceeded over tan δ = 1, the gel state of hydrogel became the liquid state because the gel network was destroyed under the US forces. In the case of C0.9 as cellulose hydrogel, the tan δ values were reached to tan δ ≈ 5 – 6, meaning that significant softening effect as the hydrogel turned to the liquid state by US exposure. In the comparison of composite hydrogels, the values of the tan δ were ≈ 1 under the US irradiation for C0.7C0.2 than C0.45Ch0.45 and C0.2Ch0.7. Nevertheless, there was a tendency of increasing the tan δ value with the US cycles. This tendency was higher in the ascending order of C0.7Ch0.2, C0.45Ch0.45 and C0.2Ch0.7. This meant that the C0.7Ch0.2 matrix could keep the gel state even though the US forced the matrix

bonds. In contrast, for the C0.45Ch0.45 and C0.2Ch0.7 composite hydrogels, at the first and second US cycles, the tan δ values were stayed below tan δ = 1, but the values exceeded tan δ = 1 at the third US cycle. For Ch 0.9, it showed much significant behavior on the same tendency. Here, the values of tan δ at the first US cycle were less than those at the second and third US cycles for Ch0.9. And at the third US cycle, the values of tan δ were reached to tan δ ≈ 5 – 6. Here, Ch0.9 matrix was more sensitive to US than the composite hydrogels. However, when the US was stopped, tan δ became tan δ < 1 for all the five hydrogel systems meaning that the matrix was returned to the gel state without permanently breaking the hydrogel networking.

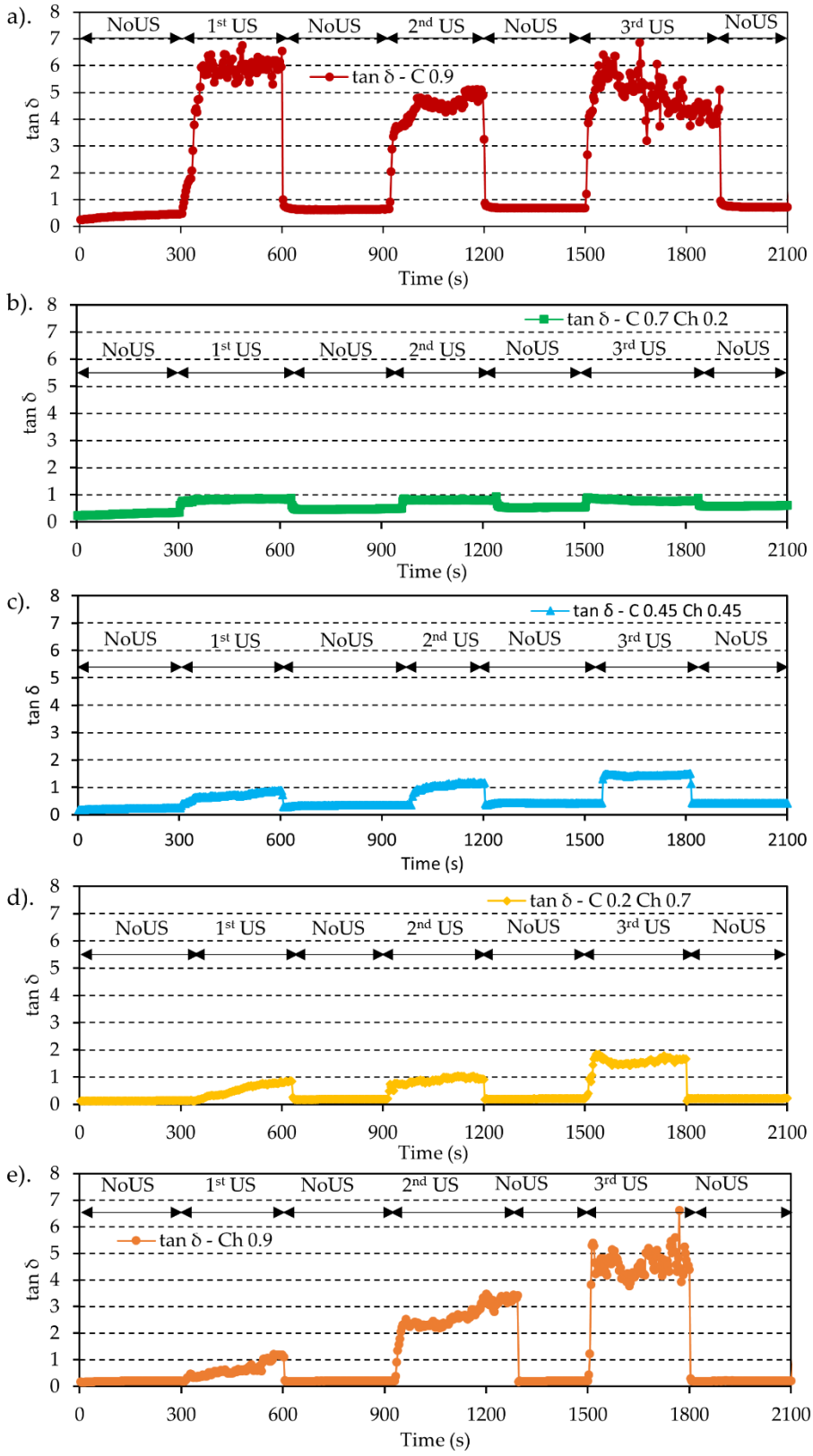

Figure 3- 5 tan δ vs time plots of a) C0.9, b) C0.7Ch0.2, c) C0.45Ch0.45 d) C0.2Ch0.7 and e) Ch0.9 during the cyclic US operation

To analyze the gradient changes of G', log G'/ G'_0 vs. time plots were drawn as shown in Figure 3- 6 for the first, second, and third US cycles. As per the plots, the negative slope meant the apparent soften rate of the hydrogels under US irradiation. In contrast, the positive slope means the bond reformation rate of the hydrogels when the US was stopped at each cycle. Here, the rates were calculated from the slope of the plots in the figure. In detail, the rate of G' drop or the softening rate of C0.9 for the first, second, and third US irradiation was 0.017, 0.058, and 0.090 sec^{-1}, respectively. The soften rates at first, second, and third cycles for C0.7Ch0.2 were 0.026, 0.060, 0.060 sec^{-1}, for C0.45Ch0.45 were 0.047, 0.056, and 0.113 sec^{-1}, for C0.2Ch0.7 were 0.004, 0.017, and 0.028 sec^{-1}, and for Ch0.9 were 0.004, 0.052 and 0.09 sec^{-1}. According to the soften rates of the hydrogels, the values were increased with the consecutive US cycles meaning that cycle by cycle, the matrix became softer than the previous state by US forces acted on the network. This might be because the US could release the physical tangles and hydrogen bonds of polymer-polymer matrix stage by stage during the US – NoUS cycles. Thus, eventually, the matrix was turning into a stable matrix. Here, when comparing different hydrogel systems, C0.45Ch0.45 exhibited the highest softening rate at the US exposure. Further, the bond reformation rates of the hydrogels when the US was stopped were, for the C0.9, 0.093, 0.171, and 0.212 sec^{-1} at first, second, and third US cycles, respectively. Similarly, the values for C0.7Ch0.2 were 0.089, 0.088 and 0.168 sec^{-1}, for C0.45Ch0.45 were 0.108, 0.182 and 0.192 sec^{-1}, for C0.2Ch0.7 were 0.163, 0.228 and 0.243 sec^{-1}, and for Ch0.9 were 0.178, 0.202 and 0.220 sec^{-1} at the first, second, and third US cycles,

adjacently. As clearly shown, bond reformation became more efficient with each cycle. This enhanced rate of bond reformation implied that the matrix has changed to be more stabilized in each US irradiation cycle. When each US cycle was compared, the bond reformation rate was higher than the softening rate. Here, it was strongly evident that the hydrogel softening happened step by step due to the breakage of hydrogel linkages in the physical entanglements and the hydrogen bonds. When the US was stopped, re-arranging the gel crosslinking points may occur, i.e., predominantly, hydrogen bond formation when removing US forces, and thus the gelation occurred more quickly. This effect was more pronounced for chitin with acetylamine groups than cellulose.

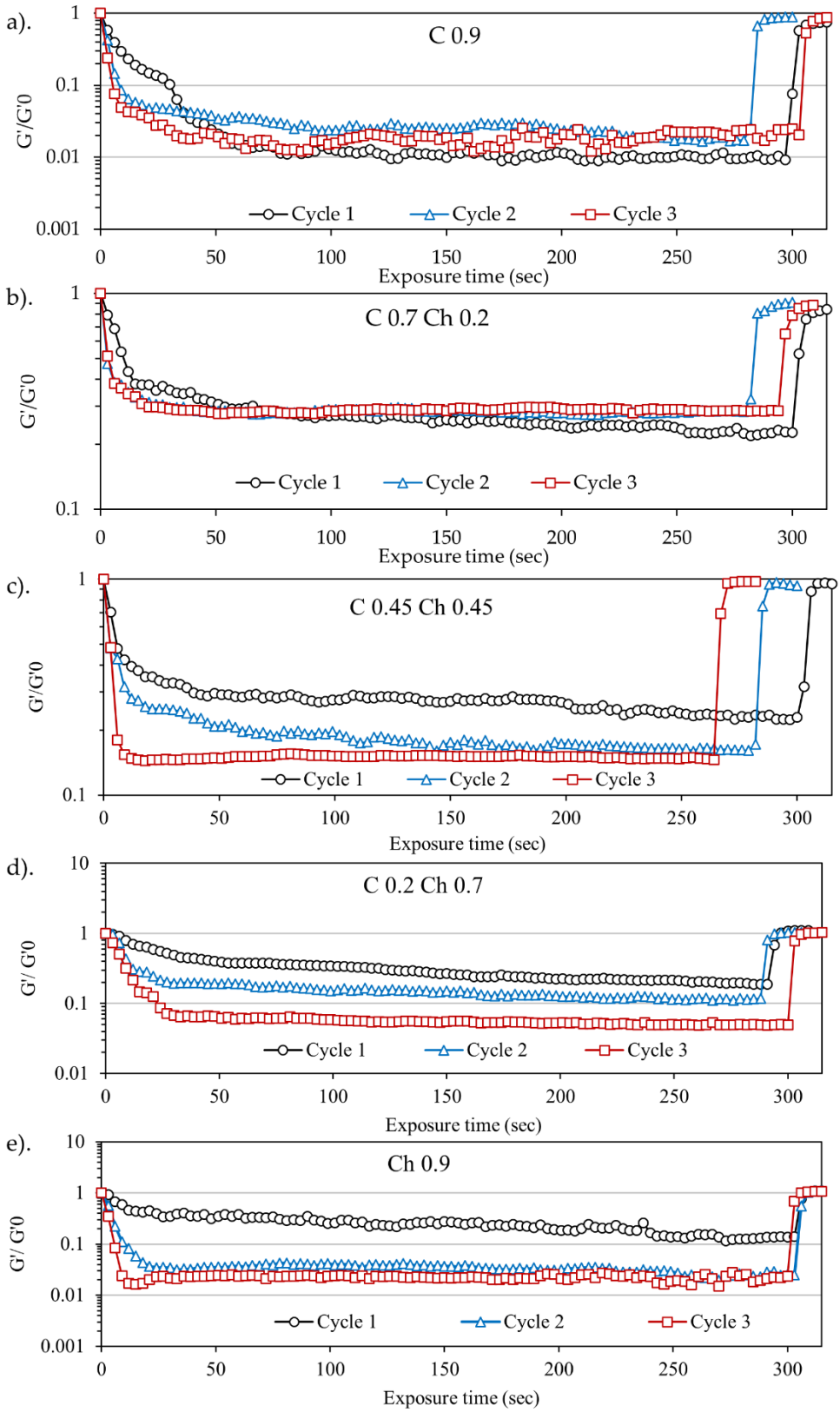

Figure 3- 6 G'/G'$_0$ vs. time plot during the first and second US cycles for a). C0.9, b) C0.7Ch0.2, c) C0.45Ch0.45, d) C0.2Ch0.7 and e) Ch0.9. US parameters were 43 kHz frequency and 30 W output power. G'$_0$ - initial G' at the point of US irradiation was started. (The max. and min points of the vertical axis scale kept different to make the plots clear to the reader)

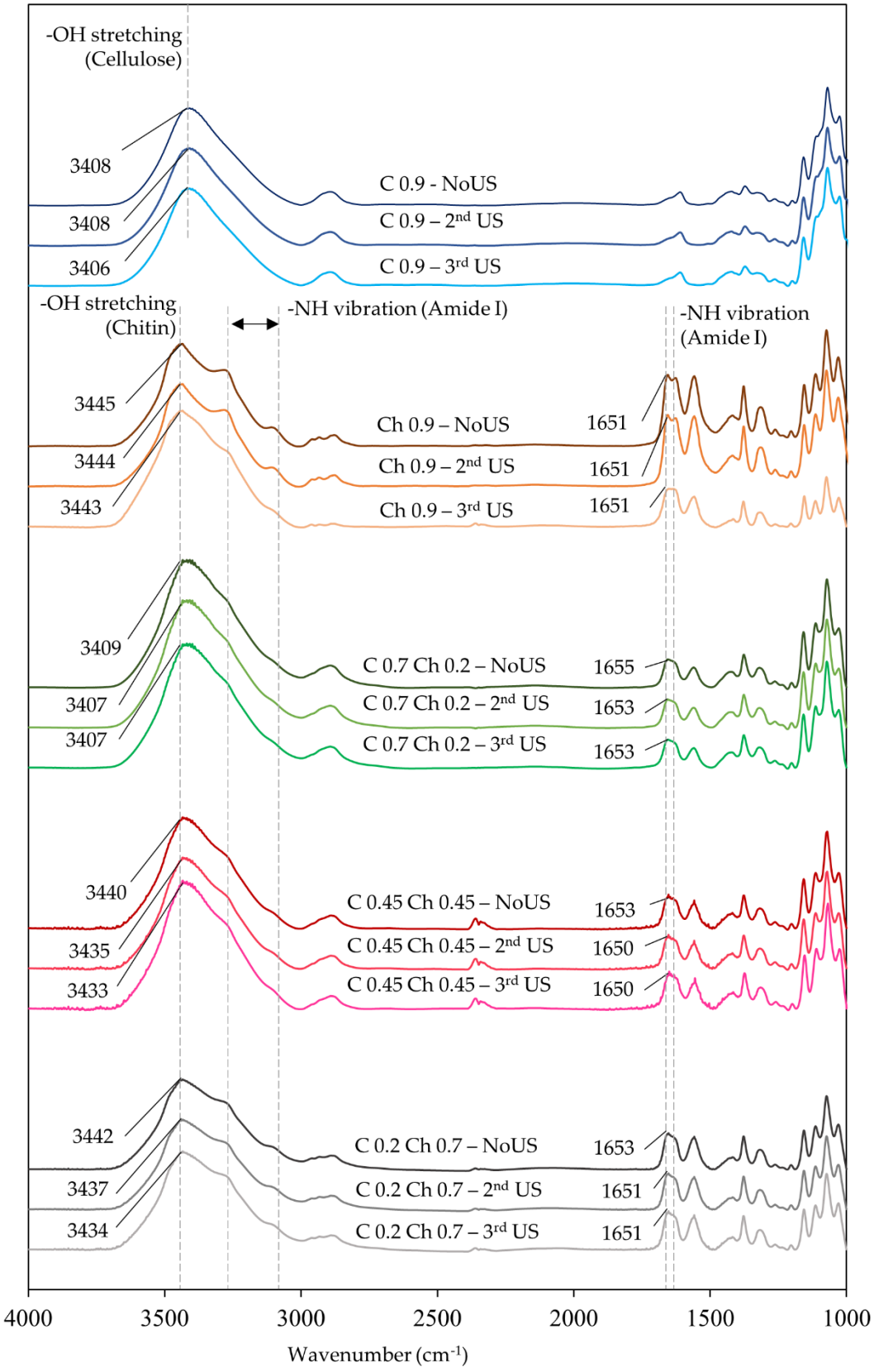

Figure 3- 7 FTIR spectra of cellulose hydrogel film, chitin hydrogel film, and cellulose-chitin composite hydrogel films before US and after third US cycle

3.3.3 FTIR analysis of cellulose-chitin composite hydrogels

In order to confirm the US effect of the hydrogels, FTIR spectra were measured and compared before the US and after the third US exposure (Figure 3- 7). In the results of -OH stretching peak of the hydrogels, the maximum wavenumber was observed at 3408, 3409, 3440, 3442, and 3445 cm^{-1} for C0.9, C0.7Ch0.2, C0.45Ch0.45, C0.7Ch0.2 and Ch0.9, respectively. Here, the original -OH stretching peaks of cellulose and chitin hydrogels at 3408 cm^{-1} and 3445 cm^{-1} were shifted towards one another in the composite hydrogels. Furthermore, the FTIR spectra of each hydrogel film when the three US cycles were over showed a slight shift in the peak wavenumber towards the lower region in the -OH stretching peak and the vibration mode of Amide I at around 1650 cm^{-1} – 1655 cm^{-1} in the chitin component [22,27]. This suggested that after the three US cycles, the wavenumber of the hydrogen bonds of the acetylamine group changed in the chitin-containing hydrogels. However, the cellulose had no change in the first, second and third cycles. In the chitin-containing hydrogels at the third cycle, the spectral change in the acetylamine group was corresponded to the change of viscoelastic behavior. While at the first and second cycles, the G' dropping and the values of tan δ of chitin containing hydrogels were increased due to releasing the physical tangles in the chitin segments. Then, the acetylamide groups were engaged in forming other hydrogen bonds to crosslink the segmental tangles. On the other hand, the composites of cellulose and chitin seemed to form tight hydrogen bonds to make compacted hydrogels. However, with the increase of the chitin

component, US caused changing the tangles of chitin with acetylamine groups. Eventually, the hydrogels were arranged to be more uniform in their networking.

3.4 Conclusions

Cellulose-chitin composite hydrogel was successfully fabricated using the phase inversion method. The sono-responsive nature of the prepared hydrogels was studied using *in-situ* viscoelasticity measuring equipment with a US device. The analytical results showed that US at 43 kHz and 30 W caused softening of hydrogels, especially significant in C0.9 and higher chitin component hydrogels. However, the gel condition was immediately recovered when the US irradiation was stopped. When the chitin contents in the hydrogels were increased, the softening effect was enhanced. Further, the hydrogel softening behavior was cycled during the US irradiation. However, the hydrogels having acetylamide groups delayed the softening in the first US cycle. However, the second and third cycles were re-arranged the segmental tangles of the hydrogels resulting in the reformation of hydrogen bonds when the US stopped.

Part 2

3.5 Application of Cellulose-Chitin Composite Hydrogel for US-triggered nicotine release

CCCH is a novel material developed in a simple, green and sustainable manners [28]. Chemical structures of cellulose and chitin alone are rich in functional groups to make strong hydrogen bonds in nature and thus in the form of a composite hydrogel, extended and stronger hydrogen bonding network is formed [28]. This extended hydrogen bonding in CCCHs make the hydrogel differ from the pure cellulose and chitin hydrogel properties. According to Part 1 of this chapter, CCCH with different cellulose and chitin loading show different manners in viscoelasticity changes during cyclic US irradiation. The key featuring behavior of those CCCHs were the softening of the hydrogel upon US irradiation and the immediate re-gelation once the US was stopped. Such cyclic softening-gelation of hydrogels against US irradiation predict their usage in applications like pulse drug release systems in smart drug delivery systems (SDDS) for controlled release of drugs. Therefore, to analyze the feasibility of using these newly studied CCCHs material, model drug of nicotine was loaded into the CCCHs in 0.1 wt% in the solution. Then, the nicotine release behaviors of the nicotine-loaded cellulose-chitin composite hydrogels (NCCCH) were studied under cyclic and continuous US irradiation. In the Part 2 of this Chapter 3, such behaviors are discussed shortly in order to consider the favorability of these hydrogels in cyclic US-triggered nicotine release applications.

3.6 Materials and Method

3.6.1 Fabrication of nicotine-loaded cellulose-chitin composite hydrogels

NCCCHs were fabricated according to the procedure similar in the Part 1 of Chapter 3. The raw materials and chemicals were also same to those which used in Chapter 3. In addition to them, nicotine, a product of Tokyo Kasei Kogyo Co., Ltd. (Tokyo, Japan) was used as the drug.

Table 3- 3 Compositions of the solution used to fabricate nicotine-cellulose-chitin composite hydrogel

Sample Name	Composition of NCCSs used to fabricate NCCCHs		
	1 wt% Cellulose (wt%)	1 wt% Chitin (wt%)	1 wt% Nicotine (wt%)
NC0.9	0.9	0	0.1
NC0.7Ch0.2	0.7	0.2	0.1
NC0.45Ch0.45	0.45	0.45	0.1
NC0.2Ch0.7	0.2	0.7	0.1
NCh0.9	0	0.9	0.1

Prior to making NCCCHs, nicotine-cellulose-chitin solutions (NCCSs) were prepared by 48 h mixing of cellulose, chitin, and nicotine solutions together in the compositions given in Table 3- 3. NCCSs were poured in 10 g for the phase inversion to fabricate hydrogels as described in Figure 3- 8. After 24 h of phase inversion, the NCCCHs were obtained, and those hydrogels were tested for US-triggered nicotine release after washing them thoroughly using 20 ml × 30 times of distilled water.

The US setup used for the cyclic US-triggered drug release is given in Figure 3- 9. This set up is same as given in the Part 1 but without the rheometer assembly. US-NoUS cycles were continued up to total 40 min total time. NCCCHs were immersed in 20 ml of distilled

water during irradiation so the water samples were analyzed by UV-Vis spectrophotometer and measured the absorption intensity of the peak at 260 nm wavelength responsible for nicotine [29]. For the continuous US irradiation, US equipment setup used in the Chapter 2 was used instead of the set up in Figure 3- 9. The reason was that the set up in Figure 3- 9 may buildup heat at the continuous irradiation. US conditions used for the drug release was 40 W US power at 43 kHz US frequency, at 25 ˚C.

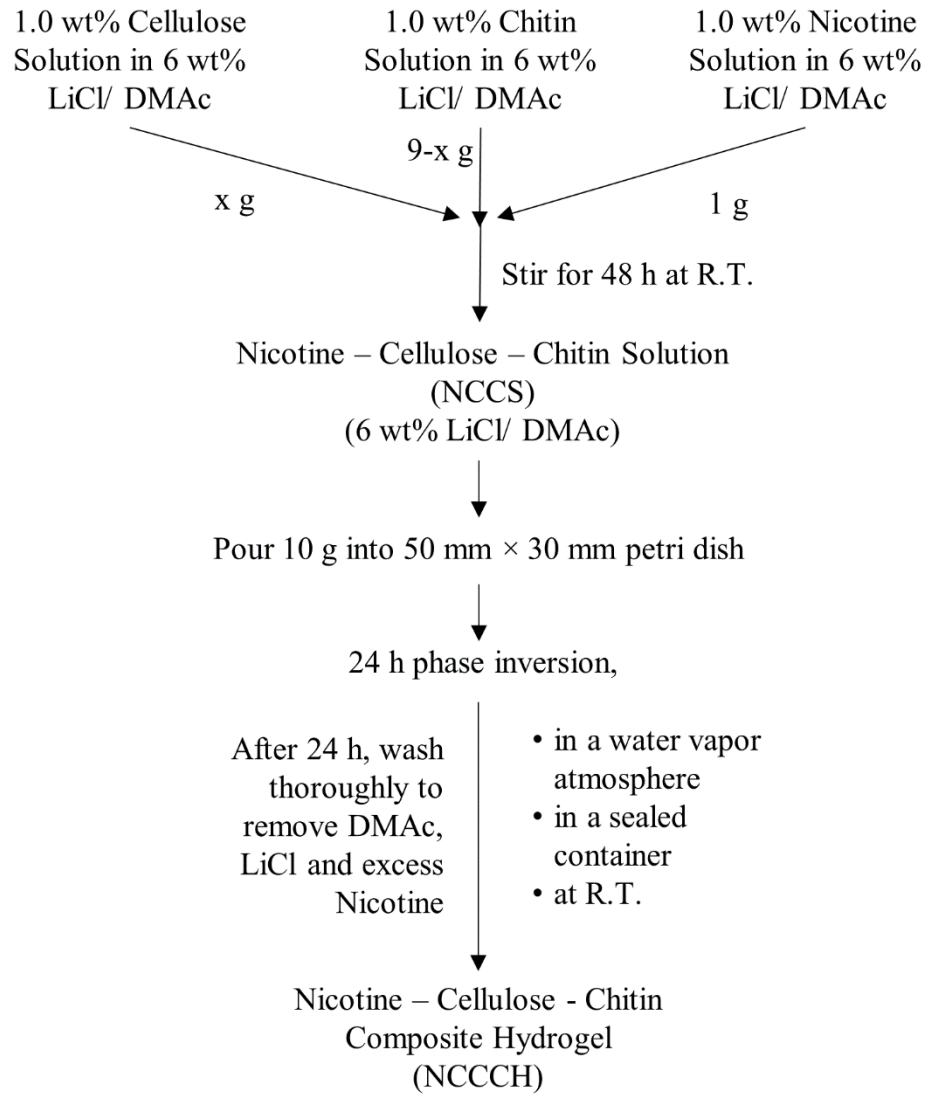

Figure 3- 8 Procedure of preparing NCCCHs

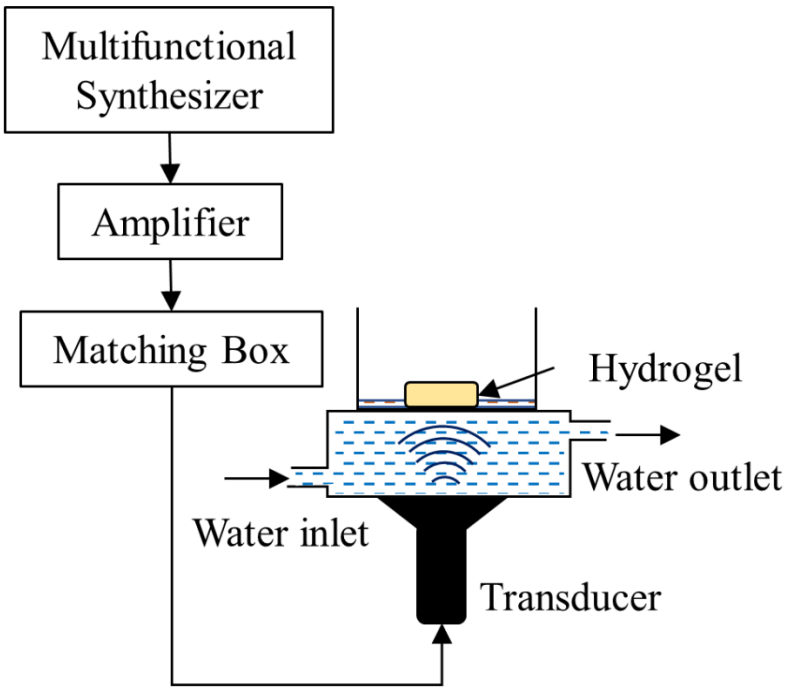

Figure 3- 9 US experimental set up for cyclic US irradiation

3.7 Results and discussion

3.7.1 US-triggered nicotine release from NCCCHs.

NCCCHs with different cellulose and chitin were successfully fabricated using 24 h phase inversion in water vapor atmosphere. The hydrogels were tested for nicotine release experiments using the method described in the previous section. Figure 3- 10 summarizes the nicotine release behavior in continuous US irradiation for total 40 min and cyclic US irradiation in 5 min intervals up to 40 min. All the five NCCCHs systems, NC0.9, NC0.7Ch0.2, NC0.45Ch0.45, NC0.2Ch0.7 and NCh0.9 shows enhanced nicotine release in both continuous and cyclic US compared to without US irradiation. Here, interestingly, the cumulative release of nicotine at 40 min exposure in cyclic irradiation was higher than that of in continuous irradiation for the five systems. According to Chapter 2, continuous irradiation to US caused the hydrogel matrix shrink and drop the viscoelastic properties [30]. This means that the shrinkage of hydrogel matrix can cause permeant entrapment of nicotine inside the matrix due to less responsiveness of the matrix after collapsing the porous structure. Therefore, the continuous US may function less in triggering nicotine to release. In contrast, the cyclic US irradiation caused repeating softening and gelation of cellulose, chitin and their composite hydrogels upon US irradiation and stop, respectively. This was reported in Part 1 and it explains the viscoelastic property drop and incline to its initial value upon cyclic US [28]. This cyclic softening – gelation of hydrogel makes the matrix more uniform in its third cycle, especially for the hydrogels containing chitin. Here, no-US step in cyclic US allows the hydrogel to

recover from effects happened during US irradiation. Thus, the hydrogel matrix does not collapse as happened in continuous irradiation. Therefore, compared to continuous US, the hydrogels under cyclic US response well against US triggering and thus higher release of nicotine even under 5 min cycles of US.

NC0.9 and NCh0.9, which are the cellulose only and chitin only hydrogels loaded with nicotine, show clear boosted nicotine release during US irradiation steps in cyclic US. However, when the number of cycles is continued, the enhanced release was lowered compared to the previous cycle. The composite hydrogels with nicotine, NC0.7Ch0.2, NC0.45Ch0.45 and NC0.2Ch0.7, this triggered nicotine release was clearly shown only during first and second US cycles. Also, in these three composite hydrogels, effect of US on nicotine release was not recognized after the second US cycle. As explained in Part 1, cellulose and chitin hydrogel response highly during US irradiation cycles compared to their composite hydrogels. Moreover, composite hydrogels showed progressive softening behavior with the US cycles and eventually it concluded a uniform matrix after the second US cycle. This was well illustrated in the plots of G' and G'' variations and tan δ. changes during cyclic US in Figure 3- 4 and Figure 3- 5 in Part 1. Therefore, this high US-responsiveness of cellulose and chitin hydrogels during US may influence the nicotine release in cyclic US and was noticeable in the plots compared to composites, especially in the last two cycles. In the composites, due to the uniformity of the matrix after the second US cycle nicotine release was permitted irrespective to the US triggering so the differences in triggered release was not noticeable in the last two cycles.

Considering the cyclic US nicotine release, non-uniformity of nicotine release in each US cycle and less responsivity of matrix in later US cycles are not favorable for DR applications. Therefore, in order to use these hydrogel systems for cyclic US drug release applications, modifications are required to increase the repeatability of the matrix for noticeable triggered nicotine release in higher number of US cycles. However, the outlook of the cyclic nicotine release behaviors predicts the applicability in DD and DR applications.

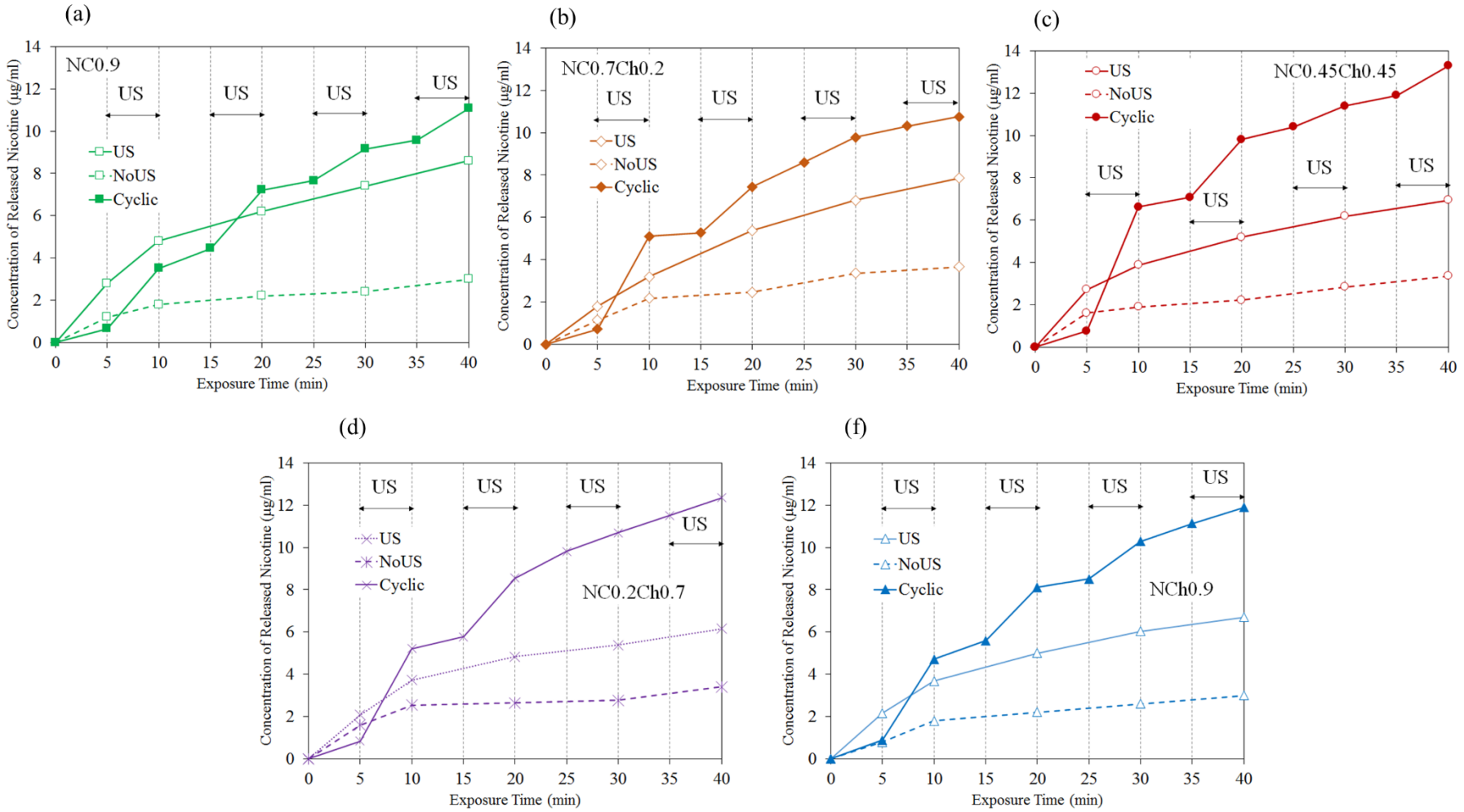

Figure 3- 10 Cyclic and continuous nicotine release behaviors of (a) NC0.9, (b) NC0.7Ch0.2, (c) NC0.45Ch0.45 (d) NC0.2Ch0.7 and (e). NCh0.9. The US conditions were 40 W US power at 43 kHz, at 25 ^{0}C

3.8 Conclusions

NCCCHs were successfully fabricated using phase inversion method. Continuous US and cyclic US was highly affected for the enhanced nicotine release. The cumulative release of nicotine at 40 min irradiation in continuous US was lesser than that of in cyclic US. Cellulose and chitin hydrogels loaded with nicotine showed step wise triggered release of nicotine compared to composite hydrogels. Overall, these hydrogel systems are not well suited for cyclic US-triggered DR applications due to non-uniform of nicotine release in continued US cycles.

References

[1] K. Nakasone, T. Kobayashi, Effect of pre-treatment of sugarcane bagasse on the cellulose solution and application for the cellulose hydrogel films, Polym. Adv. Technol. 27 (2016) 973–980. https://doi.org/10.1002/pat.3757.

[2] K.D. Nguyen, T. Kobayashi, Chitin Hydrogels Prepared at Various Lithium Chloride/N,N-Dimethylacetamide Solutions by Water Vapor-Induced Phase Inversion, J. Chem. 2020 (2020) 1–16. https://doi.org/10.1155/2020/6645351.

[3] F. Ahmadi, Z. Oveisi, M. Samani, Z. Amoozgar, Chitosan based hydrogels: Characteristics and pharmaceutical applications, Res. Pharm. Sci. 10 (2015) 1–16. /pmc/articles/PMC4578208/ (accessed June 26, 2021).

[4] L. Yan, L. Wang, S. Gao, C. Liu, Z. Zhang, A. Ma, L. Zheng, Celery cellulose hydrogel as carriers for controlled release of short-chain fatty acid by ultrasound, Food Chem. 309 (2019) 125717. https://doi.org/10.1016/j.foodchem.2019.125717.

[5] D. Burger, M. Beaumont, T. Rosenau, Y. Tamada, Porous Silk Fibroin/Cellulose Hydrogels for Bone Tissue Engineering via a Novel Combined Process Based on Sequential Regeneration and Porogen Leaching, Molecules. 25 (2020). https://doi.org/10.3390/molecules25215097.

[6] K.D. Nguyen, T.T.C. Trang, T. Kobayashi, Chitin-halloysite nanoclay hydrogel composite adsorbent to aqueous heavy metal ions, J. Appl. Polym. Sci. 136 (2018) 47207. https://doi.org/10.1002/app.47207.

[7] K. Nakasone, S. Ikematsu, T. Kobayashi, Biocompatibility Evaluation of Cellulose Hydrogel Film Regenerated from Sugar Cane Bagasse Waste and Its in Vivo Behavior in Mice, Ind. Eng. Chem. Res. 55 (2016) 30–37. https://doi.org/10.1021/acs.iecr.5b03926.

[8] K.L. Tovar-carrillo, S.S. Sueyoshi, M. Tagaya, T. Kobayashi, Fibroblast Compatibility

on Scaffold Hydrogels Prepared from Agave Tequilana Weber Bagasse for Tissue Regeneration, 52 (2013) 11607–11613. https://doi.org/doi.org/10.1021/ie401793w.

[9] D.E. Ciolacu, R. Nicu, F. Ciolacu, Cellulose-Based Hydrogels as Sustained Drug-Delivery Systems, Materials (Basel). 13 (2020) 5270. https://doi.org/10.3390/ma13225270.

[10] F. Ding, X. Shi, Z. Jiang, L. Liu, J. Cai, Z. Li, S. Chen, Y. Du, Electrochemically stimulated drug release from dual stimuli responsive chitin hydrogel, J. Mater. Chem. B. 1 (2013) 1729. https://doi.org/10.1039/c3tb00517h.

[11] H. Jiang, K. Tovar-Carrillo, T. Kobayashi, Ultrasound stimulated release of mimosa medicine from cellulose hydrogel matrix, Ultrason. Sonochem. 32 (2016) 398–406. https://doi.org/10.1016/j.ultsonch.2016.04.008.

[12] H. Jiang, T. Kobayashi, Ultrasound stimulated release of gallic acid from chitin hydrogel matrix, Mater. Sci. Eng. C. 75 (2017) 478–486. https://doi.org/10.1016/j.msec.2017.02.082.

[13] S. Noguchi, K. Takaomi, Ultrasound response of viscoelastic changes of cellulose hydrogels triggered with Sono-deviced rheometer, Ultrason. Sonochem. 67 (2020) 105143. https://doi.org/10.1016/j.ultsonch.2020.105143.

[14] N. Huebsch, C.J. Kearney, X. Zhao, J. Kim, C.A. Cezar, Z. Suo, D.J. Mooney, Ultrasound-triggered disruption and self-healing of reversibly cross-linked hydrogels for drug delivery and enhanced chemotherapy, Proc. Natl. Acad. Sci. 111 (2014) 9762–9767. https://doi.org/10.1073/pnas.1405469111.

[15] V.J. Addiel, T. Motohiro, K. Takaomi, Ultrasonics Sonochemistry Ultrasound stimulus inducing change in hydrogen bonded crosslinking of aqueous polyvinyl alcohols, Ultrason. Sonochem. 21 (2014) 295–309. https://doi.org/10.1016/j.ultsonch.2013.06.011.

[16] J.A. Venegas-sanchez, M. Tagaya, T. Kobayashi, Effect of ultrasound on the aqueous viscosity of several water-soluble polymers, Polym. J. 45 (2013) 1224–1233. https://doi.org/10.1038/pj.2013.47.

[17] J.A. Venegas-sanchez, T. Kusunoki, M. Yamamoto, T. Kobayashi, Ultraso nics Sonoch emistry Sono-respond on thermosensitive polymer microgels based on cross-linked poly (N- isopropylacrylamide-co-acrylic acid), Ultrason. - Sonochemistry. 20 (2013) 1271–1275. https://doi.org/10.1016/j.ultsonch.2013.02.003.

[18] C. Zhang, R. Liu, J. Xiang, H. Kang, Z. Liu, Y. Huang, Dissolution Mechanism of Cellulose in N,N -Dimethylacetamide/Lithium Chloride: Revisiting through Molecular Interactions, J. Phys. Chem. B. 118 (2014) 9507–9514. https://doi.org/10.1021/jp506013c.

[19] M. Rinaudo, Chitin and chitosan: Properties and applications, Prog. Polym. Sci. 31 (2006) 603–632. https://doi.org/10.1016/j.progpolymsci.2006.06.001.

[20] T. Kameda, M. Miyazawa, H. Ono, M. Yoshida, Hydrogen Bonding Structure and Stability of α-Chitin Studied by13C Solid-State NMR, Macromol. Biosci. 5 (2005) 103–106. https://doi.org/10.1002/mabi.200400142.

[21] E. Yilmaz, M. Bengisu, Preparation and characterization of physical gels and beads from chitin solutions, Carbohydr. Polym. 54 (2003) 479–488. https://doi.org/10.1016/S0144-8617(03)00211-X.

[22] M. Liu, Y. Zhang, J. Li, C. Zhou, Chitin-natural clay nanotubes hybrid hydrogel, Int. J. Biol. Macromol. 58 (2013) 23–30. https://doi.org/10.1016/j.ijbiomac.2013.03.042.

[23] K. Sato, K. Tanaka, Y. Takata, K. Yamamoto, J. ichi Kadokawa, Fabrication of cationic chitin nanofiber/alginate composite materials, Int. J. Biol. Macromol. 91 (2016) 724–729. https://doi.org/10.1016/j.ijbiomac.2016.06.019.

[24] A. Boonmahitthisud, L. Nakajima, K.D. Nguyen, T. Kobayashi, Composite effect of

silica nanoparticle on the mechanical properties of cellulose-based hydrogels derived from cottonseed hulls, J. Appl. Polym. Sci. 134 (2017) 44557. https://doi.org/10.1002/app.44557.

[25] N. Chen, H. Wang, C. Ling, W. Vermerris, B. Wang, Z. Tong, Cellulose-based injectable hydrogel composite for pH-responsive and controllable drug delivery, Carbohydr. Polym. 225 (2019) 115207. https://doi.org/10.1016/j.carbpol.2019.115207.

[26] V.L. Deringer, U. Englert, R. Dronskowski, Nature, Strength, and Cooperativity of the Hydrogen-Bonding Network in α-Chitin, Biomacromolecules. 17 (2016) 996–1003. https://doi.org/10.1021/acs.biomac.5b01653.

[27] S. Taokaew, M. Ofuchi, T. Kobayashi, Size Distribution and Characteristics of Chitin Microgels Prepared via Emulsified Reverse-Micelles, Materials (Basel). 12 (2019) 1160. https://doi.org/10.3390/ma12071160.

[28] H. Iresha, T. Kobayashi, In Situ Viscoelasticity Behavior of Cellulose–Chitin Composite Hydrogels during Ultrasound Irradiation, Gels. 7 (2021) 81. https://doi.org/10.3390/gels7030081.

[29] H. Iresha, T. Kobayashi, Ultrasound-triggered nicotine release from nicotine-loaded cellulose hydrogel, Ultrason. Sonochem. 78 (2021) 105710. https://doi.org/10.1016/j.ultsonch.2021.105710.

[30] H. Iresha, T. Kobayashi, Ultrasound-triggered nicotine release from nicotine-loaded cellulose hydrogel, Ultrason. Sonochem. 78 (2021) 105710. https://doi.org/10.1016/J.ULTSONCH.2021.105710.

Chapter 4. Summary

The current research was focused on the Ultrasound-stimulated behaviors on biomass hydrogel medicines for drug release application. Here, the nicotine-loaded cellulose hydrogel and cellulose-chitin composite hydrogel systems were investigated against US-triggered DR. In the Chapter 1, elaborative background review for the research was given. Chapter 2 focused on the nicotine release behaviors from nicotine-loaded cellulose hydrogels. Here, mainly, 3 cellulose hydrogels with three cellulose loading were prepared and loaded with nicotine. Their nicotine release behaviors were investigated under continuous US irradiation. nicotine release was enhanced by the US trigger and the hydrogel system with 0.9 wt% cellulose showed the highest release efficiency. In these systems, the matrix became softer after US irradiation and this softening was proportional to the US power. Further, nicotine release was promoted by the breakage of nicotine-cellulose hydrogen bonds by the effects of US.

In Chapter 3, novel hydrogel system from cellulose-chitin composite was investigated. Here, the *in-situ* viscoelasticity property behaviors against cyclic US irradiation were investigated using sono-deviced rheometer equipment. US-promoted viscoelasticity drops and returning the values to initials upon US stop was noticed in repeated cycles of US. This softening-gelation steps were behaved differently with the different compositions of cellulose and chitin in the composite hydrogels. When the chitin content was increased, viscoelasticity drop was gradually happened and in the third cycle a sudden drop was noticed. Presence of acetyl amide

groups in chitin make the hydrogen bonding network more complicated and act differently against US.

Chapter 4 extends the applications of the Chapter 3. Nicotine-loaded cellulose-chitin composite hydrogels were fabricated, and the hydrogels were exposed with continuous US and cyclic US irradiation to study the nicotine release behaviors. Here, the nicotine release was subjected to continuous and cyclic irradiation, so the cumulative release was lesser in continuous US than in cyclic irradiation. Further, the triggered-US release was only significant in the first two cycles of US in the composite hydrogels. So, the system identified not suitable at this stage for the cyclic irradiation of nicotine.

List of Publications

1. Harshani Iresha, Takaomi Kobayashi, **Ultrasound-triggered nicotine release from nicotine-loaded cellulose hydrogel**, *Ultrason. Sonochem*. 78 **(2021)** 105710.
2. Harshani Iresha, Takaomi Kobayashi, **In Situ Viscoelasticity Behavior of Cellulose–Chitin Composite Hydrogels during Ultrasound Irradiation**, Gels. 7 **(2021)** 81.
3. Harshani Iresha, Takaomi Kobayashi, **Smart Polysaccharide Hydrogels in Drug Delivery and Release**, in: A.K. Nayak, M.S. Hasnain (Eds.), Adv. Biopolym. Syst. Drug Deliv., Springer Nature, 6330 Cham, Switzerland, **2020**: pp. 135–149.
4. Takaomi Kobayashi, Harshani Iresha, Sarara Noguchi, Muhammad A. Wahab, **Biomass Hydrogel Medicines for Ultrasound Drug Releasing Materials**, in: Ref. Modul. Mater. Sci. Mater. Eng., Elsevier, **2022**.

Presentation in International/National Conferences and Symposiums

1. **The 26th Annual Meeting of the Japan Society of Sonochemistry, Kagoshima, Japan.** (October, 2017)
   Ranpati Devage Harshani Iresha, Takaomi Kobayashi. **Study of ultrasound triggered nicotine release from hydrogels prepared from cellulose**

2. **The 3rd Kitakanto-Ban'etsu Forum on Chemical Technology and Bioengineering, Oyama, Japan.** (December, 2017)
   Ranpati Devage Harshani Iresha, Takaomi Kobayashi. セルロースから調整されたハイドロゲルからの超音波によるニコチン放出に関する研究

3. **18th National Symposium on Polymeric Materials, Kuala Lumpur, Malaysia.** (September, 2018)
   Ranpati Devage Harshani Iresha, Takaomi Kobayashi. **Study of Ultrasound Triggered Nicotine Release from Hydrogels Prepared from Cellulose** (Best Poster Award)

4. **The 27th Annual Meeting of the Japan Society of Sonochemistry, Tokyo, Japan.** (November, 2018)
   Harshani Iresha, Takaomi Kobayashi. **Cellulose and Chitin Hydrogels as Drug Carriers in Ultrasound-Stimulated Nicotine Release System**

5. **The 28th Annual Meeting of the Japan Society of Sonochemistry, Sendai, Japan.** (November, 2019)
   Harshani Iresha, Takaomi Kobayashi. **Cellulose-Chitin composite hydrogel for ultrasound-triggered drug release** (Special Award)

6. **International Conference on "Science of Technology Innovation" (5th STI-GIGAKU 2020), Nagaoka, Japan.** (October, 2020)
   Harshani Iresha, Takaomi Kobayashi. **VISCOELASTIC PROPERTIES OF CELLULOSE-CHITIN COMPOSITE HYDROGELS: ON-SITE ULTRASOUND IRRADIATION**

7. **Global Academia-Industry Consortium for Collaborative Education Program (GAICCE) Materials Science and Technology International Symposium, Nagaoka, Japan.** (December, 2020)

   Harshani Iresha, Takaomi Kobayashi. **Viscoelastic Properties of Cellulose-Chitin Composite Hydrogels: on-Site Ultrasound Irradiation**